

DISSERTATION

HETEROTRIMERIC COILED-COILS AS
VIRAL FUSION PROTEIN MIMICS

Submitted by

Dana E. Johnson

Department of Chemistry

In partial fulfillment of the requirements

For the Degree of Doctor of Philosophy

Colorado State University

Fort Collins, Colorado

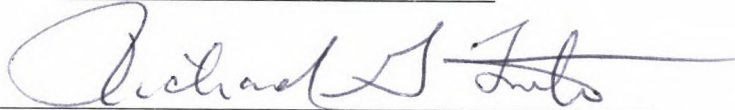
Spring 2010

COLORADO STATE UNIVERSITY

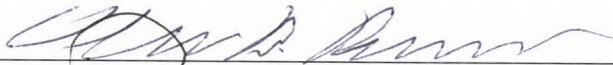
April 2, 2010

WE HEREBY RECOMMEND THAT THE DISSERTATION PREPARED UNDER OUR SUPERVISION BY DANA E. JOHNSON ENTITLED HETEROTRIMERIC COILED-COILS AS VIRAL FUSION PROTEIN MIMICS BE ACCEPTED AS FULFILLING IN PART REQUIREMENTS FOR THE DEGREE OF DOCTOR OF PHILOSOPHY.

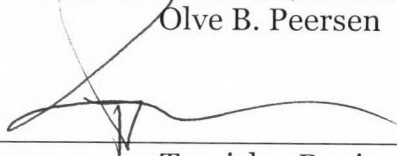
Committee on Graduate Work



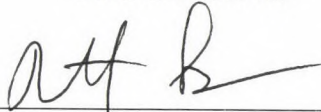
Richard G. Finke



Olve B. Peersen



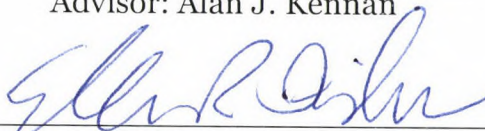
Tomislav Rovis



Matthew P. Shores



Advisor: Alan J. Kennan



Department Chair: Ellen R. Fisher

ABSTRACT OF DISSERTATION
HETEROTRIMERIC COILED-COILS AS VIRAL FUSION PROTEIN MIMICS

The α -helical coiled-coil, formed by the association and supercoiling of two or more α -helices, is a ubiquitous protein structure that mediates a wide range of biological activity. It is characterized by a heptad repeat of amino acids that serve to form both the hydrophobic core and electrostatic interfaces of the coiled-coil. Previous work in our lab showed the viability of designing a self-assembling heterotrimeric coiled-coil by sole manipulation of the hydrophobic core. This technique utilized a steric matching approach whereby one large side chain packed against two small ones. An added benefit to this type of control is that it allowed the freedom to explore additional interactions specific to the electrostatic interface.

Many enveloped viruses, including HIV-1, incorporate trimeric coiled-coils in their fusion proteins, and, consequently, are involved in the pathway to infection. Through interactions at the electrostatic interfaces of the coiled-coils, these fusion proteins form a six-helix bundle called a trimer-of-hairpins. The formation of this structure is a precursor to membrane fusion of the viral and host cells, and, as a result, it has become a therapeutic target. The steric matching technique developed in our lab allows us to graft key contacts from the native

sequences onto a stable, heterotrimeric system and construct a mimic of the trimer-of-hairpins, as was done with HIV-1 previously in our lab.

The work that follows shows that a viable mimic of the Human Respiratory Syncytial Virus is also possible. A stable, self-assembling mimic was designed, synthesized and validated through various spectroscopic methods. Additionally, a mutant study was conducted to further refine our knowledge of the importance of the residues thought to be key to the formation of the trimer-of-hairpins. Other work was performed extending the process to the Human T-cell Leukemia Virus, bringing the possibility of a complete and stable mimic ever closer.

Dana E. Johnson
Department of Chemistry
Colorado State University
Fort Collins, CO 80523
Spring 2010

ACKNOWLEDGEMENTS

First of all, I must thank my advisor Alan J. Kennan for the tremendous experience of the last 5 years. He quickly set the tone for his lab as one based on excellence and creativity, and I have grown incredibly as a researcher and problem-solver under his direction. He has also been a mentor to me as an educator, and I have been blessed by his example and encouragement. We also share a love for a good crossword and great piece of theatre.

I must thank the members of the Kennan Group as well, both past and present. Even when research was not going well, I never begrudged coming to work. There were always engaging discussions, friendly banter and abundant laughter. I have enjoyed the journey with all of you.

My family also deserves great thanks for their unending support and encouragement to me during these last 11 (!) years of college. It has been a long process, yet they were always excited for the next step and remained interested all along the way. I love you all so much!

Last but not least, I must thank my lovely wife, Kathy. She has shown incredible grace and patience toward me during these years at Colorado State. I could always count on her love and support when experiments went well or when research was nothing but frustrating. She gently pushed when I needed it, and rejoiced when I rejoiced. She has been a model to me of one who loves well. Thank you and love you!

TABLE OF CONTENTS

Chapter 1	Background	
1-1	Introduction	2
1-2	The Coiled-Coil	2
1-3	Development of the Tic-Tac-Toe System	6
1-4	Coiled Coils in HIV Infectivity	9
1-5	References Cited	13
Chapter 2	Design of Human Respiratory Syncytial Virus Mimic	
2-1	The Basics of HRSV Structure	17
2-2	Synthesis and Validation	19
2-3	Control Studies	27
2-4	Experimental	30
2-5	References Cited	33
Chapter 3	Mutant Studies of the HRSV System	
3-1	Introduction to the Mutants	36
3-2	The Mutant Studies	37
3-3	The Triple Mutant	41
3-4	Experimental	44
3-5	References Cited	46
Chapter 4	Continued Work of the Human T-cell Leukemia Virus	
4-1	Introduction	48
4-2	The HTLV Trimer	50
4-3	Synthesis and Purification of the gp21 Ligand	52

4-4 Possibilities for Future Work	58
4-5 Experimental	60
4-6 References Cited	60
Chapter 5 Conclusions	
5-1 Final Statements	63
5-2 References Cited	65
Appendix 1:Peptide Characterization	66
Appendix 2:Guanidine Denaturation Curves	88

Chapter 1
Background

1-1: Introduction

The coiled-coil motif first received attention as a secondary structure that could be identified via inspection of the primary sequence of any protein, simply by noting the location of hydrophobic residues.¹ When the yeast transcription factor GCN4 was finally crystallized, it was found to be a dimeric coiled-coil, as predicted by the primary sequence.² Since then, the coiled-coil has been found to be a ubiquitous structure in a wide variety of systems, mediating an array of protein-protein interactions.³

Trimeric α -helical coiled-coils have become the recent focus of research, much of which is based on the archetype coiled-coil, GCN4.⁴ They have shown themselves to be useful platforms for the study of self-assembling systems.

1-2: The Coiled-Coil

Coiled-coils are 2 or more α -helices that wrap around each other via a superhelical twist, much like the strands of a rope twist around a central axis (Figure 1). The primary sequence of the coiled-coil consists of a heptad repeat of residues, labeled *abcdefg*. The residues in positions *a* and *d* are hydrophobic and are the driving force behind the self-assembly of the coiled coil as they pack tightly together into a hydrophobic core.⁵ The residues in the *e* and *g* positions form what is called the electrostatic interface and are used to aid in the stability of the system.⁶ The residues in the remaining positions are solvent exposed and are less specific than the other positions. They tend to be either hydrophilic, like a serine or threonine, or helix promoting, like alanine or lysine (Figure 2).

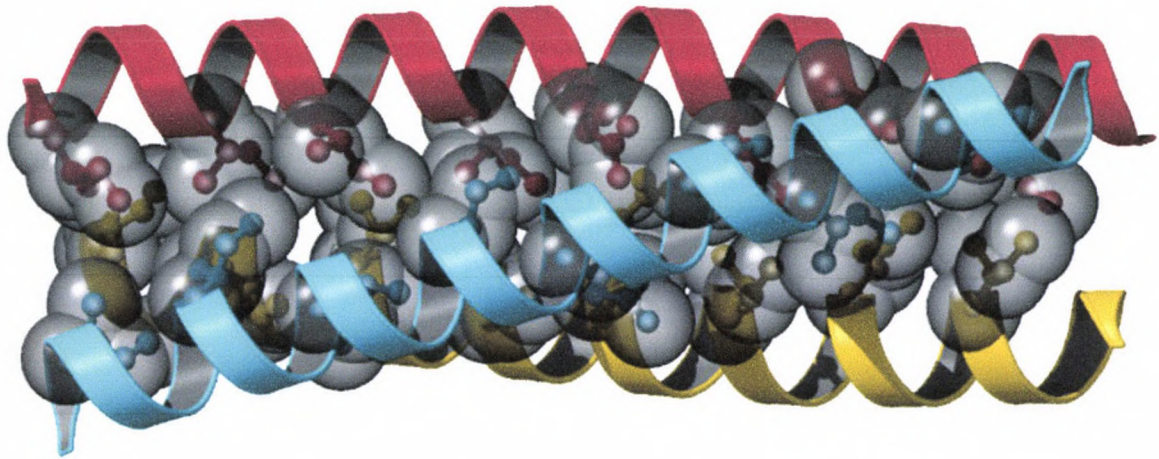


Figure 1. Side view of a trimeric coiled coil. The hydrophobic residues that make up the core are shown as a space-filling model. The peptide backbones are shown as ribbons. Notice the superhelical twist as exhibited by the fact that the red ribbon begins in front on the left and end in back on the right, and the yellow begins in back on the left and ends in front on the right.

The residues in the hydrophobic core are the most important for determining both oligomerization state and stability. Much attention has been spent to understand just how important they are. The dimeric coiled-coil of GCN4 was found to have a single asparagine in the center of the hydrophobic core.⁷ It was odd to find a polar residue in a position typically reserved for hydrophobic ones. Kim and co-workers synthesized a dimeric coiled-coil system based on GCN4, where the central asparagine and surrounding residues were all mutated to leucine, isoleucine or valine in turn. It was found that the system was much more stable but no longer specified for a dimer.⁸ Other work looked at the effect of a point mutation on a coiled coil, finding stability to be directly correlated to the hydrophobicity of the mutated residue.⁹ In effect, the burial of the asparagine into the hydrophobic core imparts structural specificity at the cost of stability.

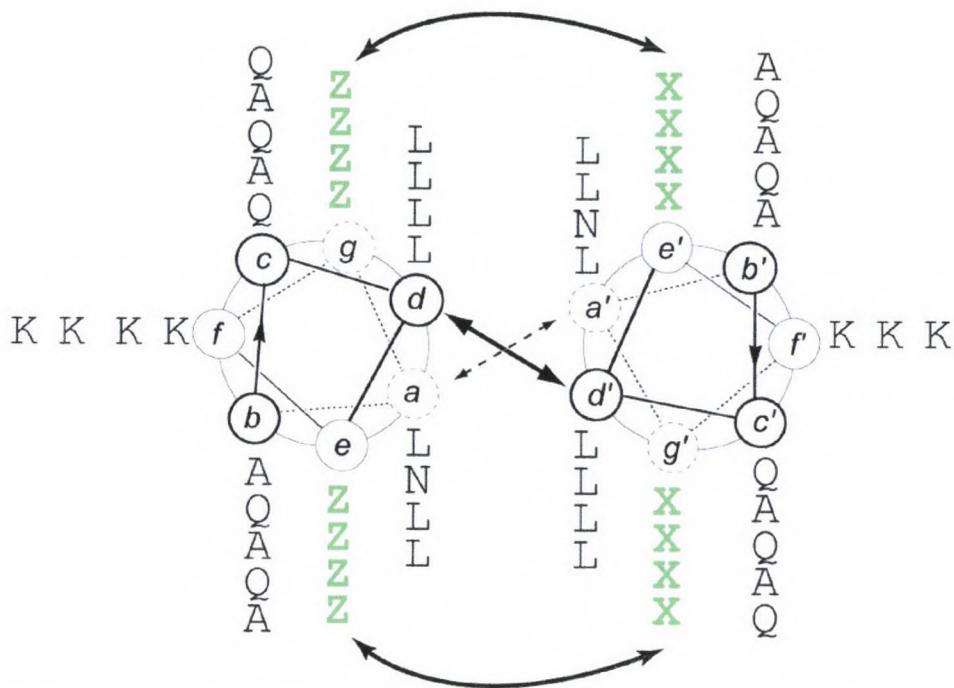


Figure 2. Helical wheel diagram of a generalized heterodimeric coiled coil. Residues in the *a* and *d* position are hydrophobic with the exception of the lone asparagine. Arrows between the green highlighted residues indicate the electrostatic interfaces. The solvent exposed positions are populated with a mixture of both polar and helix-promoting residues.

Additional work by Kim and co-workers demonstrated that the position of the buried asparagine also determined strand orientation in the coiled-coil. Simply by changing the position of the asparagine, they could specify for a parallel dimer versus antiparallel¹⁰ (Figure 3).

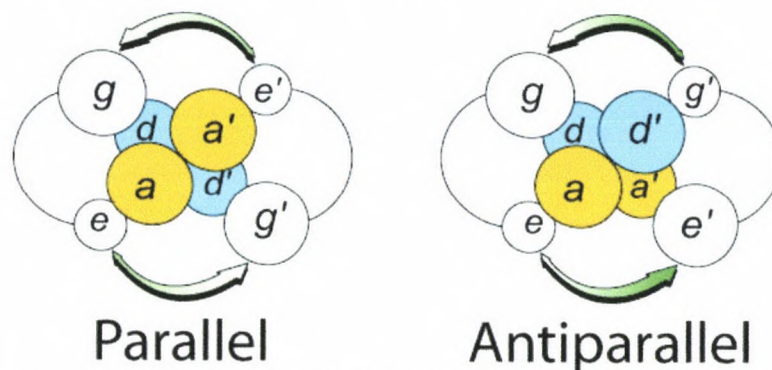


Figure 3. In parallel packing, the hydrophobic core consists of alternating all *a* and all *d* layers. In antiparallel packing, the core consists of layers with a mixture of *a* and *d* residues.

Another step in the understanding of the importance of the hydrophobic core was taken by Alber and co-workers when they mutated the central asparagine of the GCN4 system to all alanines.¹¹ The resulting system no longer specified for a dimer, but instead established an equilibrium between a dimeric state and a trimeric state. When a molecule of benzene or cyclohexane was added to the system, the small molecule served to stabilize the steric void formed by the all alanine layer, specifying a trimer over a dimer (Figure 4). Moreover, the trimeric system that resulted was stable enough for crystallographic studies. This was an important move toward the development of stable trimeric systems that could be used as scaffolds to understand the protein-protein interactions of coiled-coils in nature.

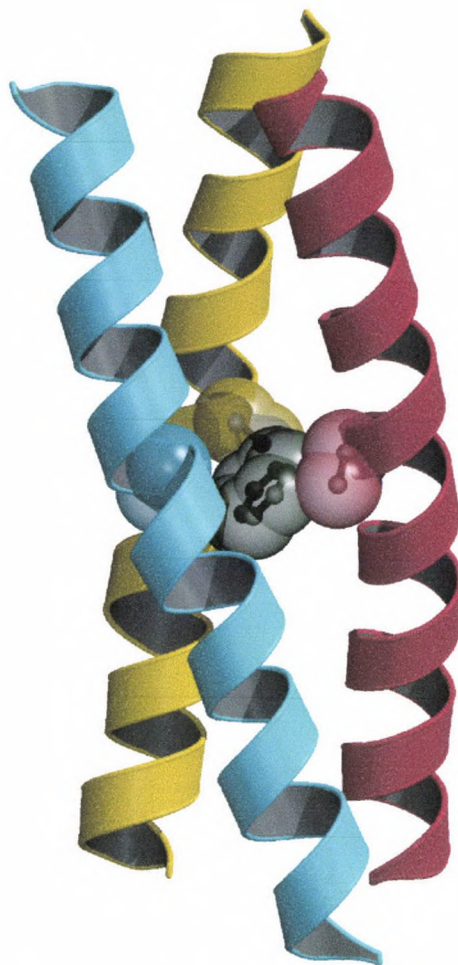


Figure 4. Crystal structure of the Alber system with benzene as the allosteric switch. The benzene molecule fits into the steric void formed by the three alanines, thus stabilizing the trimeric system.

1-3: Development of the Tic-Tac-Toe System

Our lab has sought to extend Alber's work by seeking a way to obviate the need for an additional small molecule, while still obtaining a stable trimeric system. One major step in that direction was to tether Alber's small molecule switch directly to the backbone of one of the helices of the timer. Nate Schnarr synthesized a trimeric system with a cyclohexylalanine residue meant to pack against two alanine residues in the same layer of the hydrophobic core.¹² This steric-matching technique was meant to take advantage of the steric void that

would result in an all alanine layer and a steric clash that would result upon an all cyclohexylalanine layer. The most stable system was predicted to be a 2:1 mixture of alanine:cyclohexylalanine peptides (Figure 5).

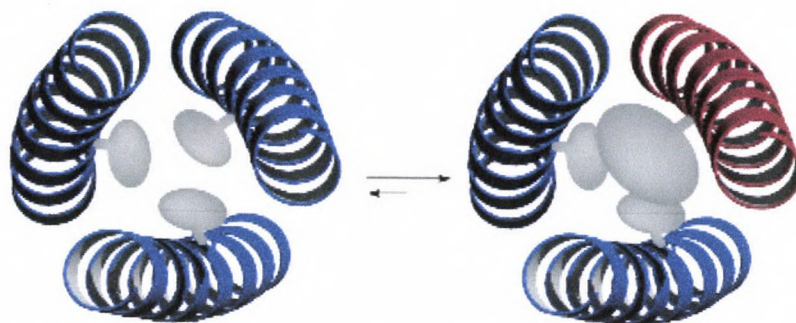


Figure 5. Steric-matching representation. The homotrimer on the left would be destabilized by the steric void of the all-alanine layer. The heterotrimer on the right would be stabilized by the large side-chain packing against the two smaller.

However, only the steric void of the all alanine layer was found to be destabilizing enough to have any effect, so the substitution pattern was extended. In three successive layers of the hydrophobic core, a cyclohexylalanine was substituted into the sequence of each peptide of the trimer in turn, while the remaining residues of each layer were alanines (Figure 6).

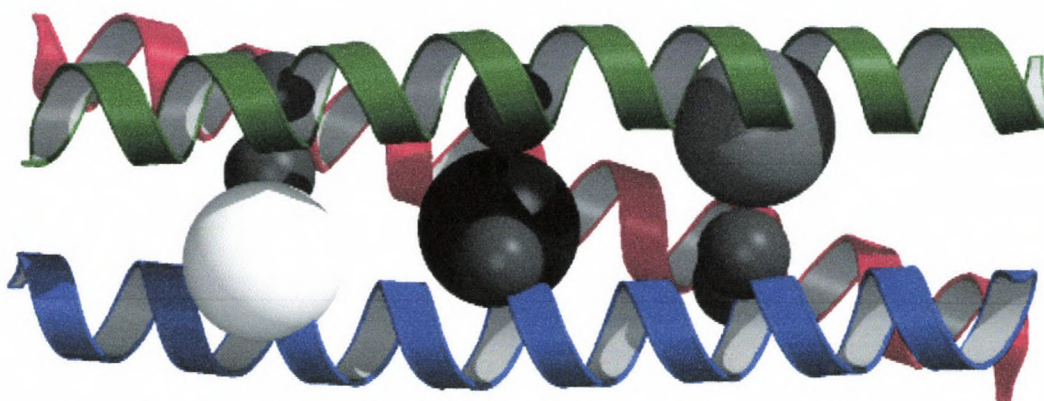


Figure 6. Cartoon side view of the new substitution pattern. Cyclohexylalanine side chains are shown much bigger than their alanine counterparts. Each peptide now has one large side chain and two small. The heterotrimeric system shown is the most stable, as it does not have any destabilizing all-alanine layers.

Therefore, the most stable structure would have three successive layers of one cyclohexylalanine packed against two alanines. Any other combination of peptides would give at least one destabilizing layer with a steric void. The three peptides of the trimer are referred to as T₉, T₁₆ and T₂₃, where the numbers refer to the residue position of the substituted cyclohexylalanine from the original GCN4 sequence. This substitution pattern was given the moniker Tic-Tac-Toe (TTT), as a schematic representation of the substitution pattern gives a picture reminiscent of the strategy game¹³ (Figure 7). This steric-matching strategy was key to allowing our lab to specify a stable heterotrimeric coiled-coil for study.

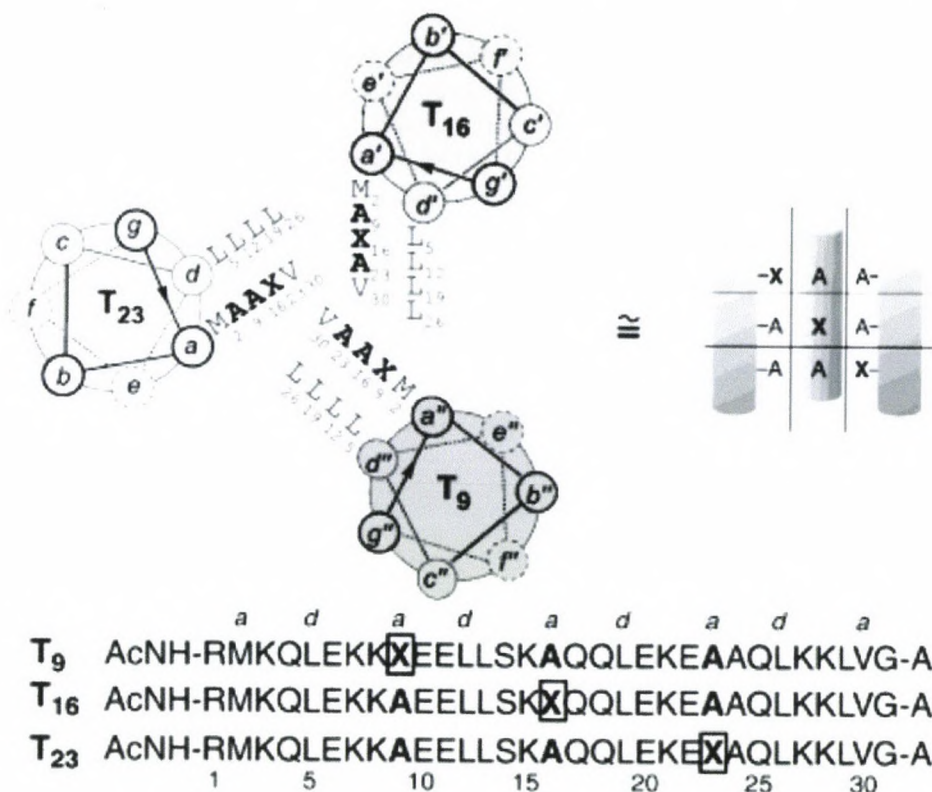


Figure 7. Schematic diagram of the TTT system. The helical wheel on the top left highlights the substitution pattern in the core, where X = cyclohexylalanine. The Tic-Tac-Toe pattern is more clearly seen in the top right as in each layer, one X packs against 2 alanines. The sequences for the GCN4-based peptides are shown on the bottom.

1-4: Coiled-Coils in HIV Infectivity

This need for a stable trimeric system is based on the fact that HIV and many other viruses depend on trimeric coiled-coils for infectivity. Looking more closely at the HIV infection pathway will highlight our interest in these structures (Figure 8). The HIV-1 fusion protein gp160 is proteolytically cleaved into two subunits, gp41 and gp120. The N-terminus of gp41 contains a fusion peptide which inserts into the membrane of the cell to be infected.¹⁴ Through a conformational rearrangement, the C-terminal end packs in an antiparallel fashion into the binding grooves formed by the N-terminal coiled coil, forming a

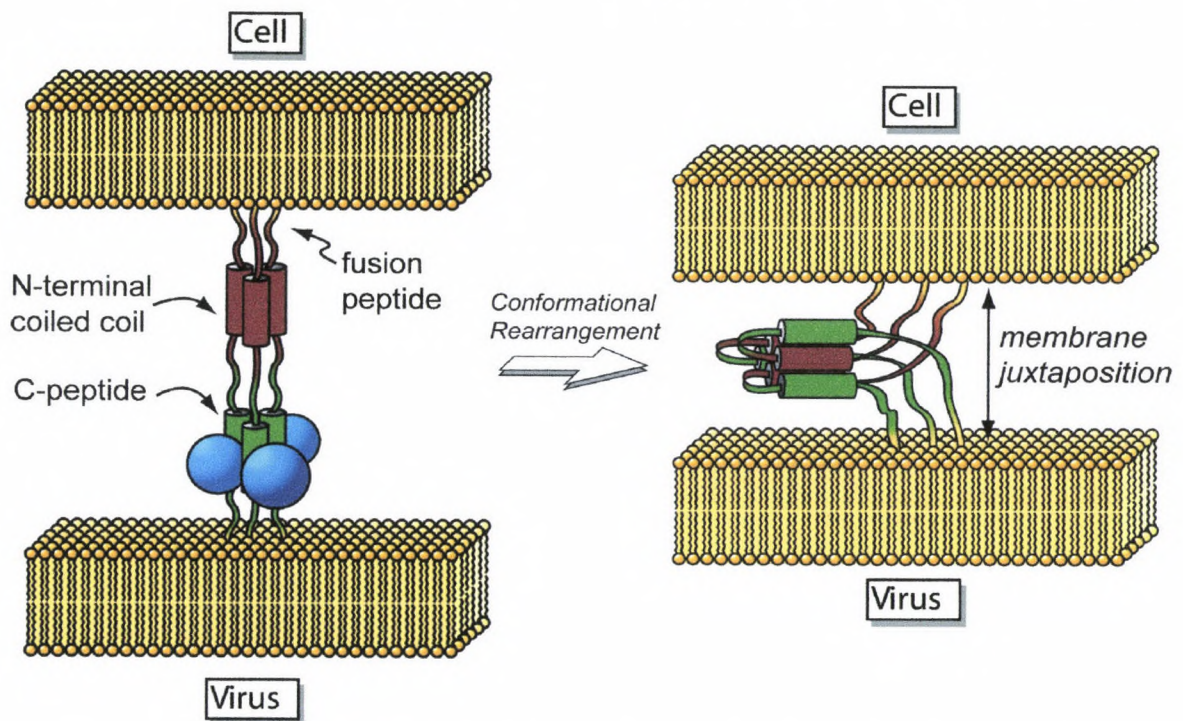


Figure 8. Model of HIV-1 membrane fusion. Pre-hairpin intermediate is shown on the left with the N-terminal trimeric coiled coil. Trimer-of-hairpins structure is shown on the right after the C-terminal peptides have bound in an antiparallel fashion into the binding grooves of the trimer. The resultant shortening of the fusion proteins leads to membrane juxtaposition and eventually fusion.

trimer-of-hairpins structure. This six-helix bundle serves to shorten the distance between viral and host cells, leading to membrane juxtaposition and infection.¹⁵ In the case of HIV-1, there are three hydrophobic residues on the C-terminal end of gp41 that are key to the formation of the trimer-of-hairpins, namely Trp628, Trp631 and Ile635. These residues bind to a specific hydrophobic pocket formed in the binding grooves of the N-terminal coiled coil¹⁶ (Figure 9).

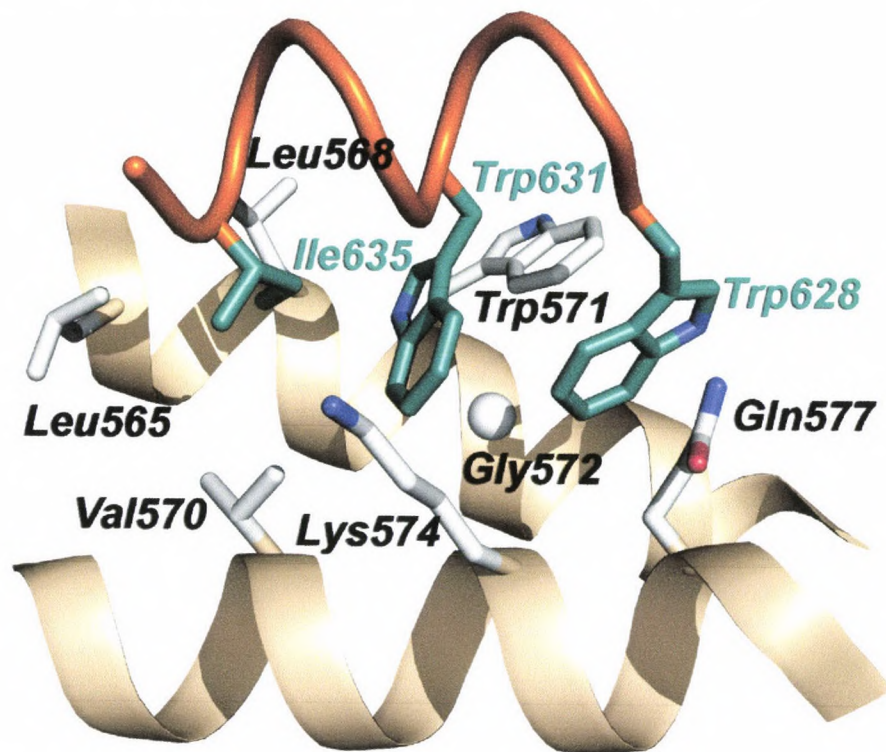


Figure 9. Key residues in the formation of the HIV-1 trimer-of-hairpins. C-terminal residues are highlighted in green. The amino acids that form the binding pocket on the N-terminus are shown in white, labeled in black.

Because of the importance of this trimer-of-hairpins to infection, it has become an important drug target.¹⁷ As the binding between the internal coiled coil and the C-terminal peptide of gp41 is dependent on the residues in the electrostatic interface, it is essential to have those residues untouched to better study the interaction. However, most research done on coiled coils rely on

electrostatic interfaces with fully matched charges for stability.¹⁸ Synthesis of the coiled coil with all three binding pockets left intact would lead to aggregation problems with so many hydrophobic residues outside the hydrophobic core. Schnarr solved this problem by mutating two of the binding pockets to a matched configuration of lysine and glutamic acid residues, making the system more soluble while leaving one binding pocket available for study.¹⁹

The resulting construct is a four-component system utilizing both the TTT strategy for heterotrimeric specificity and two matched electrostatic interfaces to improve both stability and solubility (Figure 10). The important residues of the gp41C peptide and those that form the binding pocket were determined via crystallographic studies by Kim and co-workers.²⁰ These were grafted onto our stable 4-component system and became the first viable mimic of viral fusion peptides from our lab.

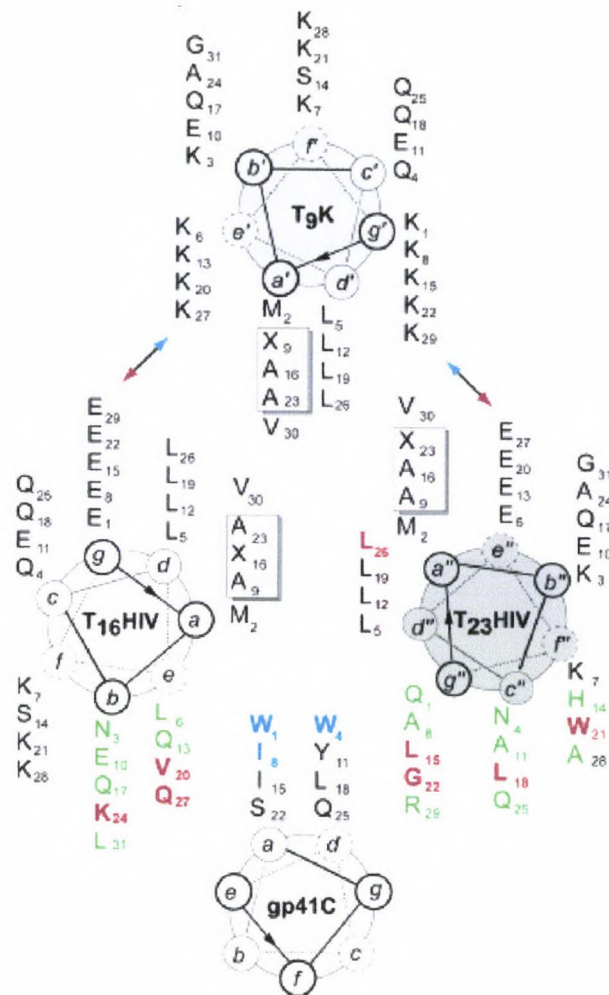


Figure 10. Helical wheel of the HIV fusion protein mimic. The boxed residues are the TTT substitutions, and the arrows indicate the electrostatically matched interfaces. Key ligand residues for binding are colored blue. Residues that form the binding pocket are red, while green residues merely surround the binding pocket. Only residues in the *a* and *d* positions are shown on gp41C for clarity.

A stable mimic of the trimer-of-hairpins structure is an important scaffold for the study of viruses outside the HIV lentiviral genus. My work was able to extend the usefulness of this construct specifically to the Human Respiratory Syncytial Virus (HRSV) and extend work done on the Human T-cell Leukemia Virus (HTLV). Additionally, my work included the use of mutant studies to further refine our understanding of the binding interactions in HRSV.

1-5: References Cited

- (1) (a) Cohen, C. and Parry, D. A. D. *Science*, **1994**, *263*, 488-489. (b) Woolfson, D. N. and Alber, T. *Protein Science*, **1995**, *4*, 1596-1607. (c) Walshaw, J. and Woolfson, D. N. *J. of Struct. Biol.*, **2003**, *144*, 349-361.
- (2) (a) Cohen, C. and Parry, D. A. D. *Science*, **1994**, *263*, 488-489. (b) O'Shea, E. K., Klemm, J. D., Kim, P. S. and Alber, T. *Science*, **1991**, *254*, 539-554.
- (3) (a) Schneider, J. P., Lombardi, A. and DeGrado, W. F. *Folding and Design*, **1998**, *3*(2), R29-R40. (b) Lombardi, A., Bryson, J. W. and DeGrado, W. F. *Biopolymer Peptide Science*, **1997**, *40*, 495-504. (c) Woolfson, D. N. and Alber, T. *Protein Science*, **1995**, *4*, 1596-1607. (d) Nautiyal, S. and Alber, T. *Protein Science*, **1999**, *8*, 84-90. (e) Burkhard, P., Stetefeld, J. and Strelkov, S. V. *Trends in Chem. Biol.* **2001**, *11*(2), 82-88.
- (4) (a) Eckert, D. M., Malashkevich, V. N. and Kim P. S. *J. Mol. Biol.*, **1998**, *284*, 859-865. (b) Zhu, H., Celinski, S. A., Scholtz, J. M. and Hu, J. C. *J. Mol. Biol.*, **2000**, *300*, 1377-1387. (c) Lear, J. D., Gratkowski, H., Adamian, L., Liang, J. and DeGrado, W. F. *Biochemistry*, **2003**, *42*, 6400-6407.
- (5) (a) Munson, M., O'Brien, R., Sturtevant, J. M. and Regan, L. *Protein Science*, **1994**, *3*, 2015-2022. (b) Lumb, K. J. and Kim, P. S. *Biochemistry*, **1995**, *34*, 8642-8648. (c) Kashiwada, A., Hiroaki, H., Kohda, D., Nango, M. and Tanaka, T. *J. Am. Chem. Soc.*, **2000**, *122*, 212-215. (d) Kiyokawa, T., Kanaori, K., Tajima, K. and Tanaka, T. *Biopolymer Peptide Science*, **2000**, *55*, 407-414.

- (6) (a) McClain, D. L., Binfet, J. P. and Oakley, M. G. *J. Mol. Biol.*, **2001**, *313*, 371-383. (b) Gurnon, D. G., Whitaker, J. A. and Oakley, M. G. *JACS*, **2003**, *125*, 7518-7519. (c) Kohn, W. D., Kay, C. M. and Hodges, R. S. *J. Mol. Biol.*, **1998**, *283*, 993-1012.
- (7) O'Shea, E. K., Klemm, J. D., Kim, P. S. and Alber, T. *Science*, **1991**, *254*, 539-554.
- (8) (a) Harbury, P. B., Zhang, T., Kim, P. S. and Alber, T. *Science*, **1993**, *262*, 1401-7. (b) Lumb, K. J. and Kim, P. S. *Biochemistry* **1995**, *34*, 8642-8648.
- (9) Wagschal, K., Tripet, B., Lavigne, P., Mant, C. and Hodges, R. S. *Protein Science*, **1999**, *8*, 2312-2329.
- (10) Oakley, M. G. and Kim, P. S. *Biochemistry*, **1998**, *37*, 12603-12610.
- (11) Gonzalez, L., Jr., Plecs, J. J. and Alber, T. *Nature Structural Biology*, **1996**, *3*(6), 510-515.
- (12) Schnarr, N. A. and Kennan, A. J. *J. Am. Chem. Soc.*, **2001**, *123*, 11081-11082.
- (13) Schnarr, N. A. and Kennan, A. J. *J. Am. Chem. Soc.*, **2002**, *124*, 9779-9783.
- (14) (a) Chan, D. C. and Kim, P. S. *Cell*, **1998**, *93*, 681-684. (b) Chan, D. C., Fass, D., Berger, J. M. and Kim, P. S. *Cell*, **1997**, *89*, 263-273.
- (15) (a) Weissenhorn, W., Dessen, A., Harrison, S. C., Skehel, J. J. and Wiley, D. C. *Nature*, **1997**, *387*, 426-430. (b) Chan, D. C. and Kim, P. S. *Cell*, **1998**, *93*, 681-684. (c) Markosyan, R. M., Ma, X., Lu, M., Cohen, F. S. and Melikyan, G. B. *Virology*, **2002**, *302*, 174-184. (d) Chan, D. C., Fass, D., Berger, J. M. and Kim, P. S. *Cell*, **1997**, *89*, 263-273.

- (16) (a) Weissenhorn, W., Dessen, A., Harrison, S. C., Skehel, J. J. and Wiley, D. C. *Nature*, **1997**, *387*, 426-430. (b) Chan, D. C., Fass, D., Berger, J. M. and Kim, P. S. *Cell*, **1997**, *89*, 263-273.
- (17) (a) Chan, D. C., Chutkowski, C. T. and Kim, P. S. *Proc. Nat. Acad. of Sci.*, **1998**, *95*, 15613-7. (b) Eckert, D. M., Malashkevich, V. N., Hong, L. H., Carr, P. A. and Kim, P. S. *Cell*, **1999**, *99*, 103-115. (c) Sia, S. K., Carr, P. A., Cochran, A. G., Malashkevich, V. N. and Kim, P. S. *Proc. Nat. Acad. of Sci.* **2002**, *99*(23), 14664-9. (d) Bewley, C. A., Louis, J. M., Ghirlando, R. and Clore, G. M. *J. of Biol. Chem.*, **2002**, *277*(16), 14238-45. (e) Tan, K., Liu, J-H., Wang, J-H., Shen, S. and Lu, M. *Proc. Nat. Acad. of Sci.*, **1997**, *94*, 12303-8.
- (18) (a) Nautiyal, S., Woolfson, D. N., King, D. S. and Alber, T. *Biochemistry*, **1995**, *34*(37), 11645-51. (b) Lumb, K. J. and Kim, P. S. *Biochemistry*, **1995**, *34*, 8642-8648. (c) Kwok, S. C. and Hodges, R. S. *J. Biol. Chem.*, **2004**, *279*(20), 21576-88. (d) McClain, D. L., Woods, H. L. and Oakley, M. G. *J. Am. Chem. Soc.*, **2001**, *123*, 3151-3152.
- (19) Schnarr, N. A. and Kennan, A. J. *JACS*, **2004**, *126*, 10260-10261.
- (20) Chan, D. C., Fass, D., Berger, J. M. and Kim, P. S. *Cell*, **1997**, *89*, 263-273.

Chapter 2

Design of a Human Respiratory Syncytial Virus Mimic

2-1: The Basics of HRSV Structure

The Human Respiratory Syncytial Virus (HRSV), a member of the *paramyxoviridae* family of viruses, is currently of concern to the world community as it remains a leading cause of bronchiolitis and pneumonia in children.¹ It is an enveloped virus that is characterized by a single strand of RNA.² Akin to HIV, HRSV utilizes a trimer-of-hairpins motif in order to bring about membrane fusion and therefore infection, which makes it a prime target for our lab.

The HRSV membrane protein, F₀, is proteolytically cleaved into two subunits, F₁ and F₂, connected by a disulfide linkage. The N-terminal end of the F₁ peptide incorporates not only a helical portion, which forms a trimeric coiled coil upon association with two other peptides, but also a fusion peptide region, which anchors into the membrane of the host cell. As in HIV, the C-terminal ends of the F₁ peptides pack in an antiparallel fashion into the binding grooves formed by the coiled coil to form the trimer-of-hairpins motif.³

Even before the trimer-of hairpins motif was identified for HRSV, it was known that portions of the F₁ protein had some inhibitory function.⁴ Since the determination of the helical nature of the F proteins in HRSV, much work has been done to identify fusion inhibitors in the form of both peptides and small molecules. Protein mimics, which are typically portions of the C-terminal end of the F₁ protein, are either toxic *in vivo* or are identified by trial and error.⁵ Some small molecules have been discovered through high throughput methods that show some inhibitory nature, although their methods of inhibition are elusive.⁶ A stable scaffold with an intact binding pocket is needed to aid in the rational

design of inhibitors of HRSV. To that end, we looked to previous X-ray crystallographic work done by Kim and co-workers to begin. Their work clearly showed not only the trimer-of-hairpins, but also the key contact points between the coiled coil and the C-peptide ligand, namely Ser509, Phe488 and Phe483⁷ (Figure 1).

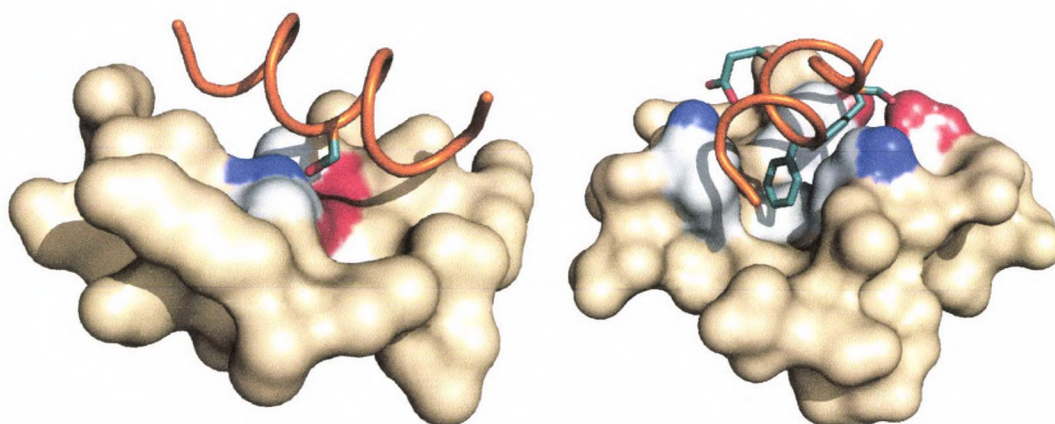


Figure 1. Depiction of the key contacts in the HRSV system highlighted in green. The C-terminal peptide backbone is shown in orange, while the N-terminal coiled coil surface is shown in tan. Serine is shown on the left. The two phenylalanines are on the right.

One unique feature of the HRSV system is a hydrophobic stutter in the primary sequence. This refers to a change in the typical occurrence of hydrophobic residues near the C-terminus. Instead of the usual 3-4-3-4-3 repeat of hydrophobic amino acid side chains, the HRSV system displays a 3-4-4-4-3 repeat on the C-terminus. This unusual characteristic causes the HRSV coiled coil to appear slightly unwound on one end.⁸ It was unclear from the start whether this partially unwound portion would disrupt trimer formation or not (Figure 2).

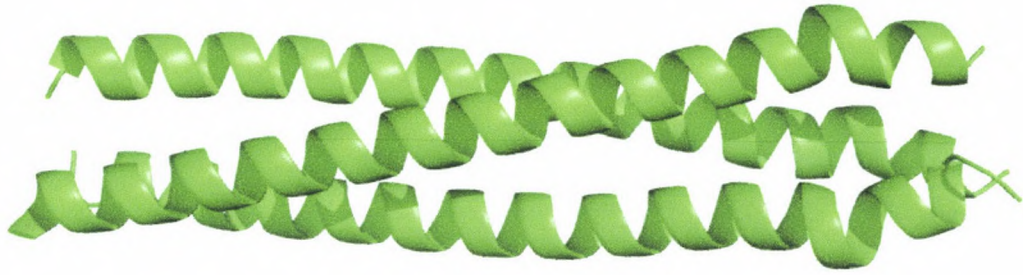


Figure 2. Ribbon drawing of the HRSV trimer. The hydrophobic stutter is seen in the partially unwound section on the right end of the structure.

2-2: Synthesis and Validation

With our stable HIV mimic in hand, we grafted the key contact points from HRSV onto the binding pocket. We continued to incorporate the successful TTT substitutions in the hydrophobic core and the matched electrostatic interfaces on two of the three possible binding grooves (Figure 3). For the initial synthetic attempt, we endeavored to make synthesis easier by trimming the sequence to include only those residues in the trimeric coiled coil that formed the binding pocket. This meant that these original sequences included the hydrophobic stutter yet did not have 9 additional residues on the N-terminus. After some initial synthetic challenges, it was decided to persubstitute all nonessential glutamine residues for alanine, which appended “Q/A” to the name. The three peptides of the coiled coil were called T₉HRSV Q/A, T₁₆HRSV Q/A and T₂₃HRSV Q/A. The initial T refers to the TTT strategy, and the number refers to the position of the cyclohexylalanine substitution taken from the original GCN4 system. The ligand peptide was referred to as F₁C, as it is near the C-terminal end of the F₁ peptide.

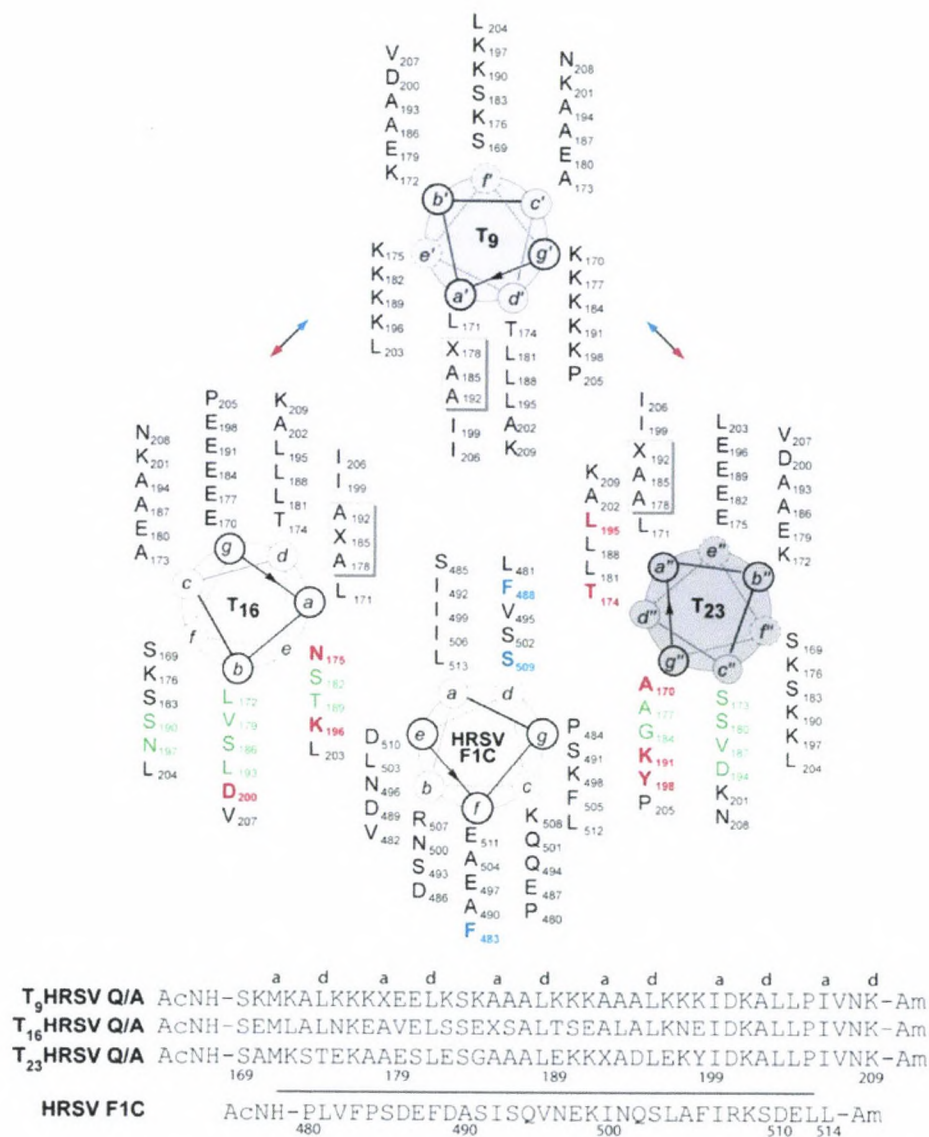


Figure 3. Helical wheel diagram of the HRSV Q/A system. The boxed residues form the TTT hydrophobic core, and the arrows show the matched electrostatic interfaces. Residues colored blue are key contact points. Those in red form the binding pocket, while those in green surround the binding pocket.

Synthesis of the T₉, T₁₆ and F_{1C} peptides was accomplished on solid phase using the *in situ* neutralization technique optimized by Kent.⁹ Access to the T₂₃ peptide proved more difficult, yet it was eventually synthesized using Fmoc chemistry on solid phase. Once the purified peptides were in hand, we tested trimer formation via a Nickel-affinity experiment. This involved appending a

Histidine tag, composed of two glycines and six histidines, to the N-terminus of the T₉ peptide, now termed T₉His. An equimolar mixture of the three trimer peptides was exposed to nickel-nitrilotriacetic acid (NTA) bound to agarose beads. The Histidine-tagged peptide will bind to the beads through interactions between the imidazole side chains of the histidine and the nickel. If the trimer forms, all three peptides will remain bound to the Ni-NTA beads through the course of the experiment and are eluted off at the end through the use of an imidazole buffer that competes for the binding sites. By analyzing both the initial solution and the final elution fraction by HPLC, we should see a clear 1:1:1 relationship among the peptides. Unfortunately, trimer formation did not occur in this case, and the sequences needed to be reevaluated (Figure 4).

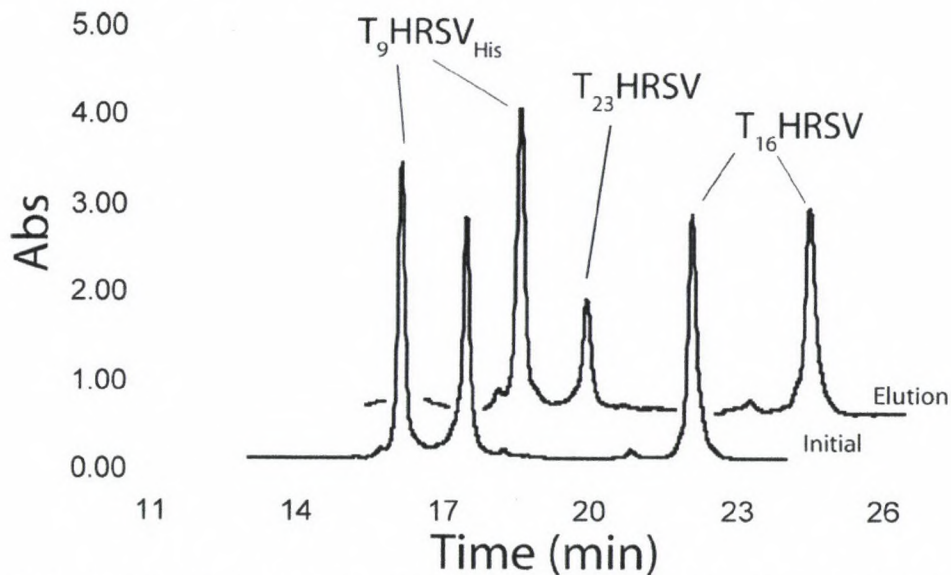
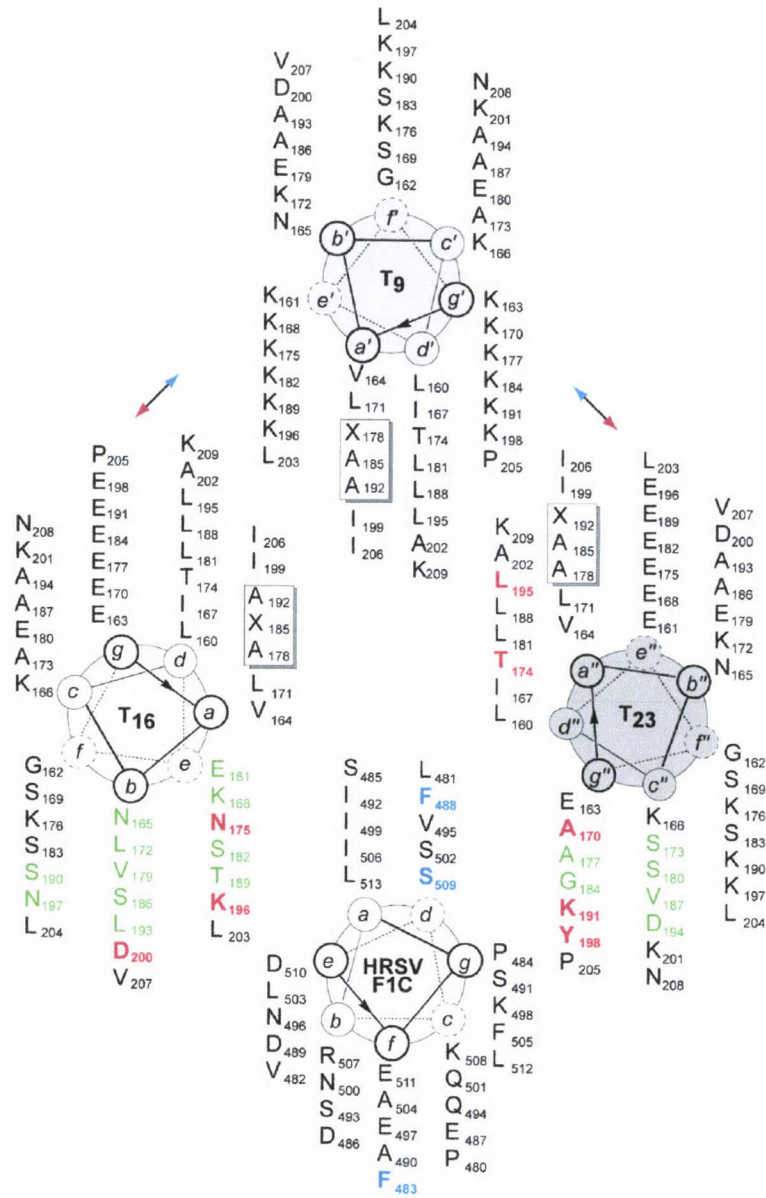


Figure 4. Ni-NTA affinity experiment of the HRSV trimer. The initial 1:1:1 relationship among the three peptides of the trimer was not maintained throughout the experiment, indicating an unstable trimer.

Upon reflection, we realized the amino acids that had originally been excised for ease of synthesis might actually have been important for stability. The hydrophobic stutter seemed to be destabilizing enough that the coiled-coil

needed the additional interactions of the nine N-terminal amino acids for stability. These nine residues were added back to the sequences and synthesis began afresh (Figure 5). It should be noted that these new sequences were the longest attempted in our lab to date and required a new protocol for their synthesis. Traditional attempts at synthesis gave numerous deletion products and incompletely cleaved material. Double coupling of residues that did not seem to react was attempted as well as several different cleavage protocols. Neither strategy gave product peptides.

Finally, a protocol was developed that gave clean products in good yields, and this protocol was applied to every 50-mer included in my work. Test splits of ~10% of the resin were removed at the 1/3 and 2/3 mark to cleave and to determine the progress of the synthesis. This allowed us to more accurately determine the identity of any deletion products. At the 2/3 mark, the resin was also reduced by half as the amount of resin hindered complete rinsing between coupling steps. Additionally, all amino acids coupled after the 2/3 mark were double coupled to insure reaction. Cleavage conditions remained unchanged as the modifications to the synthesis protocol was sufficient to give good amounts of products.



T_9 full Q/A AcNH-LKGKVNKIKSKLkATKKKXEEELKSKAAALKKKAAALKKKIDKALLPIVNK-Am
 T_{16} full Q/A AcNH-LEGEVNKIKSELLATNKEAVELSSXSALTSEALALKNEIDKALLPIVNK-Am
 T_{23} full Q/A AcNH-LEGEVNKIESALKSTEKAAESLESAAVLEKKXADLEKYIDKALLPIVNK-Am
 HRSV F1C AcNH-PLVFPSEDFDASISQVNEKINQSLAFIRKSDPELL-Am

Figure 5. Helical wheel diagram of the HRSVfull Q/A system. Boxed residues form the TTT substitution. Arrows indicate the electrostatic interface. Blue residues are key contacts; red form the binding pocket, and green surround the pocket.

Nickel-affinity experiments were conducted again with the new system. Set up of the experiment was made more difficult as the T₁₆ and T₂₃ peptides coeluted. This necessitated the set up of an initial 1:1 ratio of T₉His to T₁₆, then addition of the T₂₃ peptide to a 1:2 ratio. Trimer formation did occur with the longer sequences as evidenced by the elution fraction of the His-tag experiment (Figure 6). This indicated we had a stable, self-assembling system. We then tested to see whether the F₁C peptide would bind as the ligand. An equimolar mixture of T₉His, T₁₆, T₂₃ and F₁C was exposed to the Ni-NTA beads, and then eluted off at the end of the experiment to show intact ratios (Figure 7).

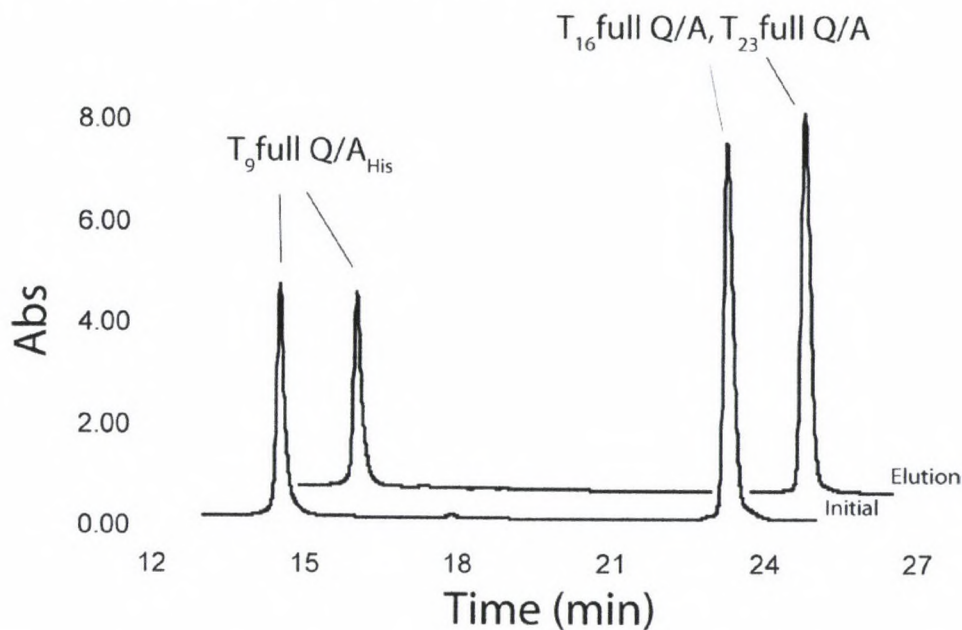


Figure 6. Ni-NTA affinity experiment of the HRSVfull Q/A trimer. Due to coelution, initial ratios are 2:1 rather than 1:1:1. Ratios remain intact through the experiment, indicating a stable trimer.

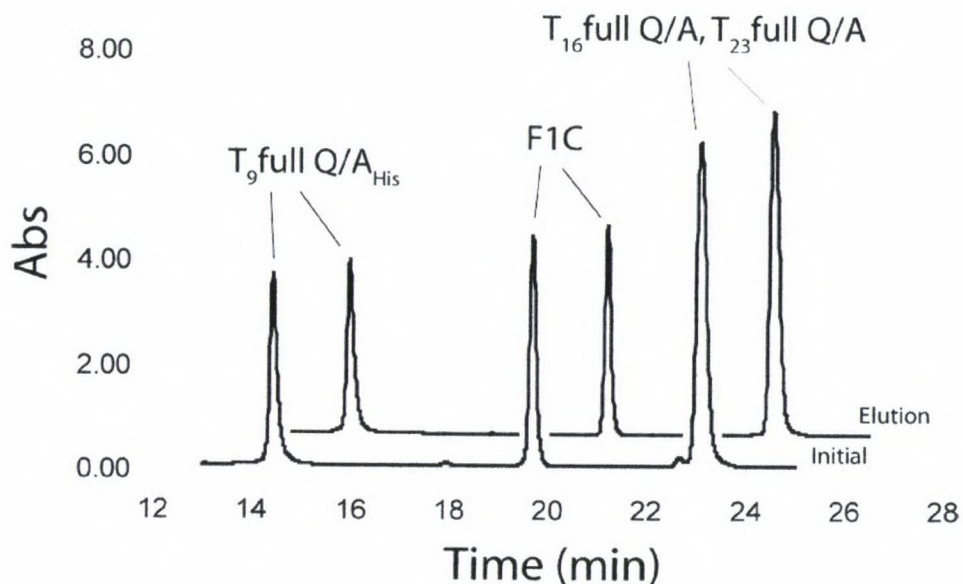


Figure 7. Ni-NTA affinity experiment of the HRSVfull Q/A system plus F₁C ligand. Intact ratios indicate binding of the ligand to the trimer.

Though we now knew the stoichiometry of the system, we also hoped to demonstrate through circular dichroism (CD) that the overall helicity of the system increased as the peptides self-assembled into a trimeric coiled-coil. CD is a method by which we can probe the secondary structure of these peptides and determine if we see an increase in helicity and stability when the peptides are present in the correct ratios. An equimolar mixture of the three trimer peptides gave a signal consistent with an α -helix with characteristic minima at 208 and 222 nm. Additionally, a forward and reverse temperature scan reveals that the trimer system refolds into a stable trimer even after thermal unfolding (Figure 8).

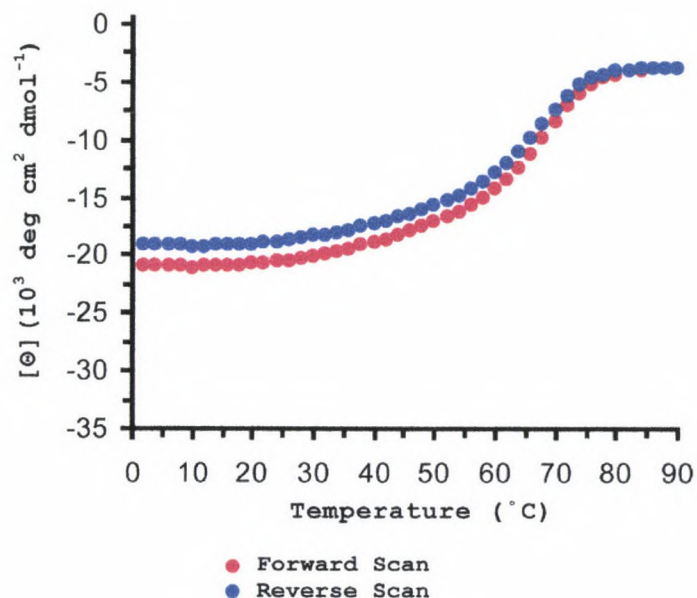


Figure 8. Thermal forward and reverse scan of the HRSV trimer. Upon cooling after thermal unfolding, the trimer reforms, indicating a self-assembling system.

Upon addition of the F₁C peptide, there was also an increase in helicity as the ligand peptide becomes helical upon binding. A temperature scan of the HRSV peptides also showed an increase in stability as the temperature at which the system cooperatively unfolded increased with the addition of the ligand peptide (Figure 9). In both cases, if the ligand were not interacting with the trimer, we would see a signal that overlaid the weighted average of the trimer and ligand signals. Instead we saw an increase in both helicity and stability, pointing to a stable, self-assembling system capable of binding the HRSV ligand.

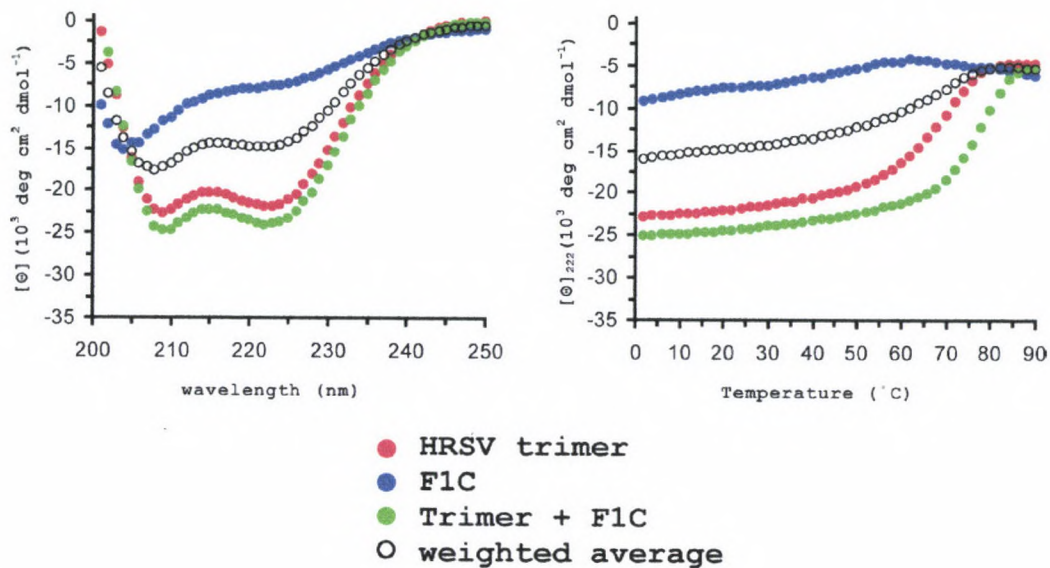


Figure 9. CD results for wavelength and thermal scans of the HRSV trimer and trimer plus ligand. Upon addition of the ligand, the system becomes more helical as shown by a more decreased signal. In addition the T_m increases from 71°C to 79°C

The apparent molecular weights could also be determined via analytical ultracentrifugation (AUC) as another means of verifying the viability of this system. Analysis of the AUC data gave an apparent molecular weight of 16.1 kilodaltons (kDa) for the trimer, which was 5.4% lower than the expected weight of 17.0 kDa. The apparent molecular weight of the trimer plus the ligand was 19.5 kDa, which was 7.3% lower than expected at 21.0 kDa. These data also point to a self-assembling system that binds our ligand.

2-3: Control Studies

To ensure that our trimer was binding our ligand in the way we assume, a series of control experiments was conducted. Half of the binding pocket was removed from the trimer by persubstituting lysines into the binding pocket of T_{16} , renaming it $T_{16}K$ (Figure 10).

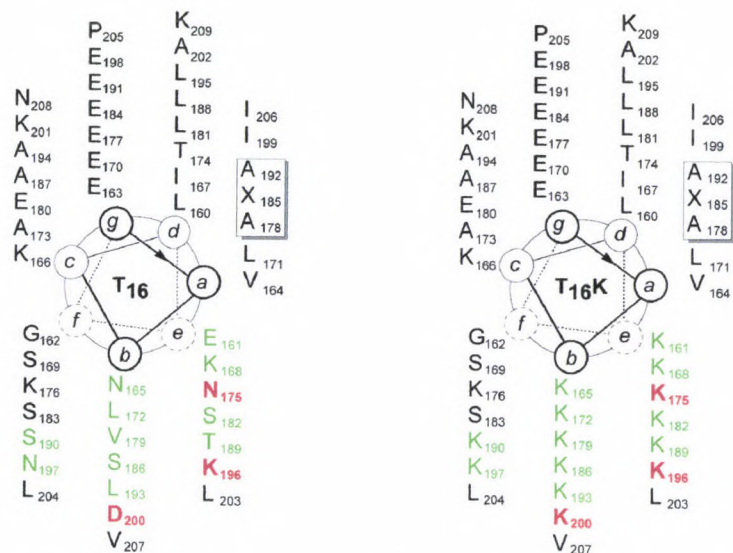


Figure 10. Helical wheel diagrams of the original T16HRSVfullQ/A, on the left, and redesigned control peptide T16K, on the right.

As only the binding pocket of the T₁₆K peptide was changed, a stable trimer should still form upon addition of the T₉ and T₂₃ peptides. A Ni-NTA affinity experiment of an equimolar mixture of the three peptides showed that to be the case (Figure 11). We could now see whether the new trimer would bind F₁C, without a complete binding pocket.

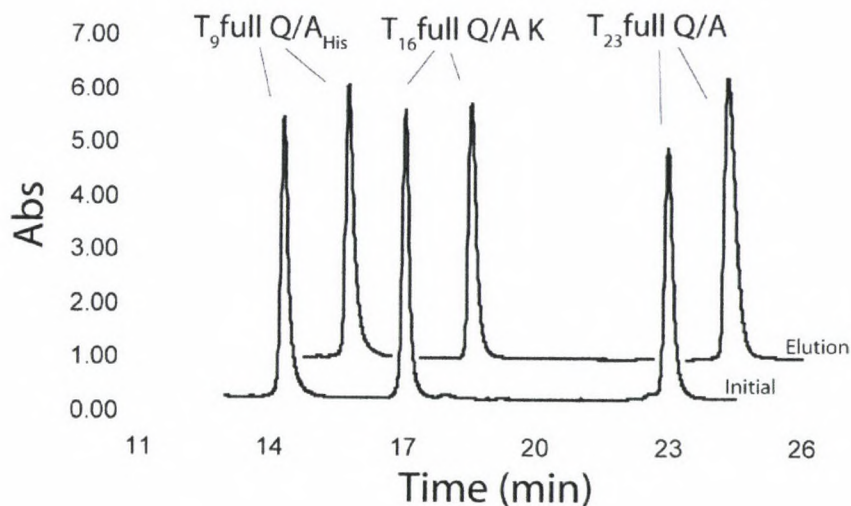


Figure 11. A Ni-NTA affinity experiment of the HRSV control trimer. Intact ratios from the initial to the elution fraction indicate stable trimer formation.

A similar experiment was done with the trimer peptides with F₁C in a 1:1:1:1 ratio. One can see two results in the data. First, the ligand peptide did not bind, as very little remained in the elution fraction. Additionally, trimer affinities were disrupted with the addition of the ligand, which point to quite an unstable system when the ligand is present (Figure 12). Since the only change was to the binding pocket of the trimer, we can conclude that the F₁C peptide was binding to the original trimer as expected. In addition to the Ni-NTA data, the CD signal of the trimer plus the ligand nearly matched that of the weighted average, which indicated that the ligand was not interacting with the trimer (Figure 13).

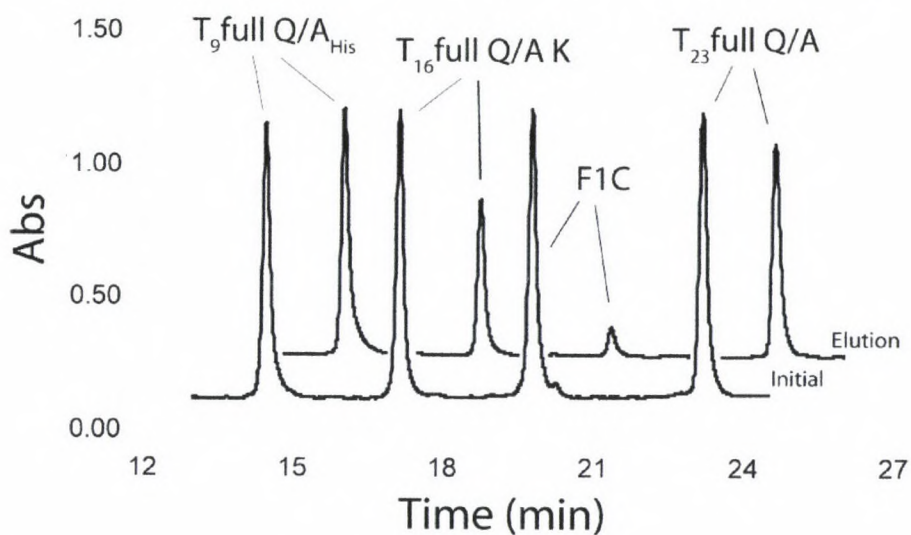


Figure 12. Ni-NTA affinity experiment of the HRSV control trimer plus the ligand. Not only does the ligand not bind, trimer affinities are also disrupted.

Apparent molecular weights also point to a successful control trimer. The apparent molecular weight of the control trimer was found to be 16.6 kDa, only 4.0% lower than the expected 17.3 kDa. The addition of the ligand showed a molecular weight of 14.0 kDa, 34.2% lower than expected at 21.3 kDa. Notice that

this is also lower than the control trimer weight alone, which confirms the His-tag data showing that the trimer is disrupted upon addition of the ligand, as well.

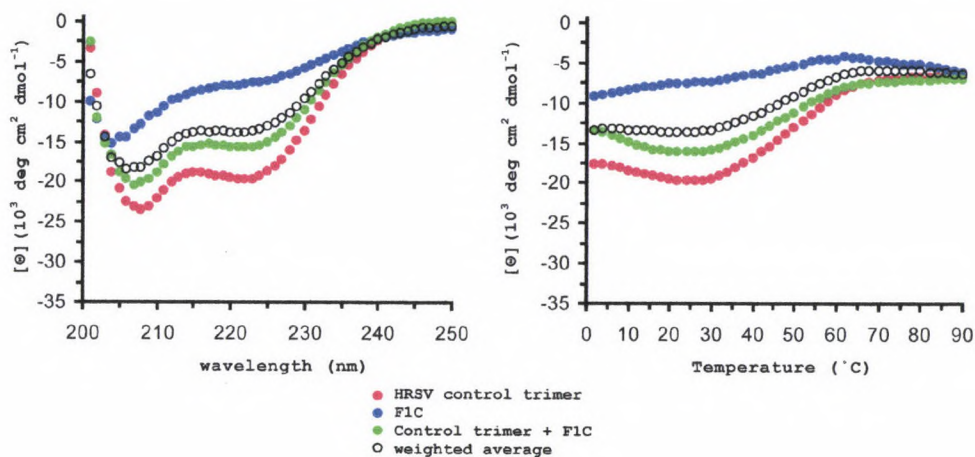


Figure 13. CD data from wavelength and thermal scans of the HRSV control trimer and the trimer plus ligand. Both helicity and stability decrease upon addition of F₁C, giving data that nearly overlays the weighted average.

All these data point to the fact that we now had a stable, well-behaved mimic of the HRSV system that self-assembled in solution and bound the F₁C ligand. My work continued to probe these interactions through a series of mutant studies to determine whether or not we could refine our understanding of the key contact points between trimer and ligand.

2-4: Experimental

Ni-NTA Affinity Experiments. All solutions were mixed in phosphate-buffered saline (PBS, 10 mM phosphate, 150 mM NaCl) to an approximate concentration of 10 μ M, using the acetamidobenzoate tag as a spectroscopic label. These concentrations assured that most of the system was in trimeric form as the k_d values are in the picomolar range. A 0.5 mL portion of 50% slurry of Ni-NTA

agarose in ethanol (Qiagen) in an Eppendorf tube was centrifuged down and the supernatant removed. A 1 mL portion of the peptide solution was added to the Eppendorf and agitated for 5 min. Upon centrifugation, the supernatant was removed as the Flow-Through Fraction. A 1 mL portion of PBS buffer was then added to the tube and agitated for 30 sec. Once centrifuged, the supernatant was removed as the Wash Fraction. Finally, 1 mL of a PBS buffer charged with 250 mM imidazole was added and agitated for 5 min. After centrifugation, the supernatant was removed as the Elution Fraction. All fractions were analyzed via HPLC on a C-4 or C-18 analytical reverse phase column (Figure 14).

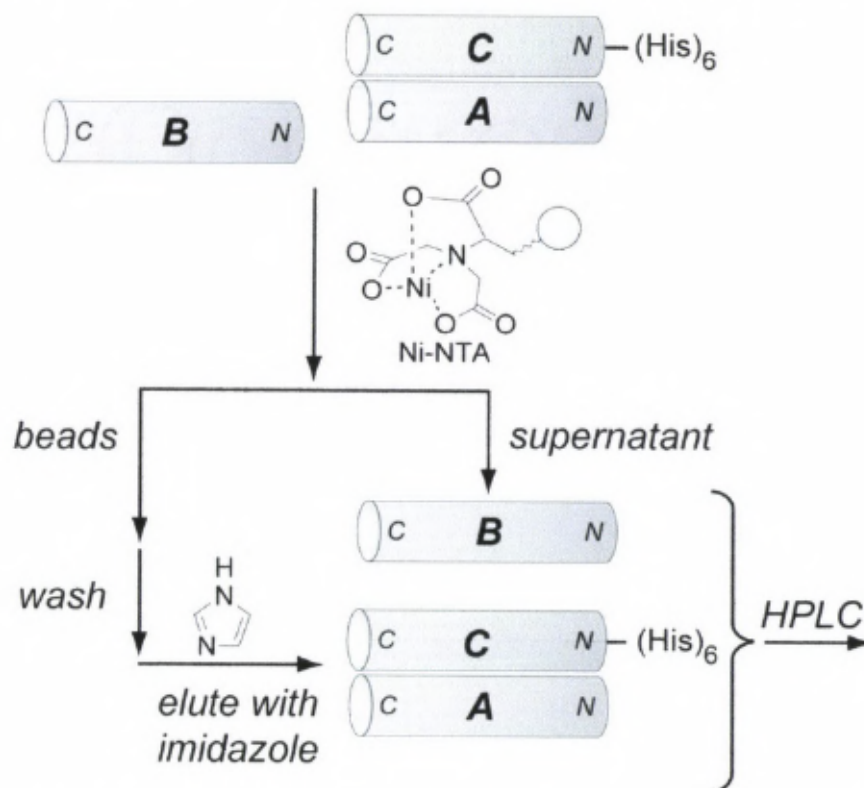


Figure 14. Schematic representation of a Ni-NTA affinity experiment. A solution of peptides, one of which has a six histidine “tag,” is introduced to the Ni-NTA beads. The his-tagged peptide and any other peptide bound to it bind to the beads through the interaction between the histidine side chains and the nickel. Any peptides not bound to the beads are washed off and collected in the supernatant. An elution step with imidazole elutes off all bound peptides, and all fractions are analyzed via reverse phase HPLC.

Circular Dichroism Experiments. All solutions were mixed in PBS buffer to a 10 μ M concentration, using the acetamidobenzoate tag as a spectroscopic label. All measurements were taken on an Aviv model 202 Circular Dichroism Spectrometer. Wavelength data were taken at 25°C and are the average of three scans from 200 to 250 nm in 1 nm steps. Thermal scans were taken at 222 nm and ranged from 0° to 90°C with a 2°/minute rate of increase and one minute equilibration and data collection times. T_m values were calculated from the minima of the first derivative of θ vs. $1/T$ plots.¹⁰ Raw data (in mdeg) was converted to mean residue ellipticity (MRE) using the following:

$$MRE = \frac{m \text{ deg}}{\# \text{ residues} * \text{conc.} * l * 10}$$

Analytical Ultracentrifugation Experiments. All experiments were performed using a Beckman XL-I analytical ultracentrifuge equipped with an An60-Ti rotor. Data was collected at 270 nm using 12 mm path length six-sector centerpieces. The concentrations of the solutions spanned 15 to 52 mM and were dialyzed against the reference buffer at 4°C overnight. Data was collected for each concentration at both 38,000 and 48,000 rpm. Samples were equilibrated at 38,000 rpm for 16 hours, and data were collected in two scans 4 hours apart. The speed increased, and the samples were allowed to equilibrate at 48,000 rpm for another 16 hours before two more scans were taken 4 hours apart. Each scan consisted of 10 replicates and 0.002 cm radial steps. Solvent densities and partial molar volumes were calculated according to that prescribed by Laue.¹¹ Data was analyzed via Ultrascan to fit an ideal one-component model.

2-5: References Cited

- (1) (a) Zhao, X., Singh, M., Malashkevich, V. N. and Kim, P. S. *Proc. Nat. Acad. of Sci.* **2000**, 97(26), 14172-14177. (b) Baker, K. A., Dutch, R. E., Lamb, R. A. and Jardetzky, T. S. *Molecular Cell* **1999**, 3, 309-319.
- (2) Melero, J. A. *Perspectives in Medicinal Virology* **2007**, 14, 1-42.
- (3) (a) Lawless-Delmedico, M. K., Sista, P., Sen, R., Moore, N. C., Antczak, J. B., White, J. M., Greene, R. J., Leanza, K. C., Matthews, T. J. and Lambert, D. M. *Biochemistry* **2000**, 39, 11684-95. (b) Yunus, A. S., Jackson, T. P., Crisafi, K., Burimski, I., Kilgore, N. R., Zoumplis, D., Allaway, G. P., Wild, C. T. and Salzwedel, K. *Virology* **2010**, 396, 226-237. (c) Russell, C. J. and Luque L. E. *Trends in Microbiology* **2006**, 14(6), 243-246.
- (4) Lambert, D. M., Barney, S., Lambert, A. L., Guthrie, K., Medinas, R., Davis, D. E., Bucy, T., Erickson, J., Merutka, G. and Petteway, S. R., Jr. *Proc. Nat. Acad. of Sci.* **1996**, 93, 2186-2191.
- (5) (a) Wang, E., Sun, X., Qian, Y., Zhao, L., Tien, P. and Gao, G. F. *Biochemical and Biophysical Research Communications* **2003**, 302, 469-475. (b) Shepherd, N. E., Hoang, H. N., Desai, V. S., Letouze, E., Young, P. R. and Fairlie, D. P. *J. Am. Chem. Soc.* **2006**, 128, 13284-13289.
- (6) (a) Douglas, J. L., Panis, M. L., Ho, E., Lin, K., Krawczyk, S. H., Grant, D. M., Cai, R., Swaminathan, S. and Cihlar, T. *Journal of Virology* **2003**, 77(9), 5054-5064. (b) Cianci, C., Langley, D. R., Dischino, D. D., Sun, Y., Yu, K-L., Stanley, A., Roach, J., Li, Z., Dalterio, R., Colonno, R., Meanwell, N. A. and Krystal, M. *Proc. Nat. Acad. of Sci.* **2004**, 101(42), 15046-51.

- (7) Zhao, X., Singh, M., Malashkevich, V. N. and Kim, P. S. *Proc. Nat. Acad. of Sci.* **2000**, 97(26), 14172-14177.
- (8) Zhao, X., Singh, M., Malashkevich, V. N. and Kim, P. S. *Proc. Nat. Acad. of Sci.* **2000**, 97(26), 14172-14177.
- (9) Schnolzer, M., Alewood, P., Jones, A., Alewood, D. and Kent, S. B. H. *International Journal of Peptide Protein Research* **1992**, 40, 180-193.
- (10) Cantor, C. R. and Schimmel, P. R. *Biophysical Chemistry of Macromolecules, Part III: The Behavior of Biological Macromolecules*; W. H. Freeman: New York, NY, 1980, p.1132.
- (11) Laue, T. M., Shah, B. D., Ridgeway, T. M. and Pelletier, S. L. in *Analytical Ultracentrifugation in Biochemistry and Polymer Science*, Harding, S. E., Rowe, A. J., and Horton, J. C., Eds., The Royal Society of Chemistry: Cambridge, 1992, pp. 90-125.

Chapter 3

Mutant Studies of the HRSV System

3-1: Introduction to the Mutants

Once a stable, well-behaved mimic for the HRSV fusion peptides was constructed and validated, we desired to better understand the binding interaction of the ligand to the trimer. Kim and co-workers had previously identified three residues that appeared to be essential for F₁C to bind to the trimer.¹ Two phenylalanines in position 483 and 488 in the sequence inserted into a hydrophobic groove formed by the trimer, while serine in position 509 was involved in a complex hydrogen bonding arrangement with Thr174, Ala170 and Asn175 (Figure 1).

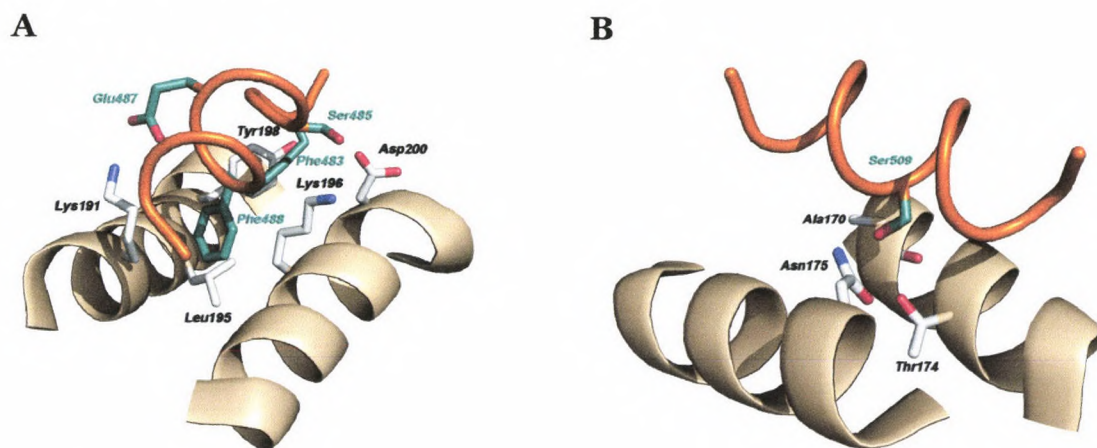


Figure 1. Close up of the key binding sites for HRSV. F₁C backbone is shown in orange, trimer in tan. A) F483 and F488 are labeled in green and important residues for the formation of the hydrophobic pocket are in white. B) S509 shown in green and the amino acids that are a part of the hydrogen bonding network in white.

This knowledge of key residues led us to consider a mutant series of ligands that would show the relative importance of each contact point to binding. Accordingly, a series of F₁C peptides were designed and synthesized mutating out F483, F488 and S509 in turn, replacing it with an alanine (Figure 2). Each new

mutant ligand was then analyzed in combination with the trimer to assess binding affinity via previously described Ni-NTA, CD and AUC experiments.

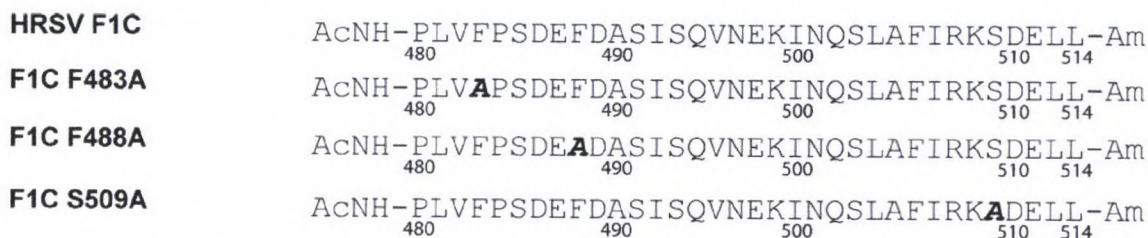


Figure 2. Sequences of the three single mutant peptides and the parent F₁C peptide for comparison. The substituted alanine has been highlighted in each sequence.

3-2: The Mutant Studies

The main experiments run on the F₁C mutant cycle were those previously mentioned: Ni-NTA affinity experiments, CD and AUC. Each gave a partial picture of the binding affinity of each ligand to the parent trimer. To understand the relative importance of each of the key residues to binding, the data must be taken cumulatively.

The Ni-NTA experiments gave a qualitative picture of binding. In each case, the trimer remained intact through the experiment while the amount of ligand varied. In truth, the F₁C F483A ligand remained bound almost as well as the parent F₁C sequence. Both the F₁C F488A and F₁C S509A ligands lost material through the assay as a result of impaired binding ability. The volume of material in both cases lessened by about 25% from the initial volumes to those in the elution fractions (Figure 3).

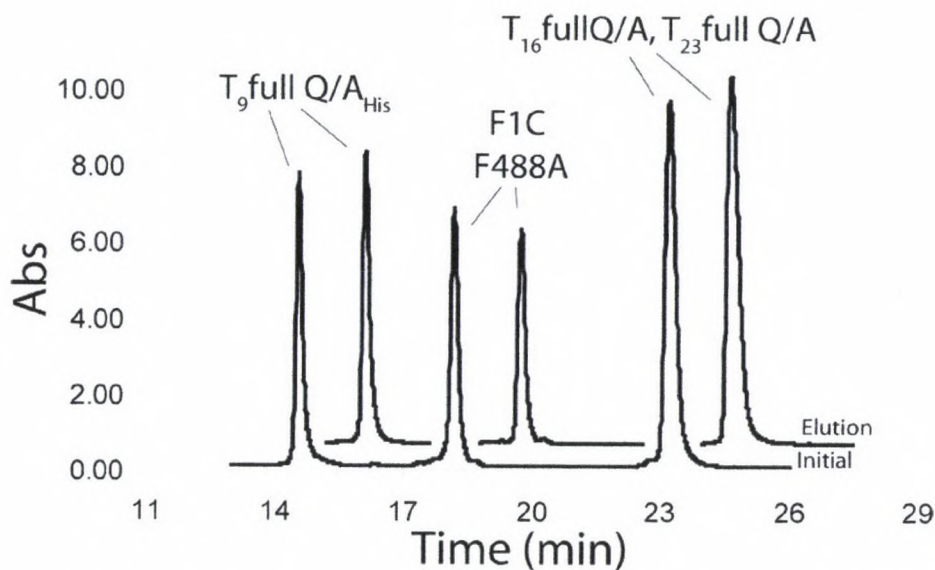


Figure 3. Ni-NTA affinity experiment of the HRSV trimer plus F₁C F488A mutant. Even though the trimer remains intact, the single mutation of the F488A peptide causes impaired binding, as seen in the smaller ligand peak in the elution fraction. The S509A experiment is similar.

Information from CD experiments gave an incomplete picture. The parent trimer had been shown to have a $T_m = 71^\circ\text{C}$, which increased to 79°C upon addition of the parent F₁C peptide. Such a ΔT was an indication that the F₁C ligand bound to the trimer and increased the overall thermal stability of the system. Each mutant gave a smaller ΔT than the parent ligand, which also indicated weaker binding. The F₁C F488A ligand increased the T_m to 73°C , while both F₁C F483A and S509A ligands increased the T_m to 77°C . The loss of any of the three key residues is obviously important for a thermally stable system, though the F488A mutation was shown here to have the greatest effect (Figure 4).

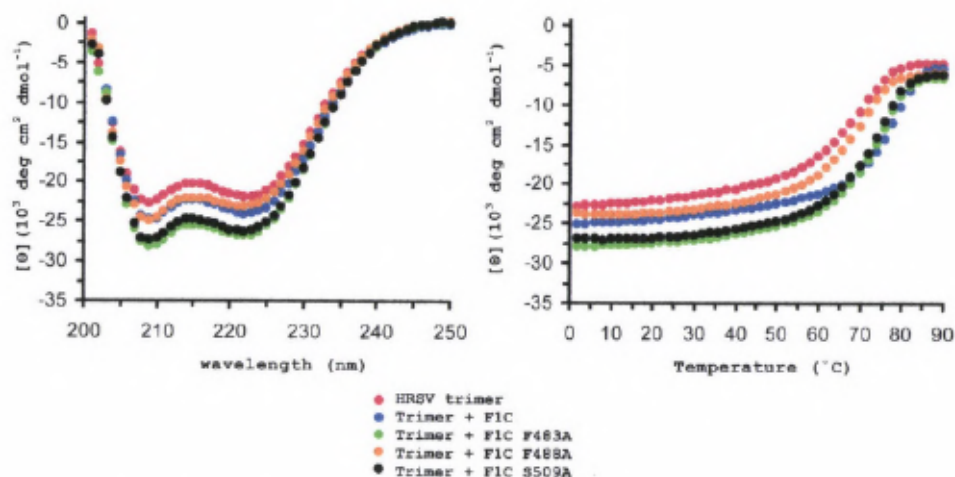


Figure 4. CD data from wavelength and thermal scans of the HRSV trimer and the trimer plus each of the mutant cycle of F₁C peptides. Most notable is the decreased T_m upon addition of the F483A mutant ligand.

Determination of apparent molecular weights via AUC also gave a picture of the key amino acids to binding (Table 1). All three mutants gave a lower molecular weight than calculated, though to different degrees. The F₁C F483A mutant had the smallest effect, giving an apparent weight 10.4% below that expected. The loss of F488 further disrupted binding, decreasing the apparent weight to 11.8% below expected. It was the S509 mutant that had the most drastic effect as the apparent weight was not only below that calculated for the 4-component system but was also 5.8% below that calculated for the 3-component system.

System	MW _{obsd}	MW _{calc}	% diff.
HRSV trimer	16.1	17.0	-5.4
+ F1C	19.5	21.0	-7.3
+ F1C F483A	18.8	20.9	-10.4
+ F1C F488A	18.5	20.9	-11.8
+ F1C S509A	16.0	21.0	-23.7

Table 1. AUC data for the HRSV trimer plus mutant cycle of ligands. Data is given in kDa.

Taken cumulatively, the data presented above give a somewhat clearer picture of the relative importance of the three amino acids identified by Kim and co-workers. There is relatively no loss of the F₁C F483A mutant via Ni-NTA affinity experiments, and its loss causes only minor changes in both the thermal stability (Trimer + F₁C T_m = 79°C vs. Trimer + F483A T_m = 77°C) and apparent molecular weight of the system (Trimer + F₁C ΔMW = 7.3% vs. Trimer + F483A ΔMW = 10.4%). The other two residues appear to be much more important for ligand binding when the data are taken cumulatively. Both F₁C F488A and S509A mutants suffer a similar loss of material via the Ni-NTA experiments. The thermal stability of the system shown by CD shows only a small increase in T_m upon addition of F₁C F488A (71°C to 73°C). The calculation of apparent molecular weight is drastically affected by the loss of S509, giving a weight below that expected if the mutant ligand were not even present.

As a result, one can see that although the loss of any one residue affects the ability of the ligand to bind to the trimer, all three do not have the same relative importance. The phenylalanine in position 483 is the least important for binding as the 4-component system forms reasonably well despite its absence. However, the data above show that F488 and S509 are clearly essential for a stable, well-behaved mimic. One possible explanation for the fact that F483 is less important than the other two residues can be traced to the fact that the amino acid is on the N-terminus of the F₁C peptide, which does not have definite secondary structure (Figure 5). The part of the F₁C peptide that is helical incorporates both S509 and F488, which would indicate specific placement of both of these residues for binding. Since F483 is located in the sequence directly after proline, which

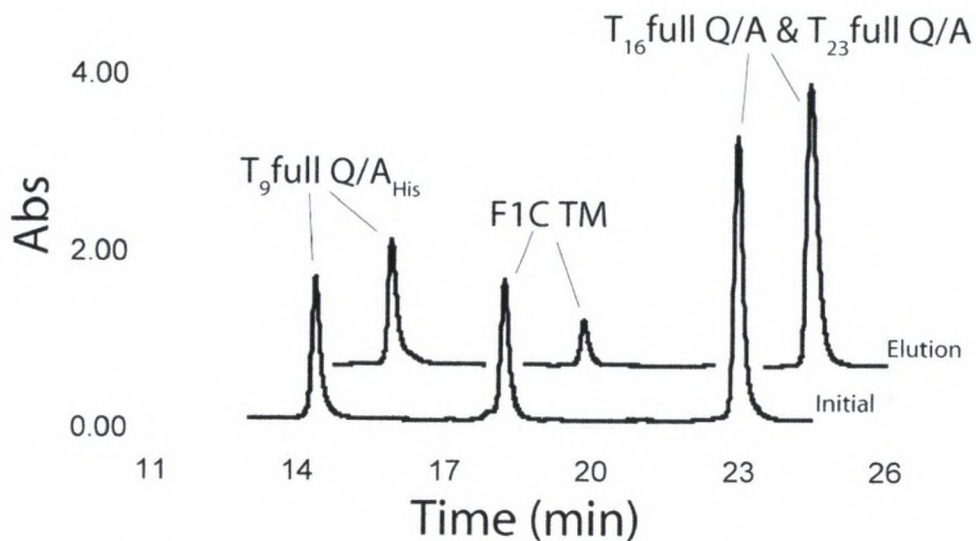


Figure 7. Ni-NTA affinity experiment with the HRSV trimer plus the F₁C TM ligand. It is clearly seen that little of the ligand remains bound, though the trimer remains intact throughout.

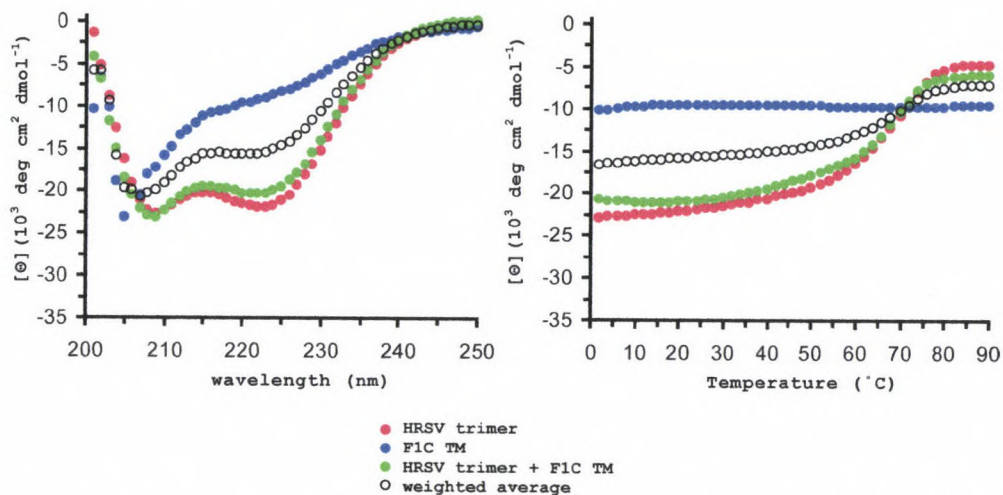


Figure 8. CD data from wavelength and thermal scans of the HRSV trimer and the trimer plus F₁C TM. The system becomes no more helical or thermally stable as a result of the addition. The T_m remains unchanged at 71°C.

An additional CD experiment was run to determine thermodynamic values for the binding of the parent ligand and F₁C TM. Guanidine hydrochloride denaturation experiments were run on the trimer alone and the trimer in solution with F₁C and F₁C TM to give ΔG_{H_2O} values for the systems, which tell us the

energy of unfolding. As the experiment progresses the amount of guanidine, a protein denaturant, increases while the amount of peptide in solution remains the same. Total helicity of the system is monitored as it goes from fully folded to fully unfolded. The curve that results is fit to an equation that gives thermodynamic information. The trimer alone has a $\Delta G_{H_2O} = 23.8 \pm 0.2$ kcal/mol, which increases to 25.0 ± 0.1 kcal/mol upon addition of the F₁C ligand. The F₁C TM gives an intermediate value of 24.3 ± 0.1 kcal/mol, which is in agreement with the Ni-NTA affinity experiments, which show slight binding. Data curves are shown in Appendix 2.

These mutant studies definitively show the essential nature of these three key residues for binding, as their cumulative absence destroys the ability of the F₁C ligand to bind to the trimer. In addition, the mutant cycle highlights differences among the three amino acids and gives a means of determining relative importance.

This information as well as the stable, heterotrimeric coiled-coil mimic could potentially be useful in the rational design of therapeutics against HRSV infection. As the relevant residues that form the HRSV binding pocket have been grafted onto our sterically-matched, self-assembling heterotrimeric system, the HRSV coiled-coil described above could be used to test the binding affinities or mechanisms of small molecule drugs. Additionally, work on the development of small molecule inhibitors should be able to disregard the F483 residue as a key contact point and focus attention elsewhere.

3-4: Experimental

Ni-NTA Affinity Experiments: as described in 2-4.

Circular Dichroism Experiments: as described in 2-4.

Analytical Ultracentrifugation Experiments: as described in 2-4.

Guanidine Denaturation Experiments. All measurements were taken on an Aviv Model 202 Circular Dichroism Spectrometer fitted with a Microlab 500 series titrator. A peptide solution in PBS was titrated with a second solution identical to the first except that it contained 6M guanidine hydrochloride (GdnHCl). Helicity was monitored at 222nm, and the raw data were converted to MRE values using the model below.

Observed MRE values (θ_{obs}) were fitted with the assumption that the folded and unfolded baselines are linear functions of denaturant concentrations (Equation 1),

$$\theta_{obs} = f_u(\theta_u + a[GdnHCl]) + (1 - f_u)(\theta_f + b[GdnHCl]) \quad (1)$$

where f_u = fraction of peptide unfolded, θ_u and θ_f are the MRE values of the unfolded and folded peptides, respectively, and a and b are parameters

describing the guanidine dependence of the observed unfolded and folded baselines. The fraction unfolded (f_u) is calculated using equation (2), assuming that the equilibrium constant for the monomer-trimer equilibrium is K_{unf} .

$$f_u = \sqrt[3]{k \left(\frac{1}{2} + \frac{\sqrt{3}\sqrt{4k+27}}{18} \right)} - \frac{1}{3} \frac{k}{\sqrt[3]{\frac{1}{2} + \frac{\sqrt{3}\sqrt{4k+27}}{18}}} \quad (2)$$

where,

$$k = \frac{K_{unf}}{27C_{tot}^2} \quad (3)$$

$$K_{unf} = e^{-\Delta G_{H_2O}/RT} \quad (4)$$

and $C_{tot} = [\text{trimer}] = 1/3[\text{total peptide}]$.² The equilibrium constant is then calculated from the observed unfolding energy, assuming a linear extrapolation model in which the true unfolding energy (ΔG_{H_2O}) is a linear function of the observed value and the denaturant concentration³ (Equation 5).

$$\Delta G_{H_2O} = \Delta G_{obs} + m[GdnHCl] \quad (5)$$

The observed data were fit using this model and a non-linear least squares fit approach, using a Microsoft Excel macro⁴ and ΔG_{H_2O} , θ_u , θ_f , a , b and m as parameters. Estimates of error were calculated using another macro by de Levie.⁵

3-5: References Cited

- (1) Zhao, X., Singh, M., Malashkevich, V. N. and Kim, P. S. *Proc. Nat. Acad. of Sci.* **2000**, 97(26), 14172-14177.
- (2) Jelesarov, I. and Lu, M. *Journal of Molecular Biology* **2001**, 307, 637-656.
- (3) Santoro, M. M. and Bolen, D. W. *Biochemistry* **1988**, 27, 8063-8068.
- (4) Harris, D. C. *Journal of Chemical Education* **1998**, 75(1), 119-121.
- (5) de Levie, R. *Journal of Chemical Education* **1999**, 76(11), 1594-1598.

Chapter 4

Continued Work on the Human T-cell Leukemia Virus

4-1: Introduction

As the name implies, the Human T-cell Leukemia Virus has been detected in patients with T-cell type leukemia.¹ Although the number of people who carry the virus is much larger than those who will contract the disease, it remains a target for active study.² As a member of the same family of retroviruses as HIV-1, HTLV utilizes a similar mode of infection, and crystal structures reveal the fusion proteins to associate in the familiar trimer-of-hairpins motif³ (Figure 1). As a result, it was a prime target for our tunable, self-assembling heterotrimeric coiled coils.

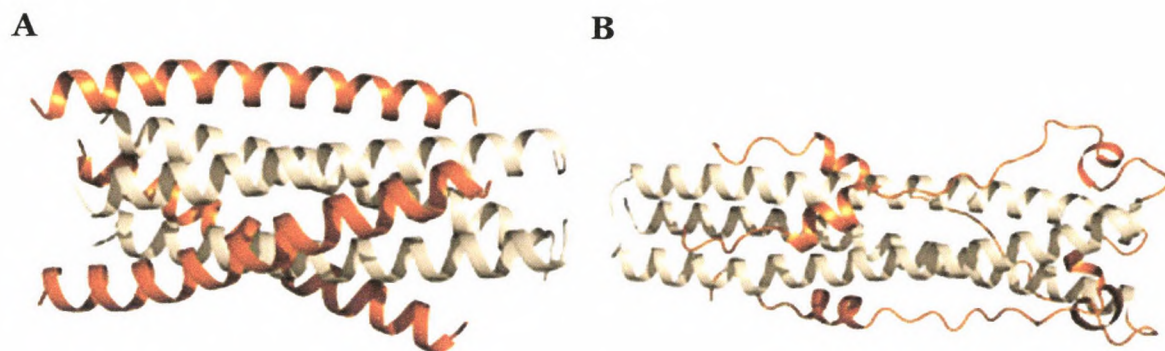
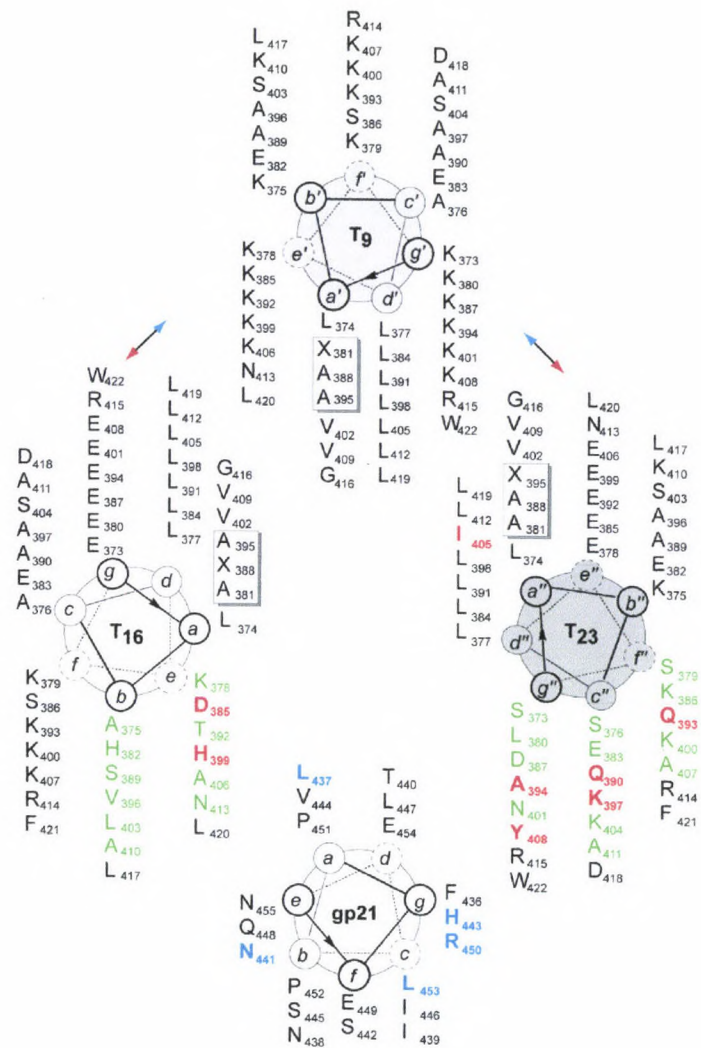


Figure 1. Comparison of the HIV trimer-of-hairpins (A) and the HTLV (B). Trimer peptides are shown in tan, while ligand peptides are in orange. Though the trimeric coiled coils are quite helical, notice the unstructured nature of the HTLV ligand.

Work on the HTLV system was begun by a previous Kennan group member, Brent Mann. He worked to successfully apply the TTT steric matching technique to the HTLV trimeric coiled-coil in order to synthesize a self-assembling system that could be used to further study how it binds to the ligand, named gp21. His synthesis incorporated trimmed sequences for the trimer to match a ligand that had also been trimmed for ease of synthesis. Despite the

successful synthesis of a self-assembling trimer, it was found that gp21 failed to bind.⁴ Additionally, gp21 proved difficult to purify.

Upon reevaluation of the trimer sequences, it was decided to reintroduce the 11 residue C-terminal sequence that had been trimmed from each peptide in the hopes that gp21 binding affinity would be restored. This addition lengthened the trimer peptides to 50-mers, which have since been shown to be viable synthetic targets, as seen in HRSV. In addition to the TTT substitutions and the matched electrostatic interfaces, we also persubstituted all unnecessary glutamines for alanines, a mutation that worked well for HRSV (Figure 2).



T_9 full Q/A AcNH-KL**K**AL**K**KK**X**EEL**K**SKAAAL**K**KKAAAL**K**KKV**S**SL**K**KKV**K**AL**N**RRGLD**L**L**L**FW-Am
 T_{16} full Q/A AcNH-EL**A**AL**K**KE**A**HELD**S**EX**S**AL**T**KE**A**VAL**H**KE**V**LS**L**AKE**V**AAL**N**RRGLD**L**L**L**FW-Am
 T_{23} full Q/A AcNH-S**L**KS**L**ES**L**AE**E**LE**K**DA**A**Q**L**E**Q**AX**A**KL**E**KN**V**SK**I**E**A**Y**V**K**L**N**R**RGLD**L**L**L**FW-Am
 HTLV gp21 AcNH-FL**N**I**T**NS**H**VS**I**L**Q**ER**P**PLE**N**-Am
 436 440 450 455

Figure 2. Helical wheel of the lengthened HTLV system. Coding and characteristics remain the same as all other wheels presented.

4-2: The HTLV Trimer and Control

Accessing the new 50-mer peptides was much easier with the protocol established during work on HRSV. Once these longer peptides were obtained, a Ni-NTA experiment was run to determine if we still were dealing with a self-

assembling system. Indeed, the trimer held up throughout the experiment with no indication that material was eluting off before the imidazole step (Figure 3). The trimer integrity was not harmed by the addition of the C-terminal residues.

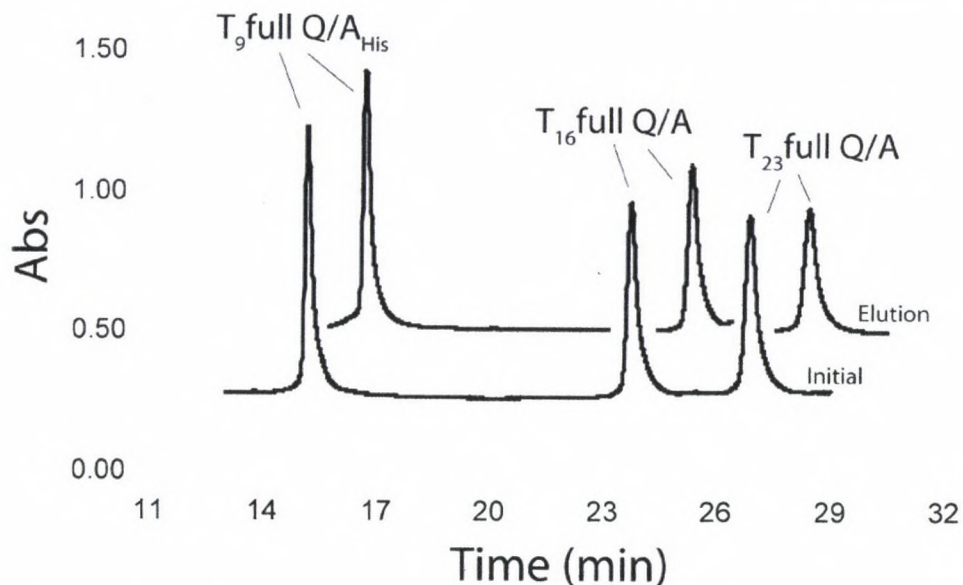


Figure 3. Ni-NTA affinity experiment of the HTLV trimer. Despite differences in peak shape, initial ratios remain intact through the experiment, indicating a stable system.

A control trimer was also constructed in the same manner as in HRSV, namely, half the binding pocket was removed by mutating out the key residues that form it. In the case of HTLV, the T₁₆ peptide was modified with lysine and alanine mutations in the binding pocket to maintain helicity and solubility. As the electrostatic interface and TTT substitutions remained untouched, trimer formation was still expected and was confirmed through a Ni-NTA experiment as well (Figure 4). We now had a stable, self-assembling heterotrimeric system and a control that could be used to test for gp21 binding. Unfortunately, synthesis of a pure, well-behaved gp21 ligand remained a difficulty.

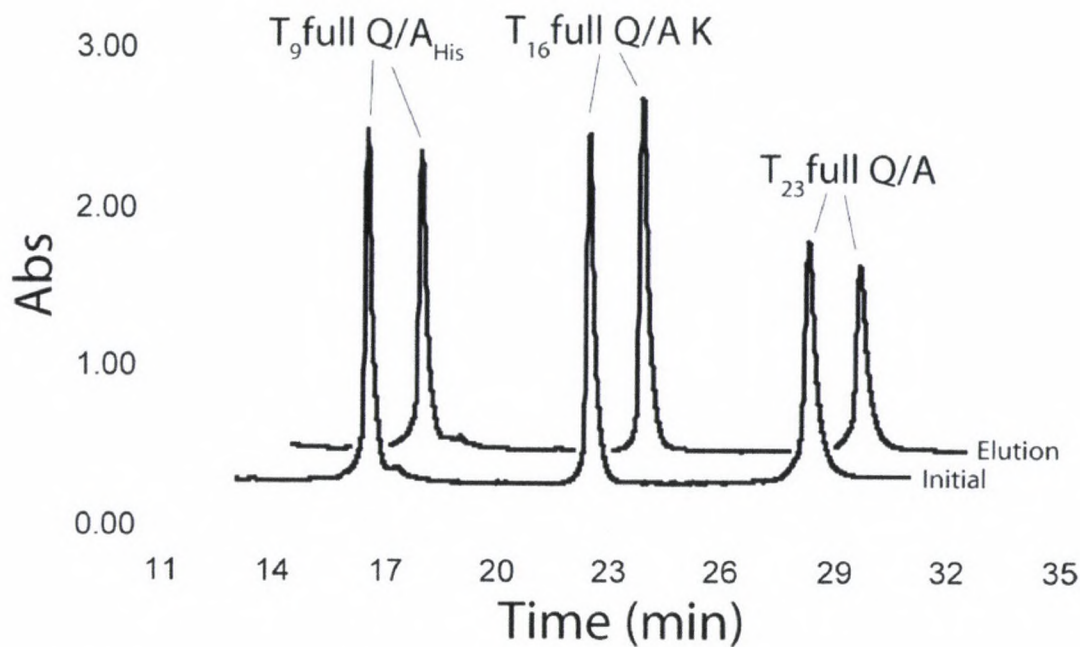


Figure 4. Ni-NTA affinity experiment of the HTLV control trimer. Ratios remain generally intact from the initial to the elution fraction.

4-3: Synthesis and Purification of the gp21 Ligand

In all previous attempts by Mann, in our labs, the synthesis of the gp21 ligand exhibited a persistent deletion product (-129 amu), which made purification difficult. This particular deletion carried over into all my initial attempts as well and corresponded to the loss of glutamic acid, lysine or glutamine. All of these possible amino acids were in the gp21 sequence. Lysine was quickly eliminated as the problem as it was the location of the spectroscopic label. After a series of test peptides, it was determined that the most C-terminal glutamic acid was the culprit. Additionally, the test peptides also showed that the initial asparagine at the C-terminus was also not coupling well during synthesis, and both offending amino acids were mutated out as they were not key contacts for binding. This new peptide was purifiable and renamed gp21 E&N, signifying

the two mutant residues. Unfortunately, the Ni-NTA experiment failed to show quantitative binding of the gp21 mutant as only ~70% of the material remained throughout the assay (Figure 5).

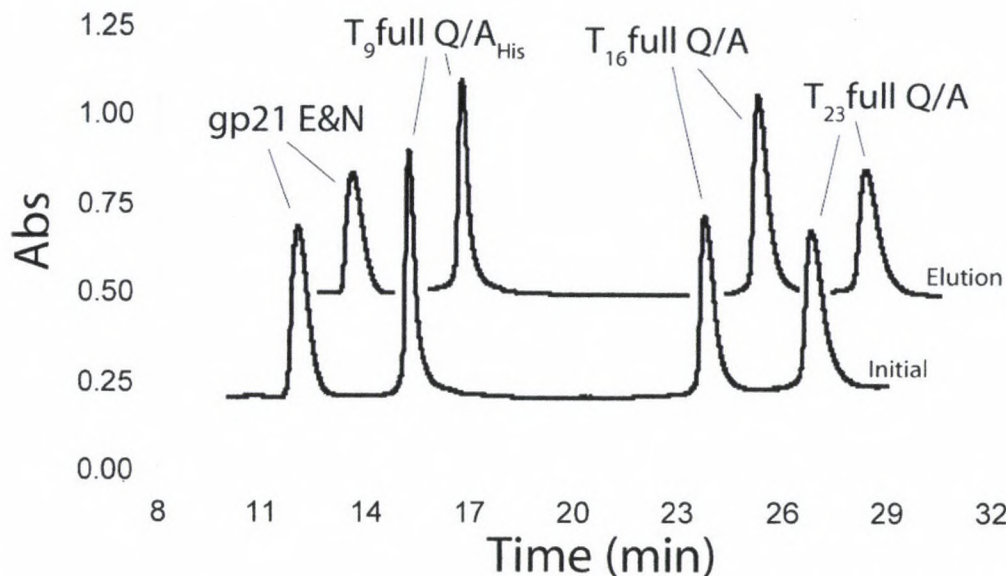


Figure 5. Ni-NTA affinity experiment for the HLTV trimer plus the trimmed gp21 ligand. Trimer behaves normally, while gp21 does not remain quantitatively bound.

The sequence for the gp21 ligand had originally been trimmed to excise the part of the sequence that includes three cysteine residues, two of which are involved in an internal disulfide bond. The trimer sequences were originally trimmed to accommodate a shorter gp21, so it might stand to reason that the longer trimeric sequences required the full-length gp21 for binding (Figure 6). To aid in synthesis, the full sequence was attempted, but all three cysteines were originally mutated out. This was to preclude any intermolecular disulfide bridges that might occur. The two previously beneficial mutations were kept, and the new peptide was referred to as gp21full C/S E&N, as all cysteines had been mutated to serines.

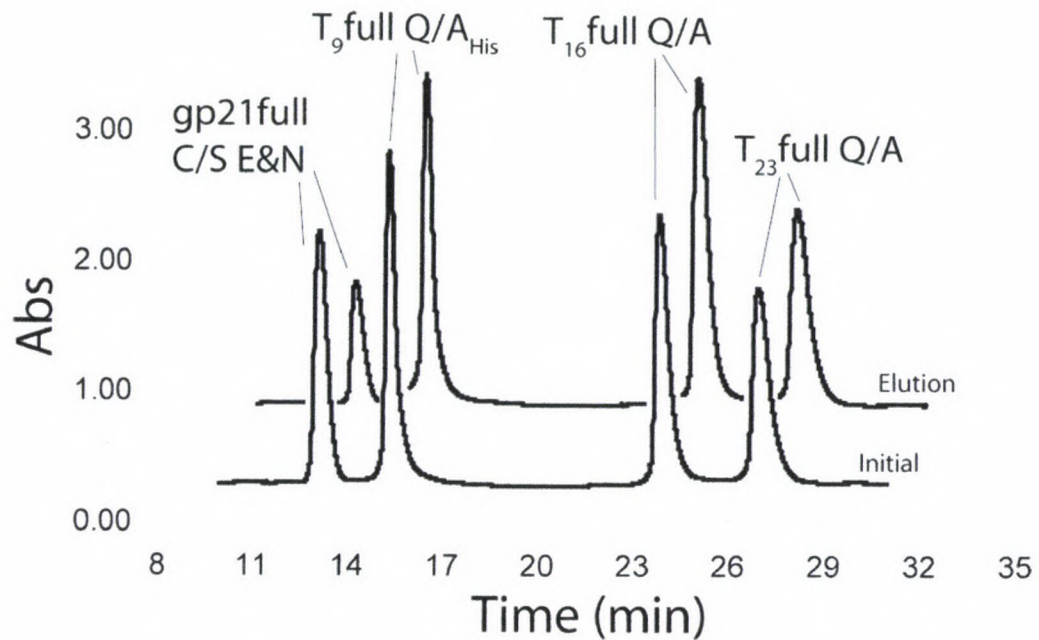


Figure 7. Ni-NTA affinity experiment of the HTLV trimer plus the gp21full C/S E&N ligand. Trimer maintains 1:1:1 ratio, and less ligand binds here than in the trimmed gp21 experiment. The longer length does not guarantee better binding.



Figure 8. Single dimer of the trimer-of-hairpins structure. Original trimmed gp21 shown in blue, and the additional residues of the full gp21 are in green. The three cysteine side chains are depicted as green balls, and two are shown in the intramolecular disulfide bridge.

The original plan to remove the cysteine residues from the initial gp21 sequence quickly made sense as the new peptide, synthesized to incorporate an internal disulfide bridge, was quite difficult to purify. Repeated attempts to purify solely through HPLC proved futile as persistent impurity peaks showed in every analytical trace of purified material. A series of experiments were undertaken to manipulate the disulfide bridge to aid in purification. Reduction of the disulfide was attempted through exposure to triscarboxyethylphosphine (TCEP)⁵, which resulted in a consistent impurity peak in every HPLC trace (Figure 9). Oxidation was attempted by exposure to high pH and air, which resulted in a clearly defined shoulder in the material. Even combinations of the two above strategies only served to give material with both an impurity peak and a shoulder (Figure 10).

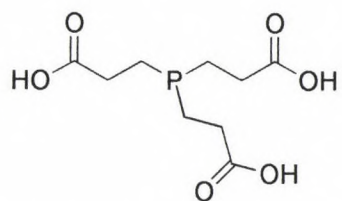


Figure 9. Triscarboxyethylphosphine (TCEP)

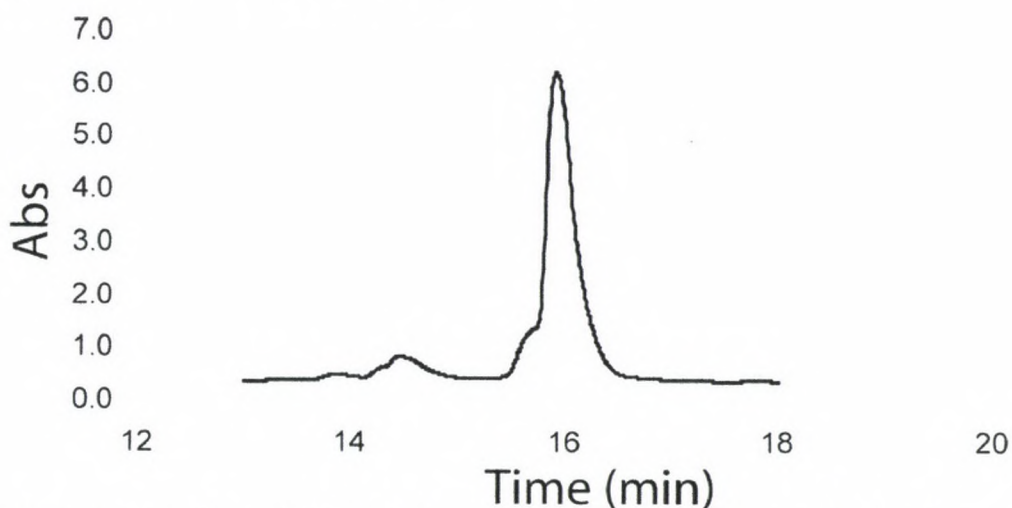


Figure 10. Analytical HPLC trace of gp21full CEN after oxidation for two hours, then reduction by TCEP overnight. Leading shoulder indicative of oxidation and the TCEP impurity is seen around 14.5 minutes.

In either reduction or oxidation, one should be able to see a change in the HPLC trace of the crude material as the disulfide is reduced or the free thiols oxidized. This change can take the form of a shifted product peak or a new peak appearing while the old peak disappears, depending on the placement of the disulfide bridge in the secondary structure. Several attempts were made to determine if we could see such a change in the oxidation of the crude material over time. The first experiment tracked the changes in the HPLC trace during oxidation over a 180 minute period. Aliquots were removed, quenched and analyzed at set intervals, though nothing more than a slight shift in the product peak was seen over the course of the experiment (Figure 11).

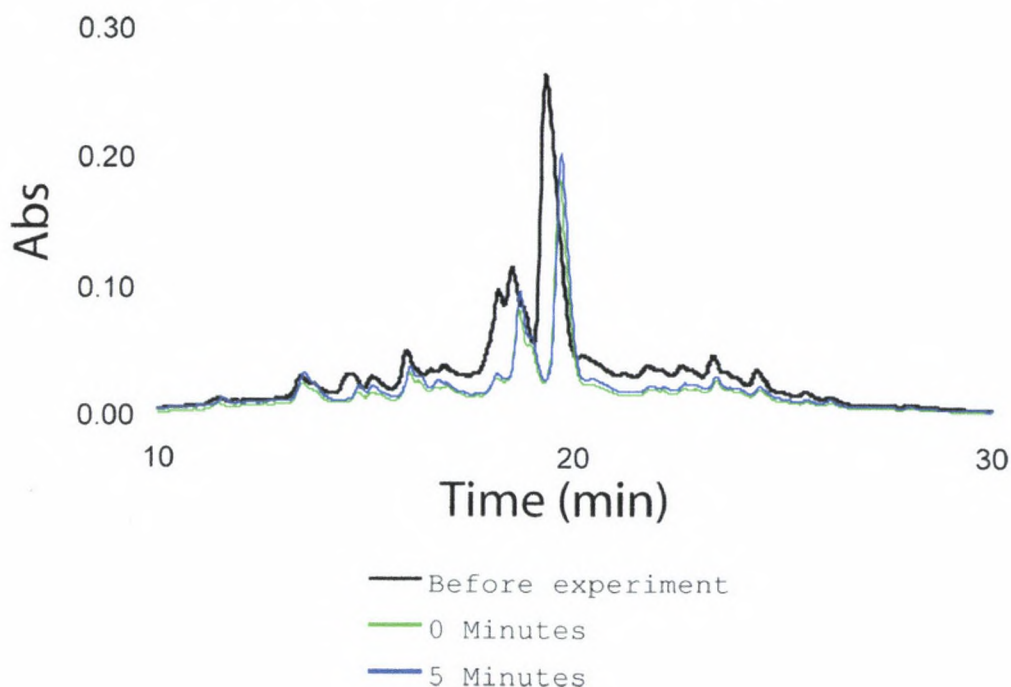


Figure 11. Comparison HPLC traces of crude material and oxidized material. Original trace is shown in black. Aliquots from time zero and after 5 minutes of oxidation are shown in green and blue, respectively. The other aliquots are left off for clarity as there was no additional change.

It was thought that an experiment over a longer period of time might show more of a change, so a 24-hour oxidation experiment was attempted. The shift in the position of the product peak was still observed, though the amount of material in that peak lessened greatly over 24 hours, while the material in the B wash dominated by the end of the experiment (Figure 12).

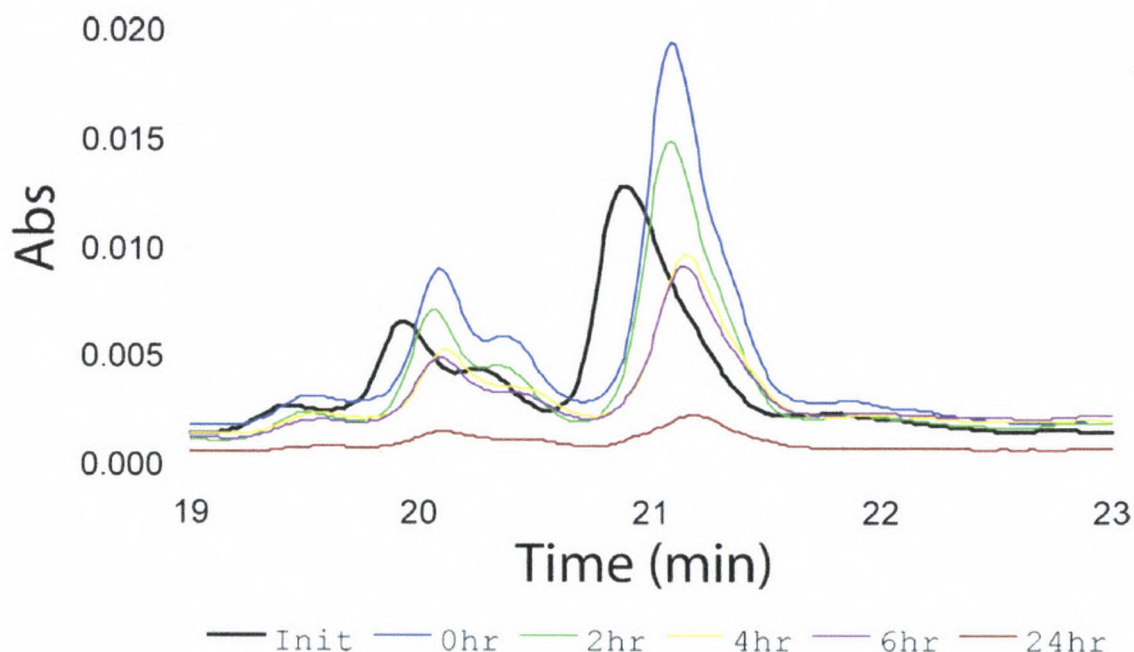


Figure 12. Close-up comparison HPLC traces of crude material and oxidized material. Original crude trace is shown in black. Each aliquot was removed, quenched and analyzed on the same gradient. A peak shift is immediate, though material in the product peak greatly lessens by the 24 hour mark.

4-4: Possibilities for Future Work

Though both the HTLV trimer and control have been synthesized and shown to be stable, it is the gp21 ligand that proved the most troubling. While working with the purification of the gp21full CEN ligand, it became clear that the original trimmed gp21 was not as soluble in PBS buffer as first believed. It was demonstrated through Ni-NTA experiment that the ligand was consistently

centrifuged down in each step with PBS buffer. The imidazole buffer served to solubilize the ligand much more effectively, which explains its appearance in the elution fraction. (Figure 13)

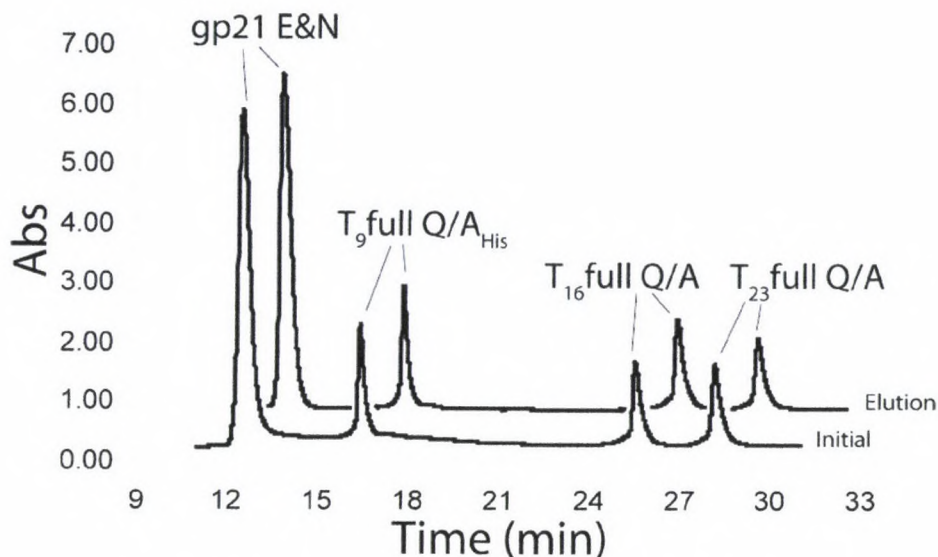


Figure 13. A Ni-NTA affinity experiment in which the ligand is at five times the concentration of the trimer. Rather than observing an 80% reduction in material to restore proper ratios, we see the same ratio of material appear in the elution as in the original experiment. (See Figure 5)

A redesign of the trimmed ligand to aid in solubility failed to aid in binding the ligand to the trimer. The latest sequence of the gp21full ligand had proved difficult to purify by either reduction or oxidation. It is possible that these solubilizing mutations from the trimmed ligand, if added to the full sequence, could make a peptide that is more amenable to attempts to purify it. Without the need to manipulate the disulfide prior to purification, it could be possible to form the proper disulfide conformation by using the trimer itself as a template in solution. We are a few steps closer to realizing a fusion protein mimic for HTLV.

4-5: Experimental

Ni-NTA Affinity Experiments: as described in 2-4.

Reduction of Peptides. A stock solution of TCEP was prepared in water to a concentration of 0.2M. Peptide stock solutions were also prepared in water. In an eppendorf tube, the TCEP and peptide stock solutions were mixed to give the TCEP ten times the concentration of the peptide. Target concentrations were 0.001M TCEP and 0.0001M peptide. The solution was allowed to stir overnight, then analyzed via reverse phase HPLC.

Oxidation of Peptides. Peptides were dissolved in PBS buffer pH = 8.4 in an eppendorf that had a hole bored in the lid. The solution was allowed to stir for various times. Each aliquot was quenched with TFA in water to pH = 7 before analysis by reverse phase HPLC.

4-6: References Cited

- (1) Poiesz, B. J., Ruscetti, F. W., Gazdar, A. F., Bunn, P. A., Minnan, J. D. and Gallo, R. C. *Proc. Nat. Acad. of Sci.* **1980**, 77(12), 7415-7419.
- (2) (a) Poiesz, B. J., Ruscetti, F. W., Gazdar, A. F., Bunn, P. A., Minnan, J. D. and Gallo, R. C. *Proc. Nat. Acad. of Sci.* **1980**, 77(12), 7415-7419. (b) Wang, J. J. G., Steel, S., Wisniewolski, R. and Wang, C. Y. *Proc. Nat. Acad. of Sci.* **1986**, 83, 6159-6163. (c) Li, M., Laco, G. S., Jaskolski, M., Rozycki,

- J., Alexandratos, J., Wlodawer, A. and Gustchina, A. *Proc. Nat. Acad. of Sci.* **2005**, *102*(51), 18332-7.
- (3) (a) Kobe, B., Center, R. J., Kemp, B. E. and Pountourios, P. *Proc. Nat. Acad. of Sci.* **1999**, *96*, 4319-4324. (b) Center, R. J., Kobe, B., Wilson, K. A., The, T., Howlett, G. J., Kemp, B. E. and Pountourios, P. *Protein Science* **1998**, *7*, 1612-1619.
- (4) Mann, Brent (2007). *Designed Coiled Coils as Viral Fusion Protein Mimics*. (MS Thesis). Colorado State University.
- (5) Burns, J. A., Butler, J. C., Moran, J. and Whitesides, G. M. *J. Org. Chem.* **1991**, *56*, 2648-50.

Chapter 5
Conclusions

5-1: Final Statements

Coiled-coils have been found to exist in a wide range of biological contexts performing a variety of functions.¹ Since the initial crystallization of the yeast transcription factor GCN4, the sequence for that dimeric coiled-coil has been the foundation of much research to understand the mechanisms of these self-assembling systems.² Our lab has successfully harnessed a steric matching technique, which has allowed for the synthesis of heterotrimeric systems that rely solely on the hydrophobic core for specificity.³ This technology has given us the opportunity to design, synthesize and study mimics of viral fusion proteins, which utilize the electrostatic interfaces of a coiled-coil.⁴

My research continued this work and extended the application of this steric matching technique to the synthesis of the HRSV fusion protein mimic. The three peptides of the coiled-coil, though longer than any other peptide previously synthesized in our lab, were accessed through an adapted synthetic protocol and shown to bind together to form a heterotrimeric coiled-coil. The full 4-component system, which included the ligand peptide, was synthesized and validated through various spectroscopic means as a well-behaved, stable mimic of the HRSV fusion protein.

The ligand of the HRSV system, the F₁C peptide, was demonstrated to bind to the trimeric coiled-coil through His-tag affinity experiments, circular dichroism (CD) and analytical ultracentrifugation (AUC). Control experiments to remove half of the binding pocket clearly showed that the F₁C peptide was binding where expected.

The key contact points for F₁C binding were probed through a mutant cycle of ligands. By removing each of the key contact points in turn and testing binding, the relative importance of these three residues became clear. Removal of the phenylalanine in position 483 did not have a great effect on the demonstrated binding of the parent F₁C ligand, indicating that it is not essential for binding. The other mutant ligands, which removed F488 and S509 in turn, both showed a much greater effect on binding through His tags, CD and AUC. These residues were shown to be essential for the binding of the F₁C peptide to the trimeric coiled-coil.

In addition to HRSV, my research included work on the HTLV system. A former group member had previously worked on this system, though was unsuccessful in demonstrating ligand binding to the trimer. The trimer sequences were lengthened to be on par with the length of the HRSV peptides. With the new synthetic protocol in place, access was gained to these longer peptides, and their association into heterotrimeric coiled-coils was demonstrated through spectroscopic means. A control trimer was also synthesized and validated for future use.

Unfortunately, synthesis of the ligand peptide, gp21, proved elusive. My work clearly showed that the trimmed sequence for gp21 does not bind effectively to the trimer. Additionally, simply lengthening the gp21 peptide without incorporating the cysteines that form an internal disulfide bridge is not sufficient to promote binding. Binding may be dependent on the correct formation of the internal disulfide bridge, accessed through correct oxidation of the thiols or possibly an unnatural linkage.

In both the HRSV and HTLV systems, the steric matching technique pioneered in our lab has proven effective in promoting heterotrimeric coiled-coil formation. These coiled-coils have then been used both to elucidate the finer details of ligand binding (HRSV) and to demonstrate constructs that are ineffective for binding to the trimer (HTLV).

5-2: References Cited

- (1) (a) Schneider, J. P., Lombardi, A. and DeGrado, W. F. *Folding and Design*, **1998**, 3(2), R29-R40. (b) Lombardi, A., Bryson, J. W. and DeGrado, W. F. *Biopolymer Peptide Science*, **1997**, 40, 495-504. (c) Woolfson, D. N. and Alber, T. *Protein Science*, **1995**, 4, 1596-1607. (d) Nautiyal, S. and Alber, T. *Protein Science*, **1999**, 8, 84-90. (e) Burkhard, P., Stetefeld, J. and Strelkov, S. V. *Trends in Chem. Biol.* **2001**, 11(2), 82-88.
- (2) (a) Eckert, D. M., Malashkevich, V. N. and Kim P. S. *J. Mol. Biol.*, **1998**, 284, 859-865. (b) Zhu, H., Celinski, S. A., Scholtz, J. M. and Hu, J. C. *J. Mol. Biol.*, **2000**, 300, 1377-1387. (c) Lear, J. D., Gratkowski, H., Adamian, L., Liang, J. and DeGrado, W. F. *Biochemistry*, **2003**, 42, 6400-6407.
- (3) Schnarr, N. A. and Kennan, A. J. *J. Am. Chem. Soc.*, **2002**, 124, 9779-9783.
- (4) Schnarr, N. A. and Kennan, A. J. *JACS*, **2004**, 126, 10260-10261.

Appendix 1
Peptide Characterization

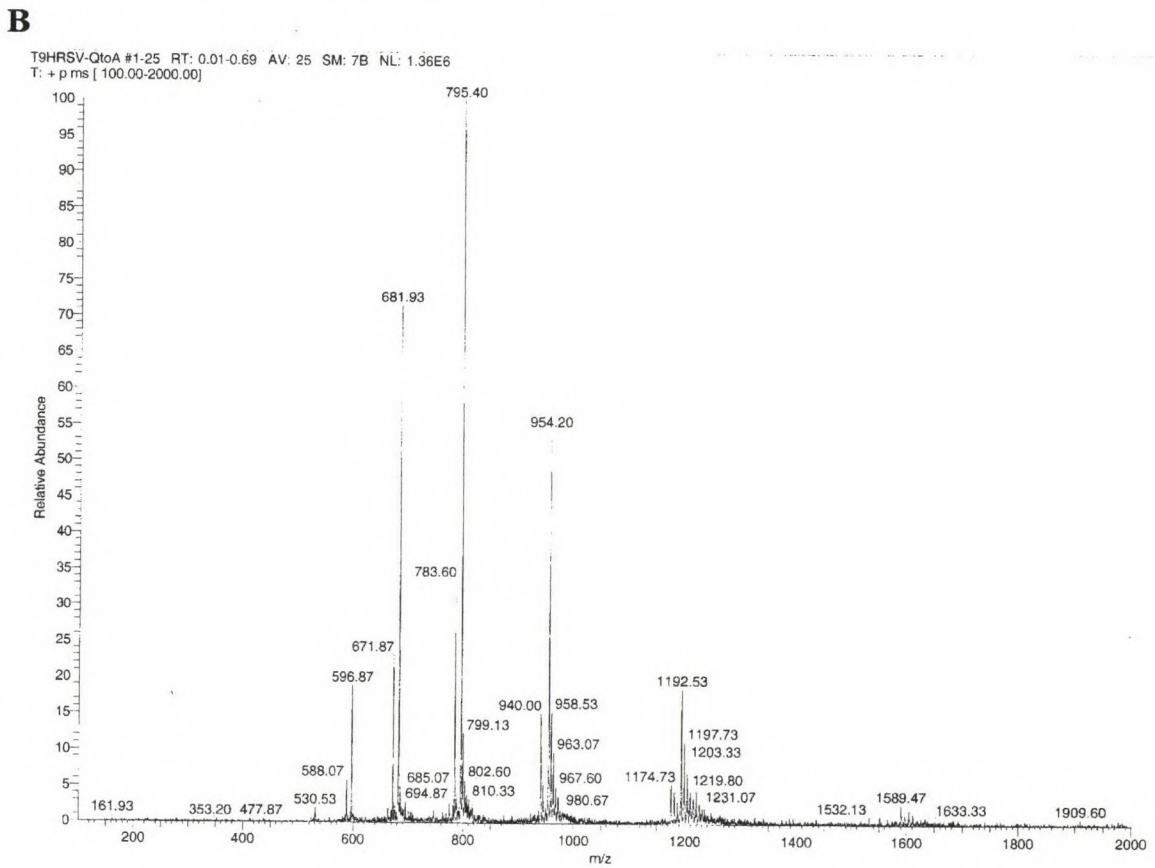
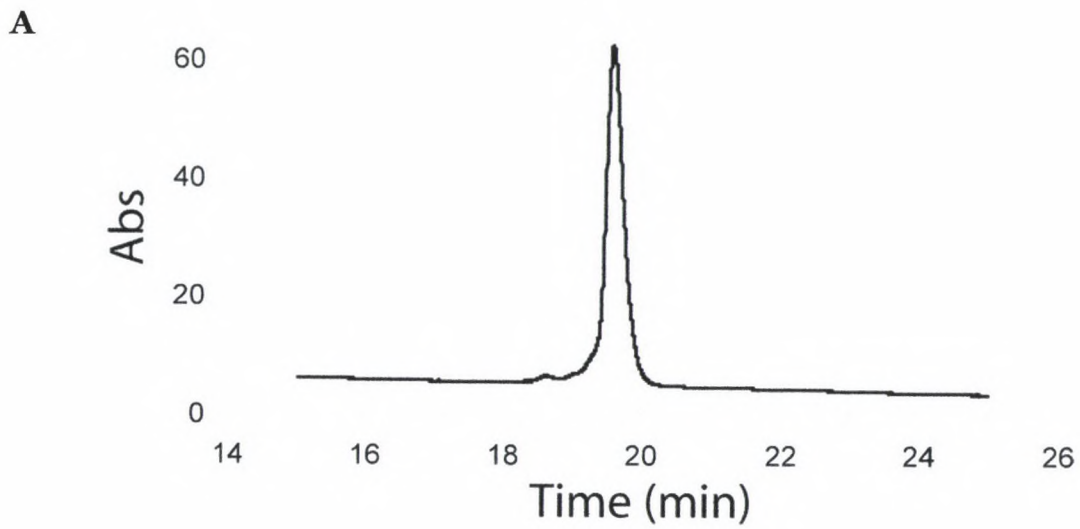


Figure 1. Characterization of T₉HRSV Q/A. (A) HPLC of purified material. (B) Electrospray mass spec raw data for purified material ($MW_{calc} = 4759$; $MW_{obsd} = 4759$).

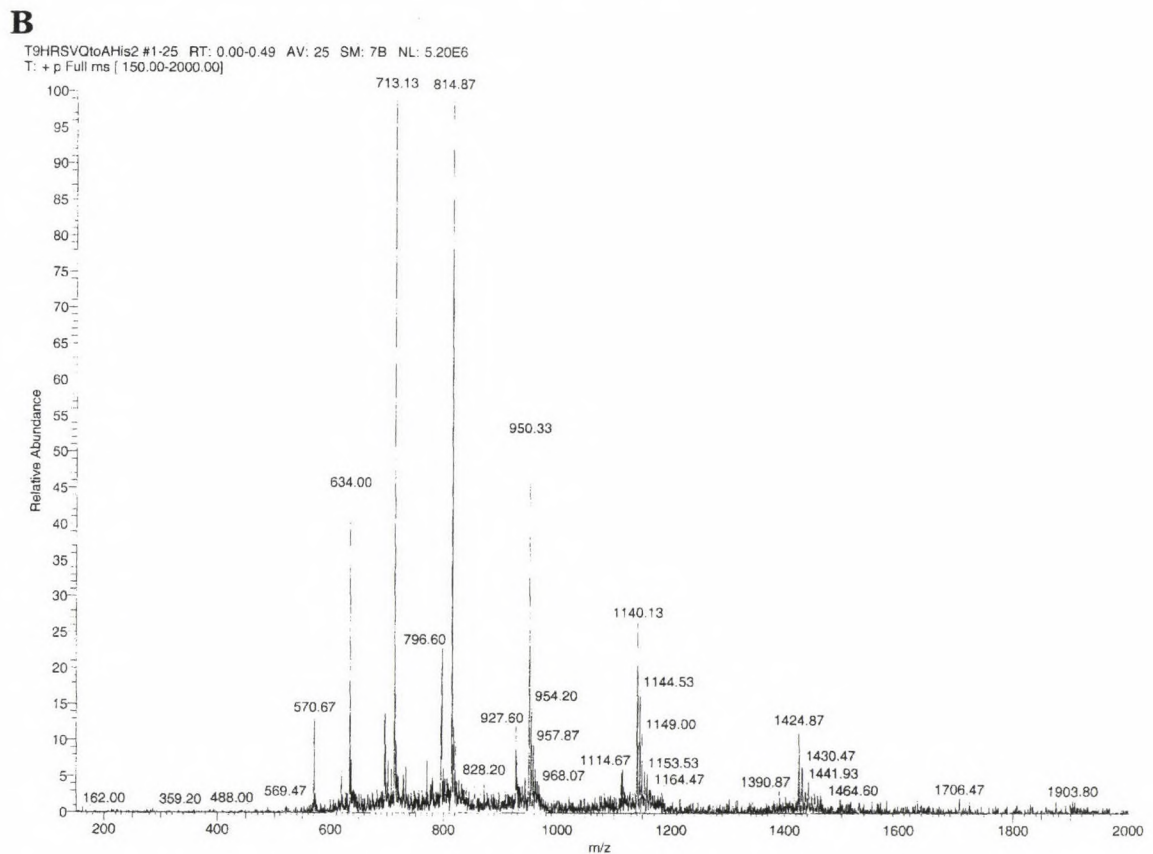
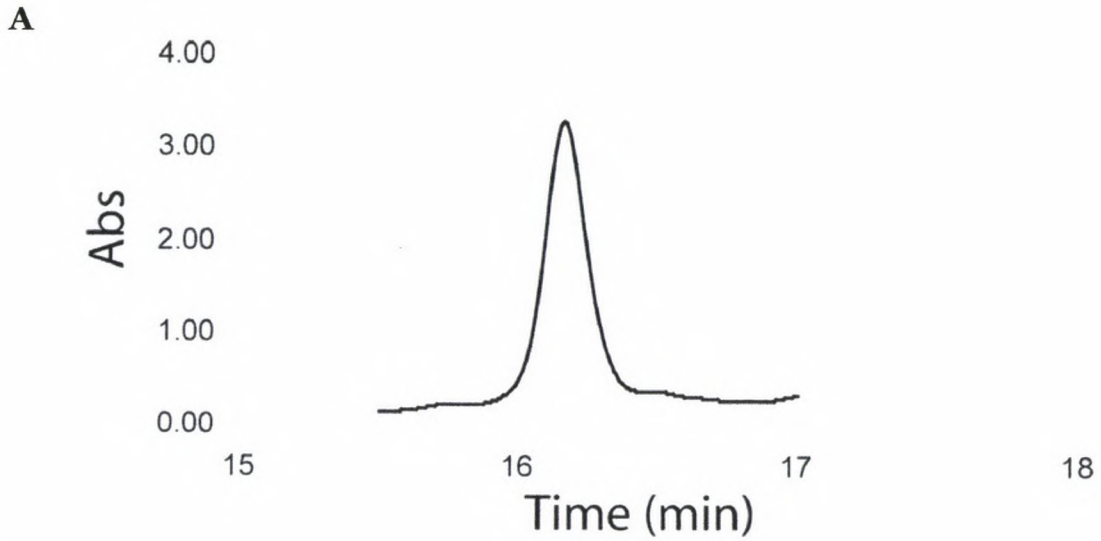


Figure 2. Characterization of T₉HRSV Q/A His. (A) HPLC of purified material. (B) Electrospray mass spec raw data for purified material ($MW_{calc} = 5696$; $MW_{obsd} = 5696$).

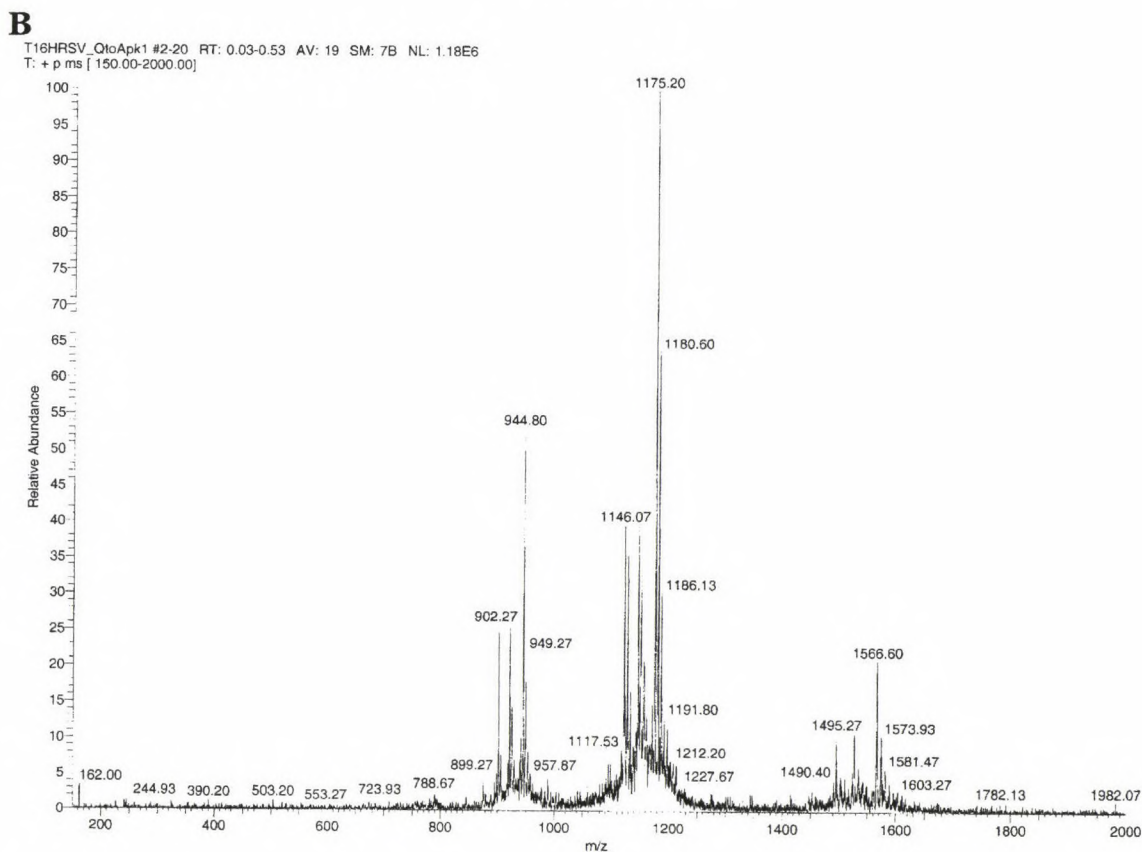
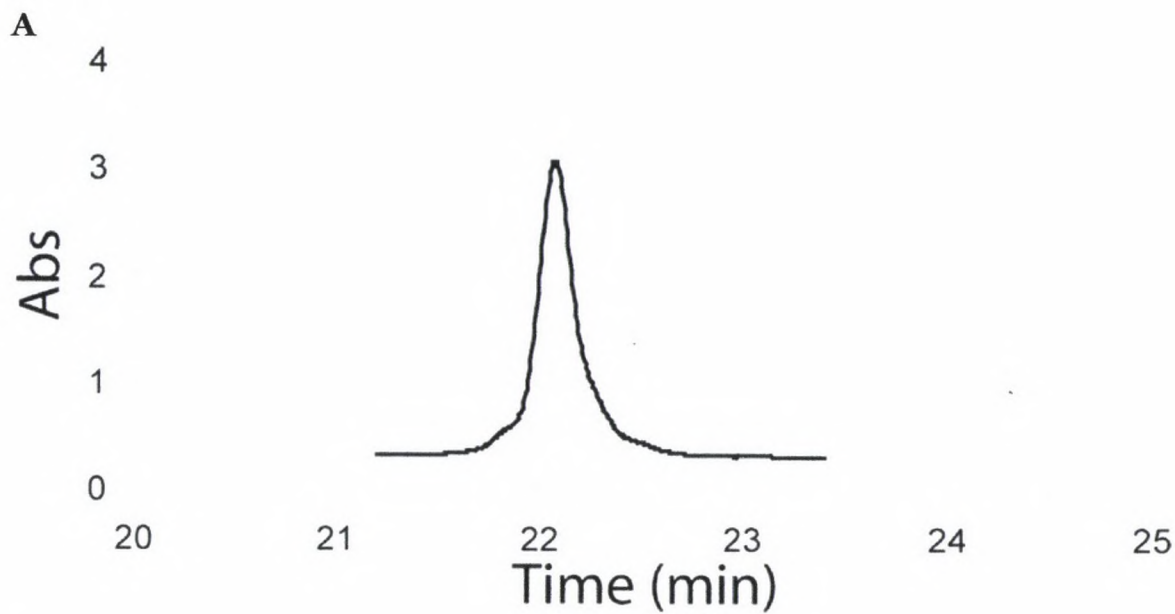


Figure 3. Characterization of T₁₆HRSV Q/A. (A) HPLC of purified material. (B) Electrospray mass spec raw data for purified material ($MW_{calc} = 4696$; $MW_{obsd} = 4697$).

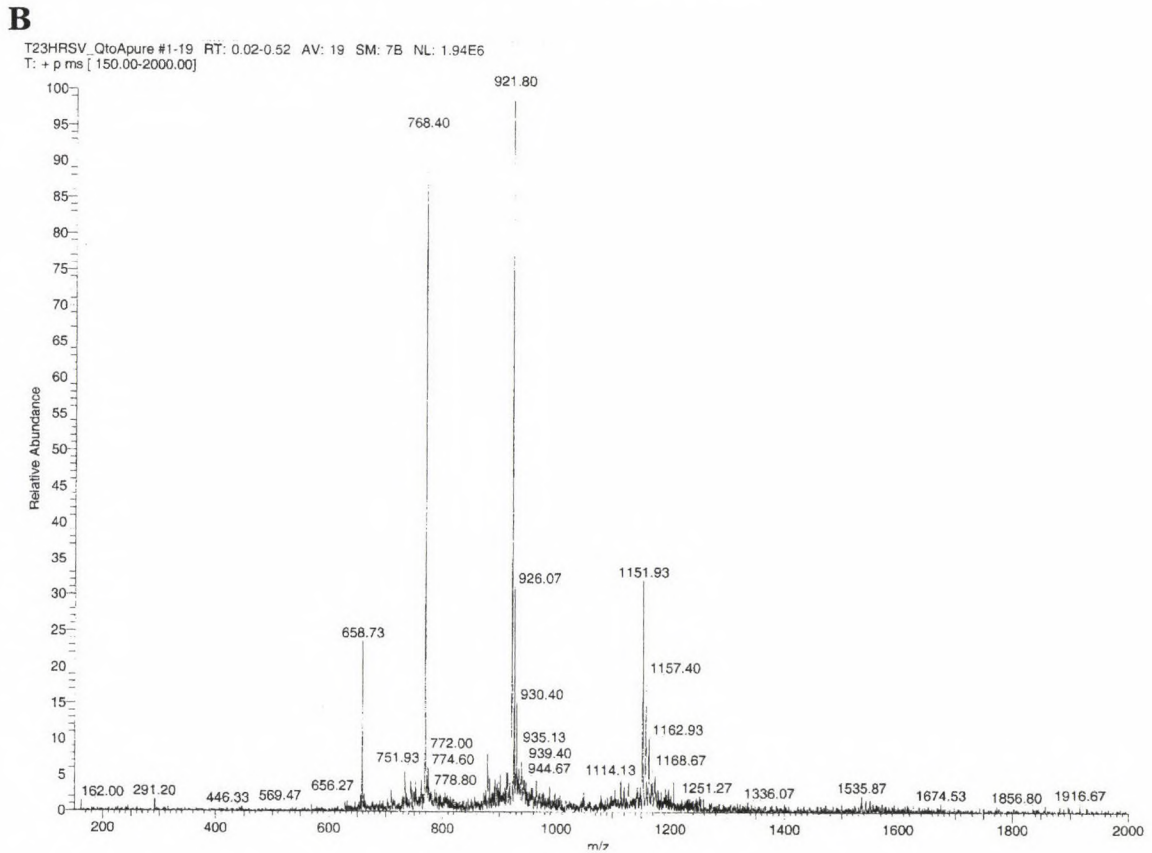
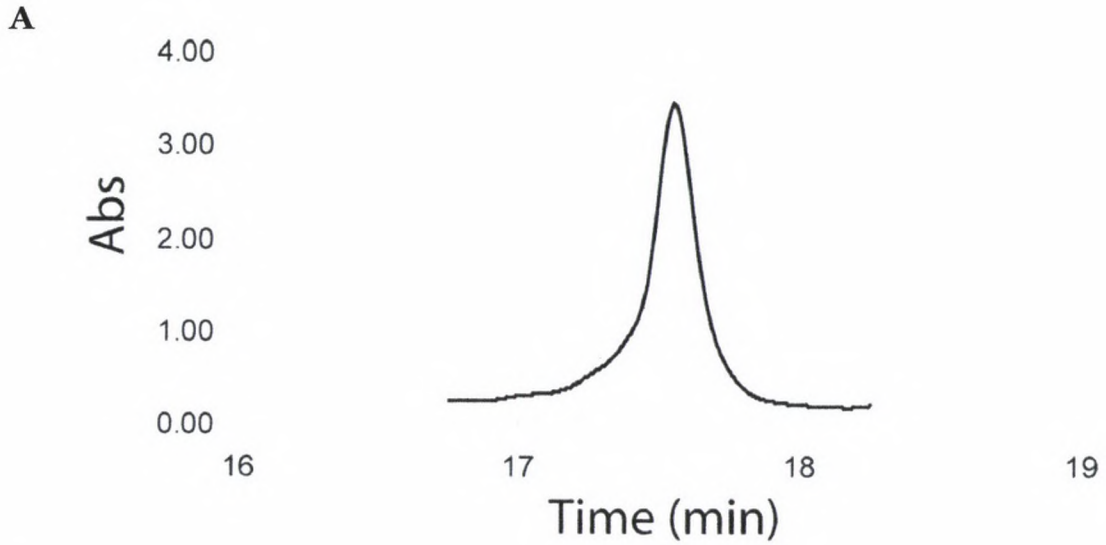


Figure 4. Characterization of T₂₃HRSV Q/A. (A) HPLC of purified material. (B) Electrospray mass spec raw data for purified material (MW_{calc} = 4603; MW_{obsd} = 4604).

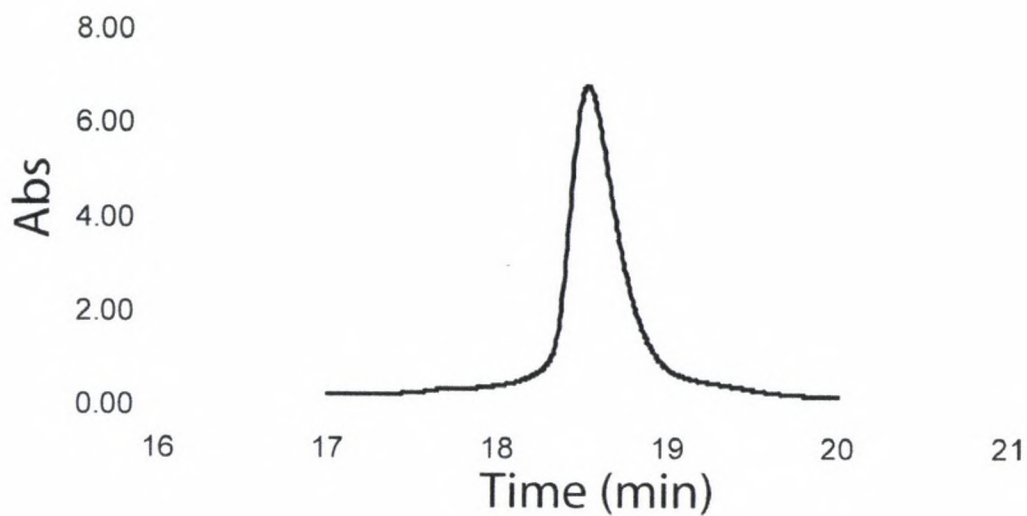
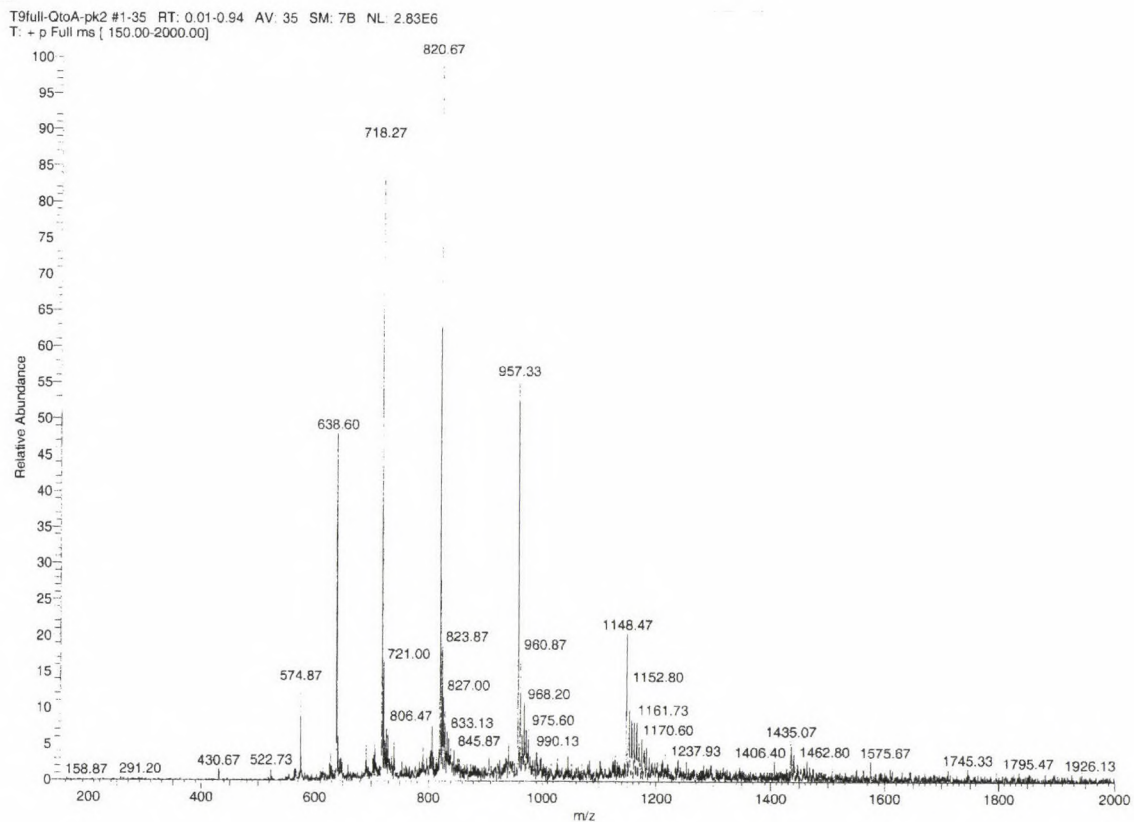
A**B**

Figure 5. Characterization of T₉HRSVfull Q/A. (A) HPLC of purified material. (B) Electrospray mass spec raw data for purified material ($MW_{\text{calc}} = 5738$; $MW_{\text{obsd}} = 5738$).

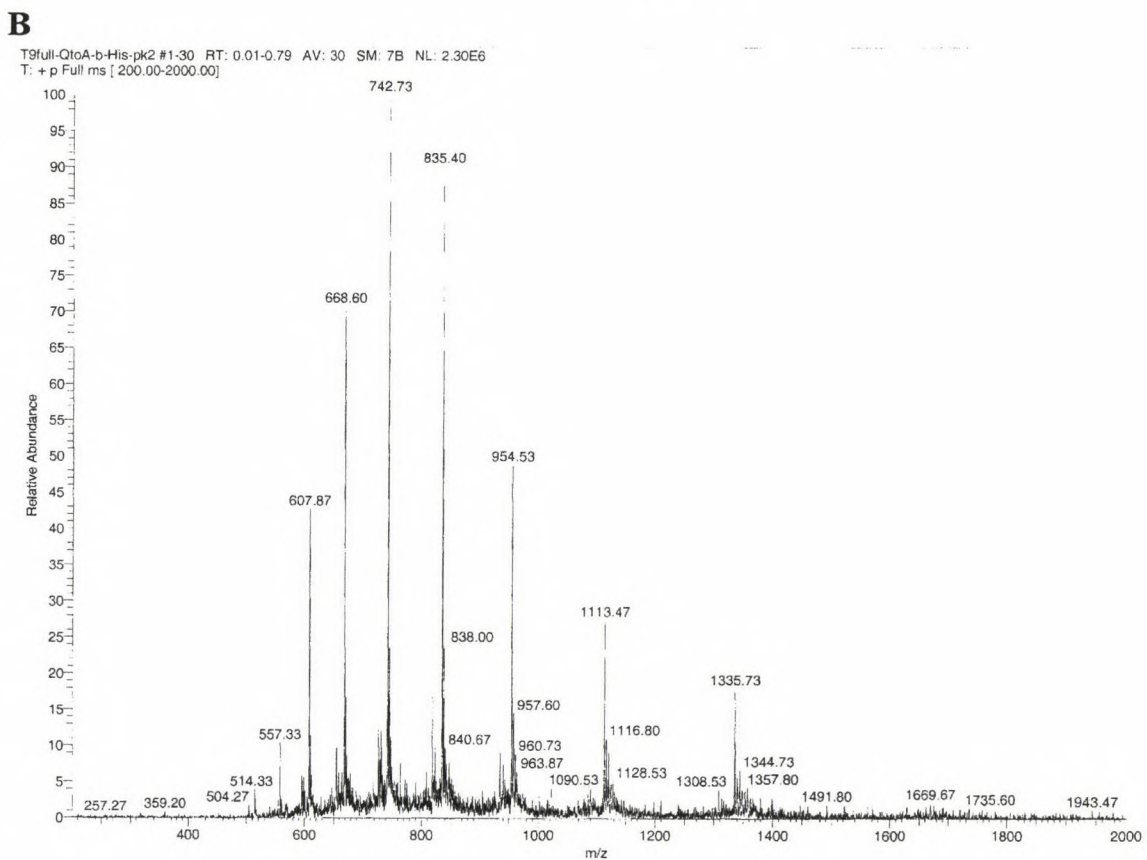
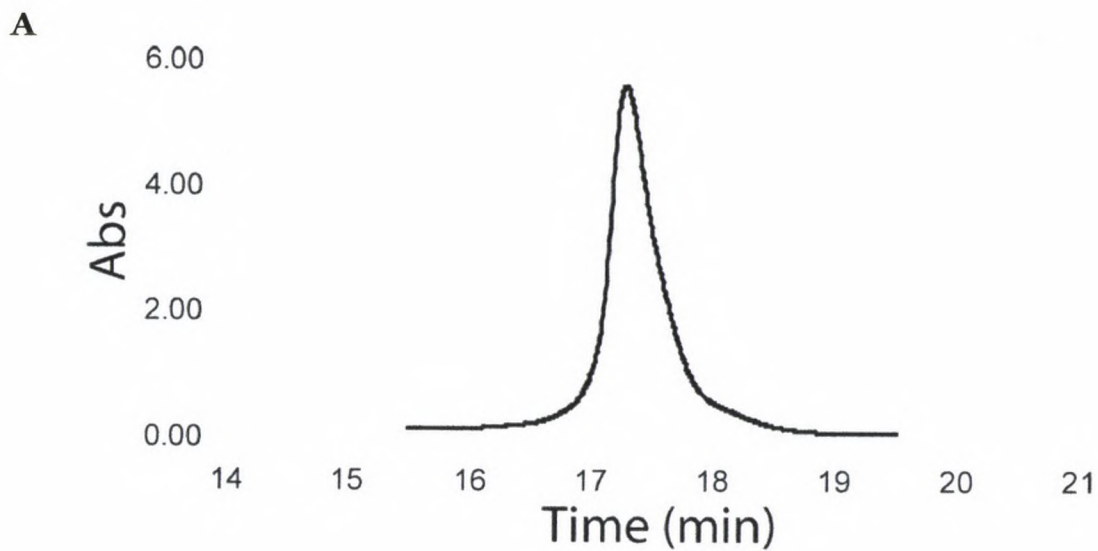


Figure 6. Characterization of T₉HRSVfull Q/A His. (A) HPLC of purified material. (B) Electrospray mass spec raw data for purified material ($MW_{\text{calc}} = 6675$; $MW_{\text{obsd}} = 6675$).

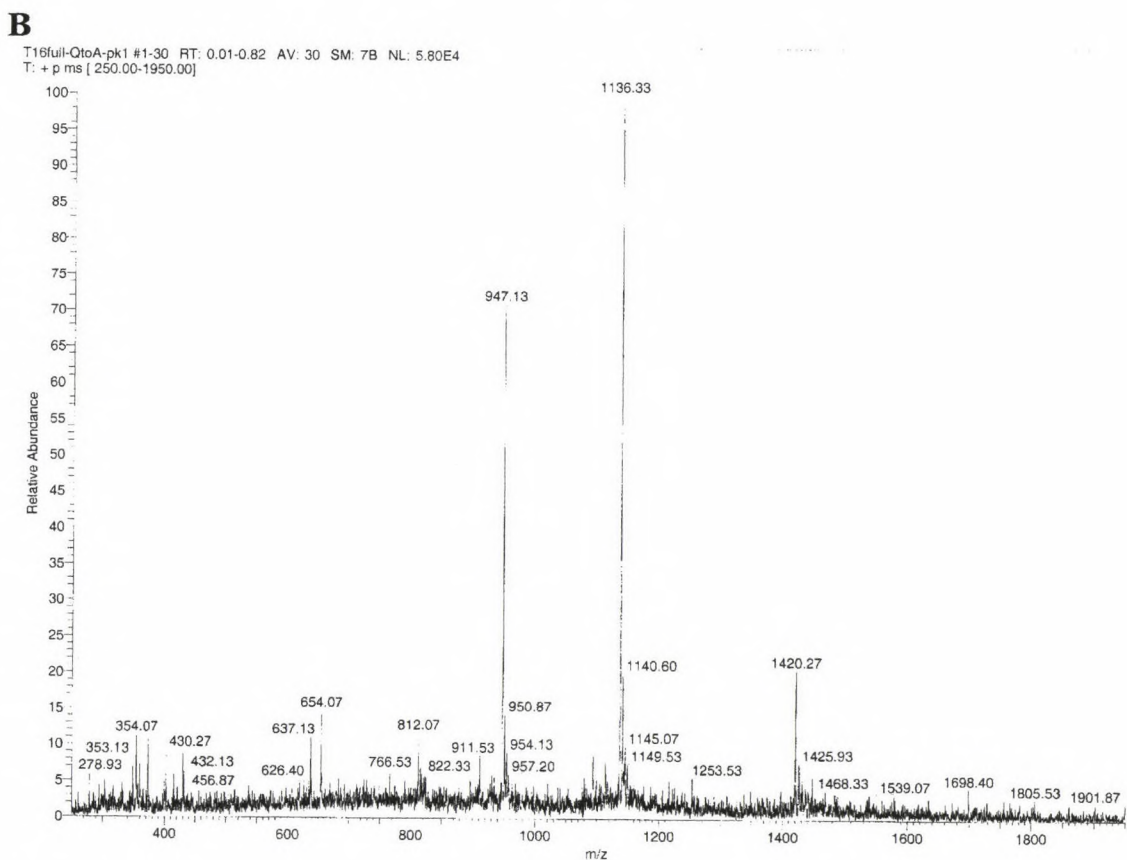
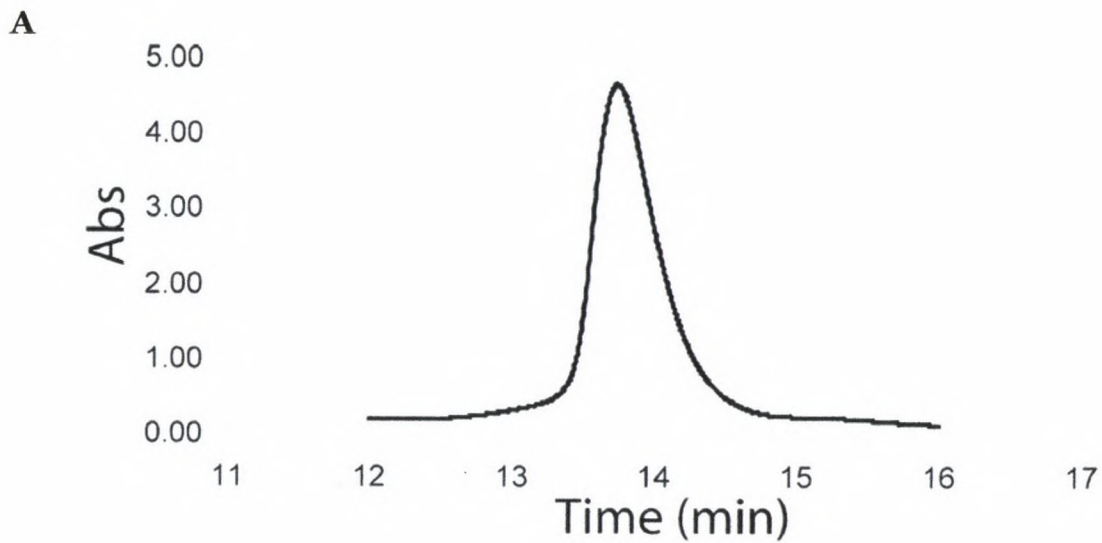


Figure 7. Characterization of T₁₆HRSVfull Q/A. (A) HPLC of purified material. (B) Electrospray mass spec raw data for purified material ($MW_{calc} = 5678$; $MW_{obsd} = 5676$).

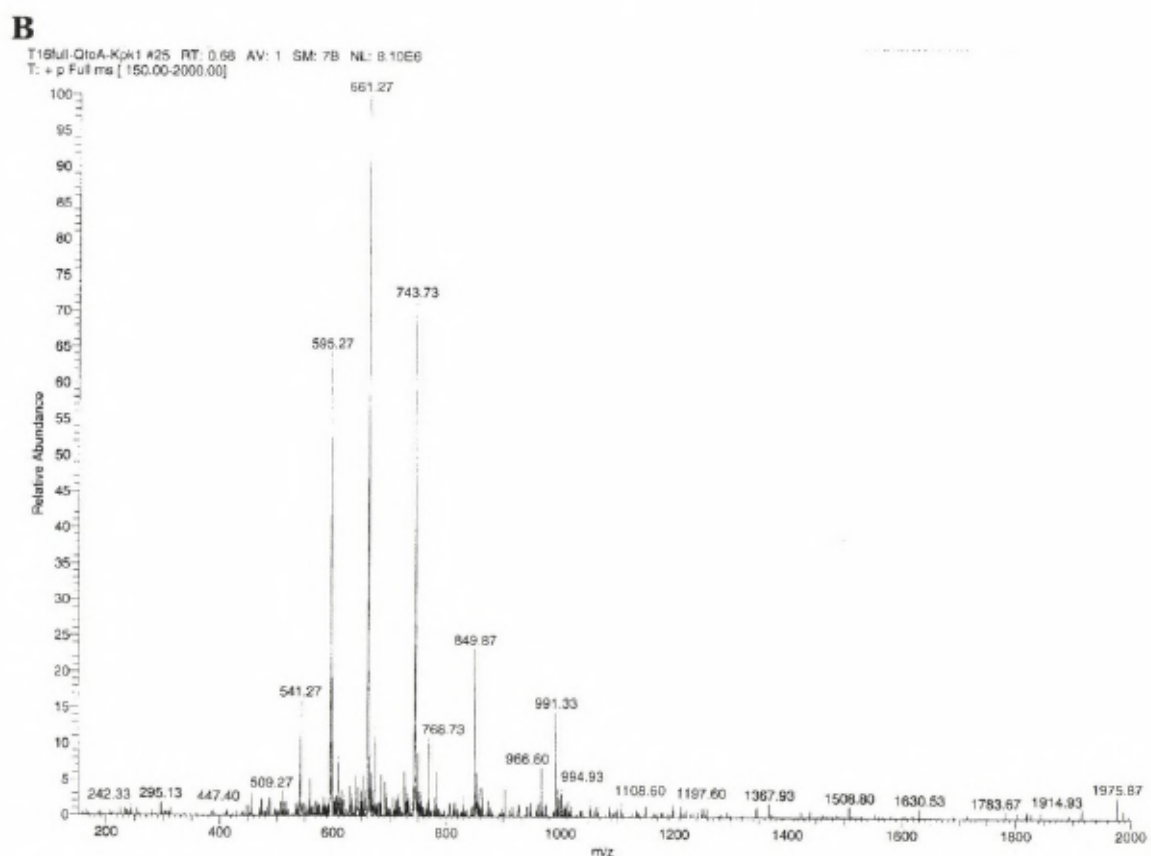
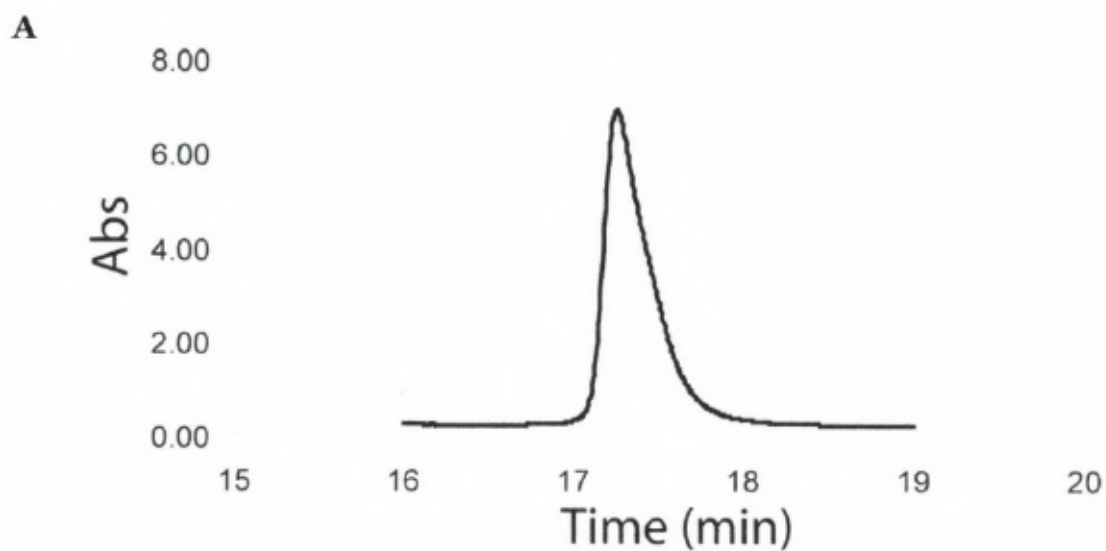


Figure 8. Characterization of T₁₆HRSVfull Q/A K. (A) HPLC of purified material. (B) Electrospray mass spec raw data for purified material (MW_{calc} = 5941; MW_{obsd} = 5942).

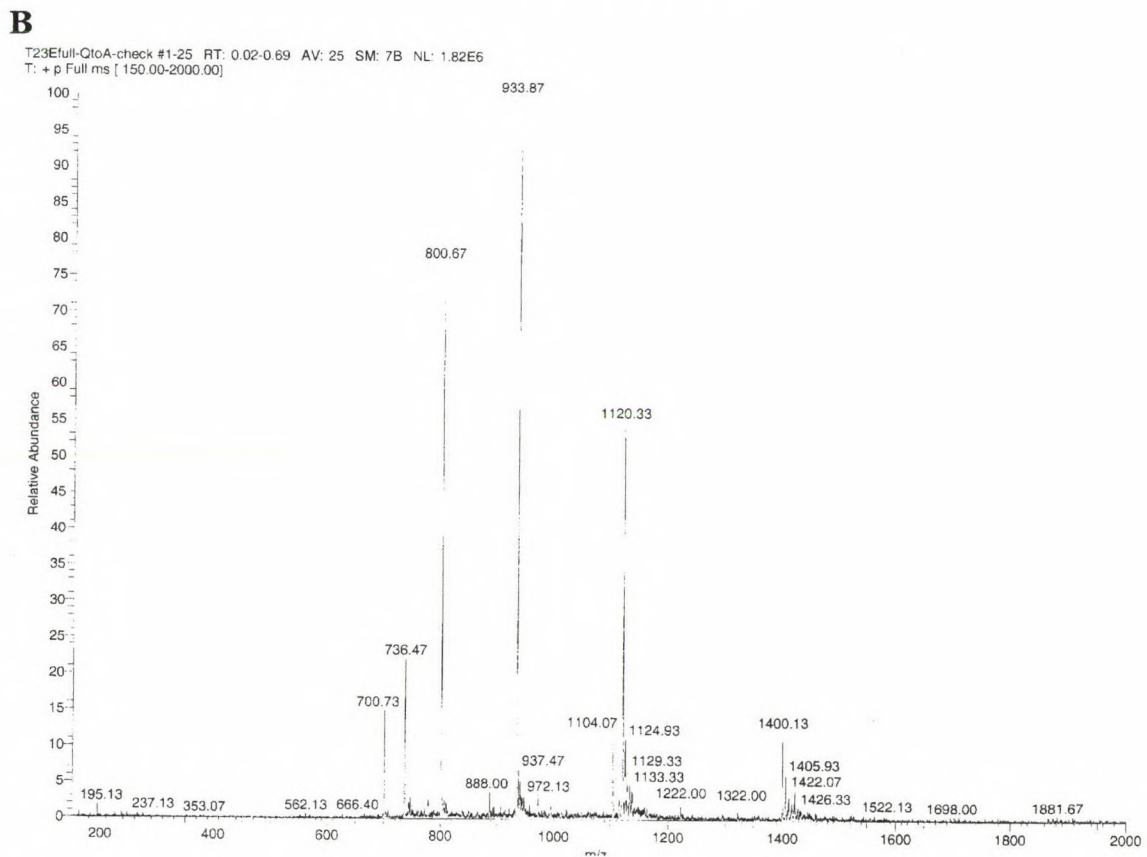
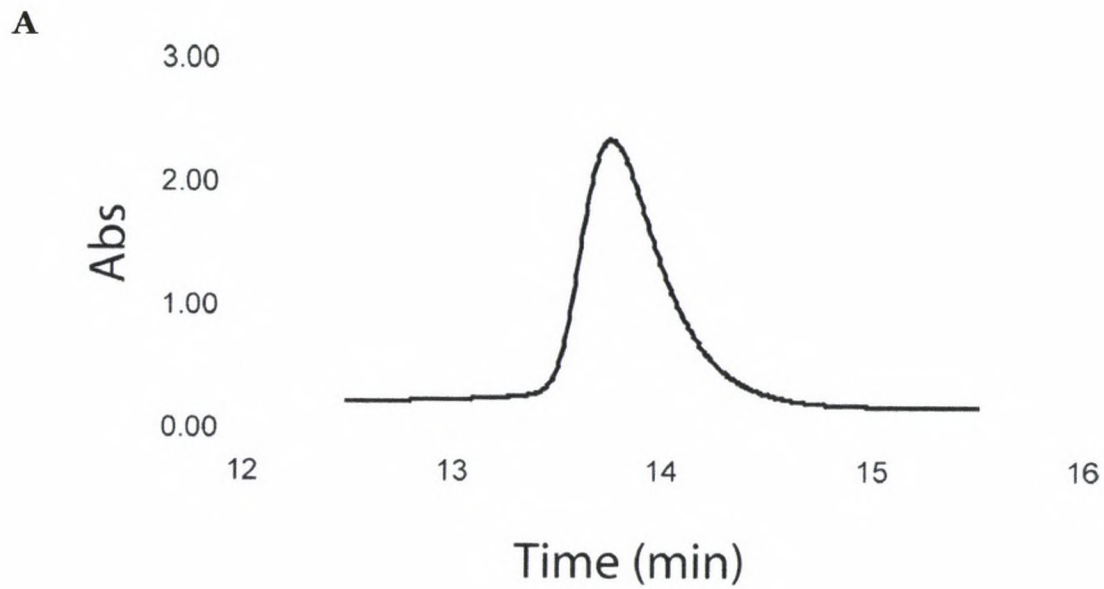


Figure 9. Characterization of T₂₃HRSVfull Q/A. (A) HPLC of purified material. (B) Electrospray mass spec raw data for purified material (MW_{calc} = 5598; MW_{obsd} = 5597).

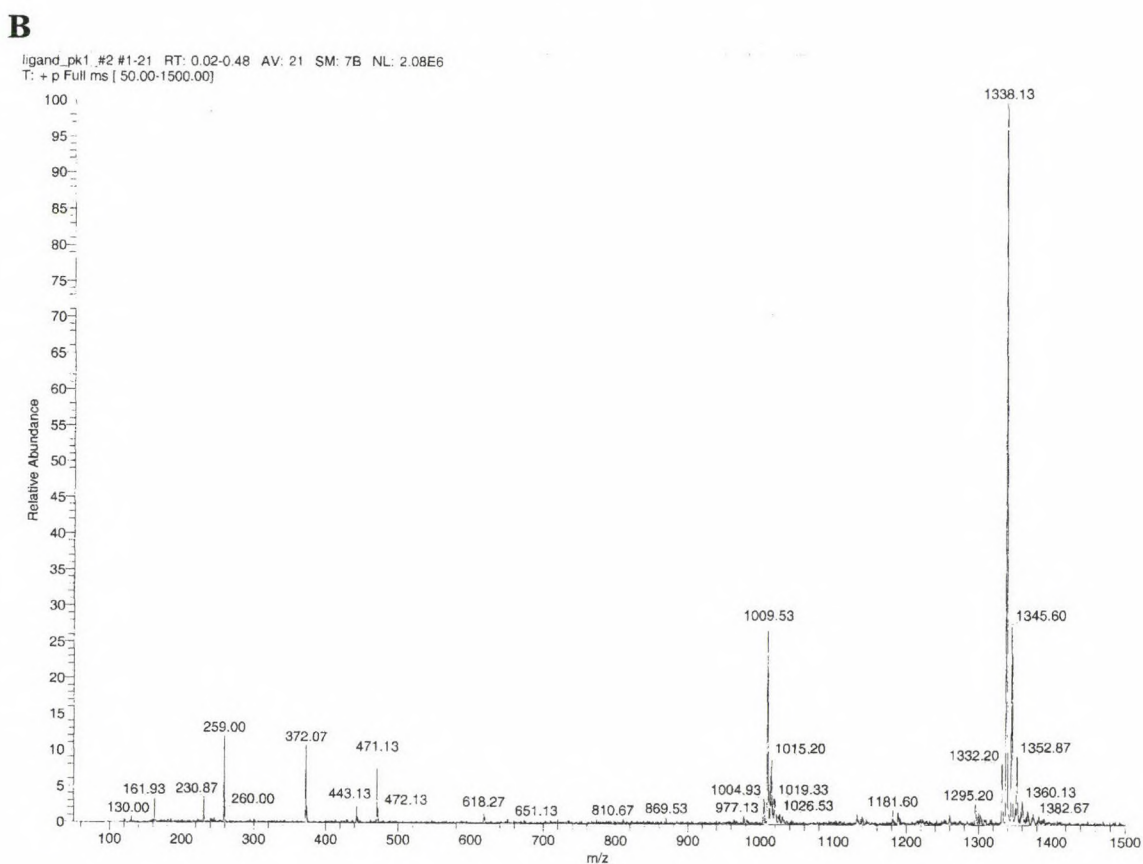
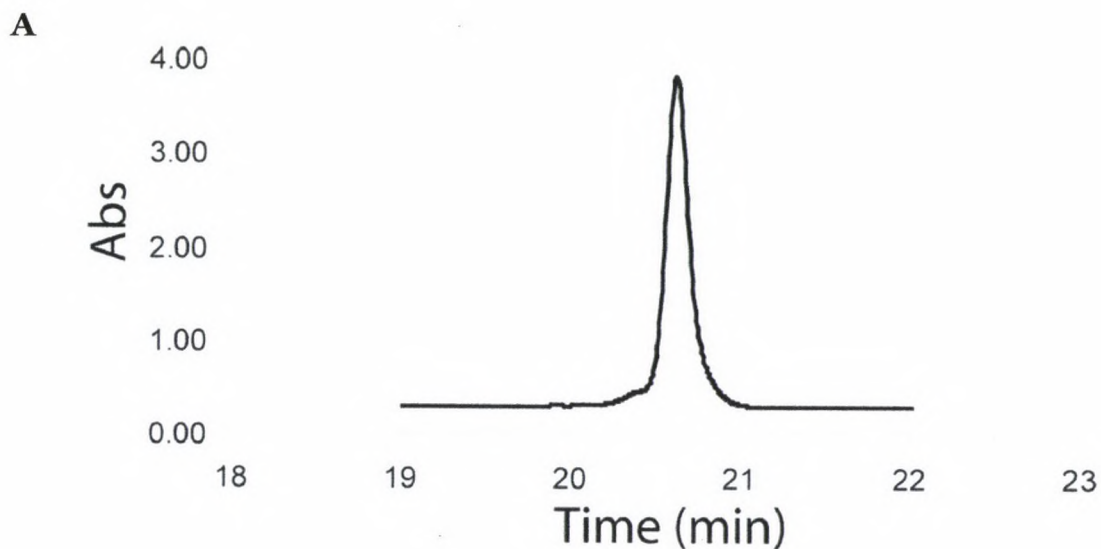


Figure 10. Characterization of HRSV F₁C. (A) HPLC of purified material. (B) Electrospray mass spec raw data for purified material ($MW_{calc} = 4012$; $MW_{obsd} = 4012$).

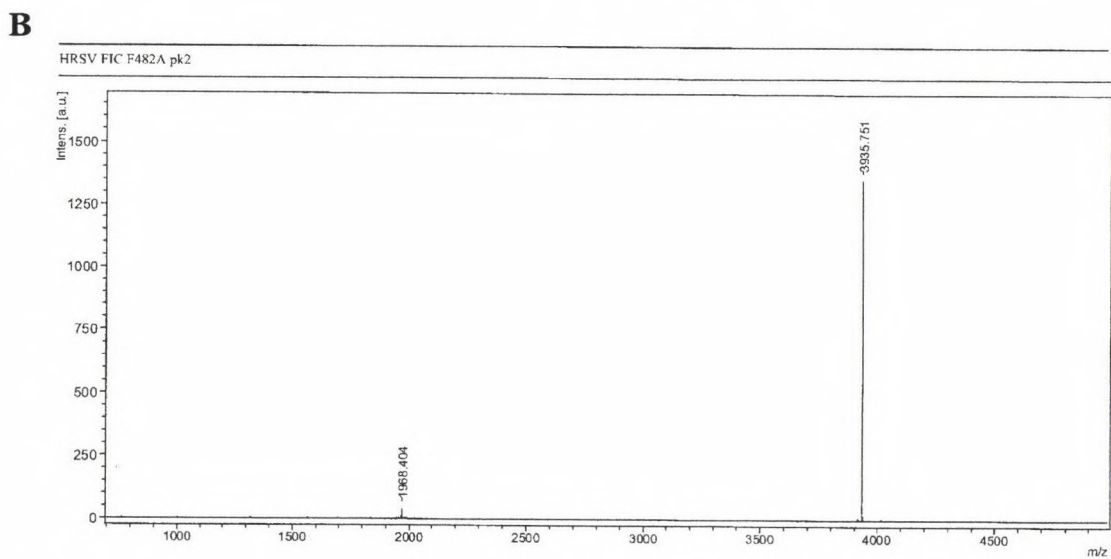
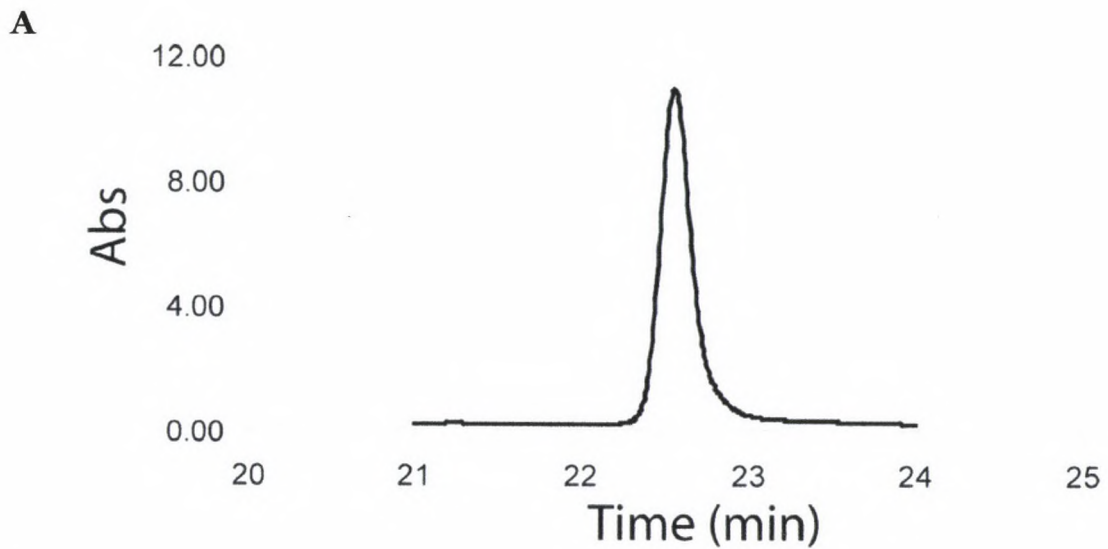


Figure 11. Characterization of HRSV F₁C F483A. (A) HPLC of purified material. (B) MALDI mass spec raw data for purified material ($MW_{\text{calc}} = 3935$; $MW_{\text{obsd}} = 3936$). NB: The name of this peptide was mistyped by the technician who ran the mass spec.

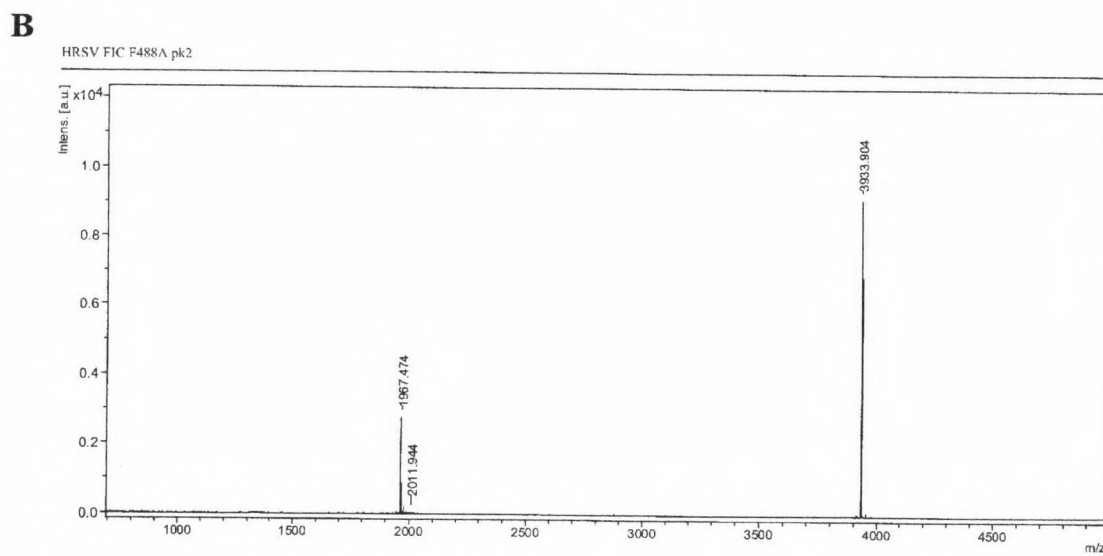
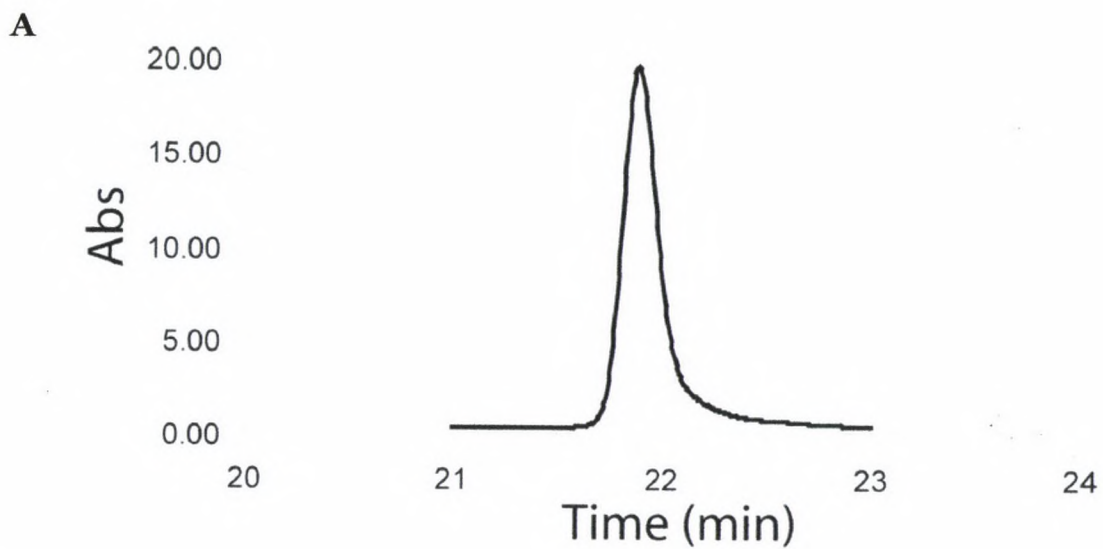


Figure 12. Characterization of HRSV F₁C F488A. (A) HPLC of purified material. (B) MALDI mass spec raw data for purified material ($MW_{\text{calc}} = 3935$; $MW_{\text{obsd}} = 3934$).

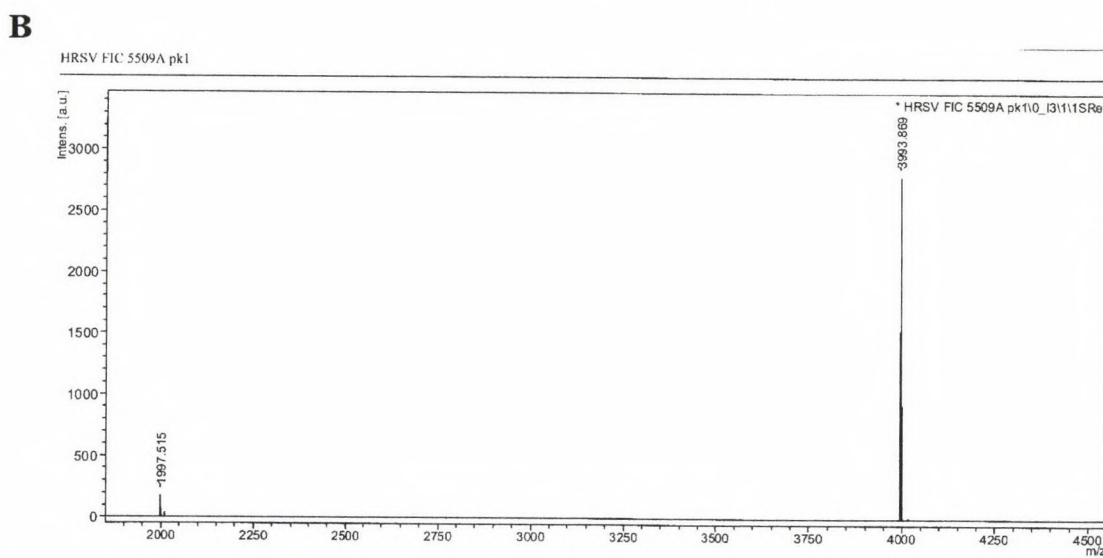
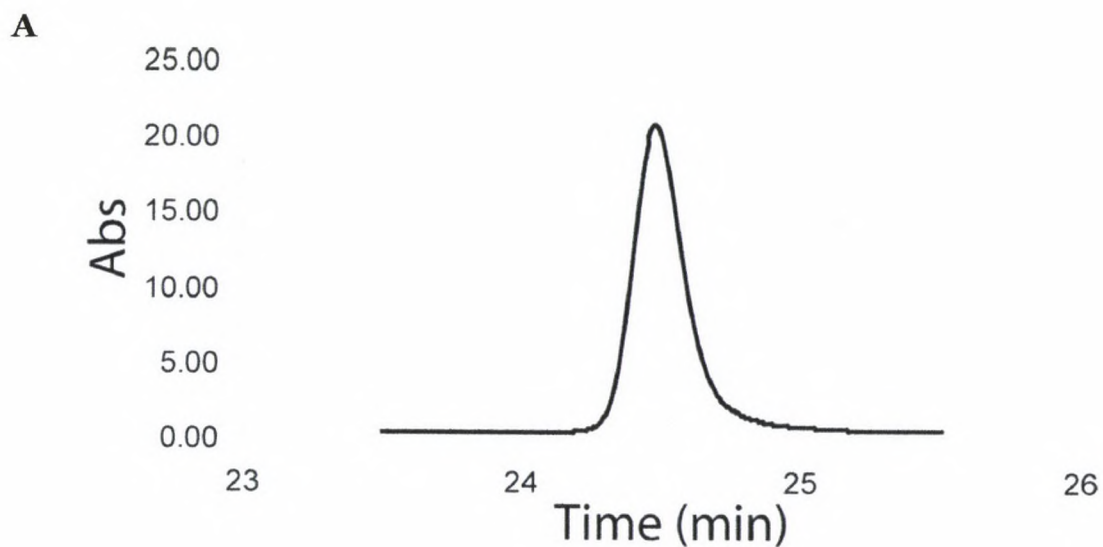


Figure 13. Characterization of HRSV F₁C S₅₀₉A. (A) HPLC of purified material. (B) MALDI mass spec raw data for purified material ($MW_{\text{calc}} = 3996$; $MW_{\text{obsd}} = 3994$).

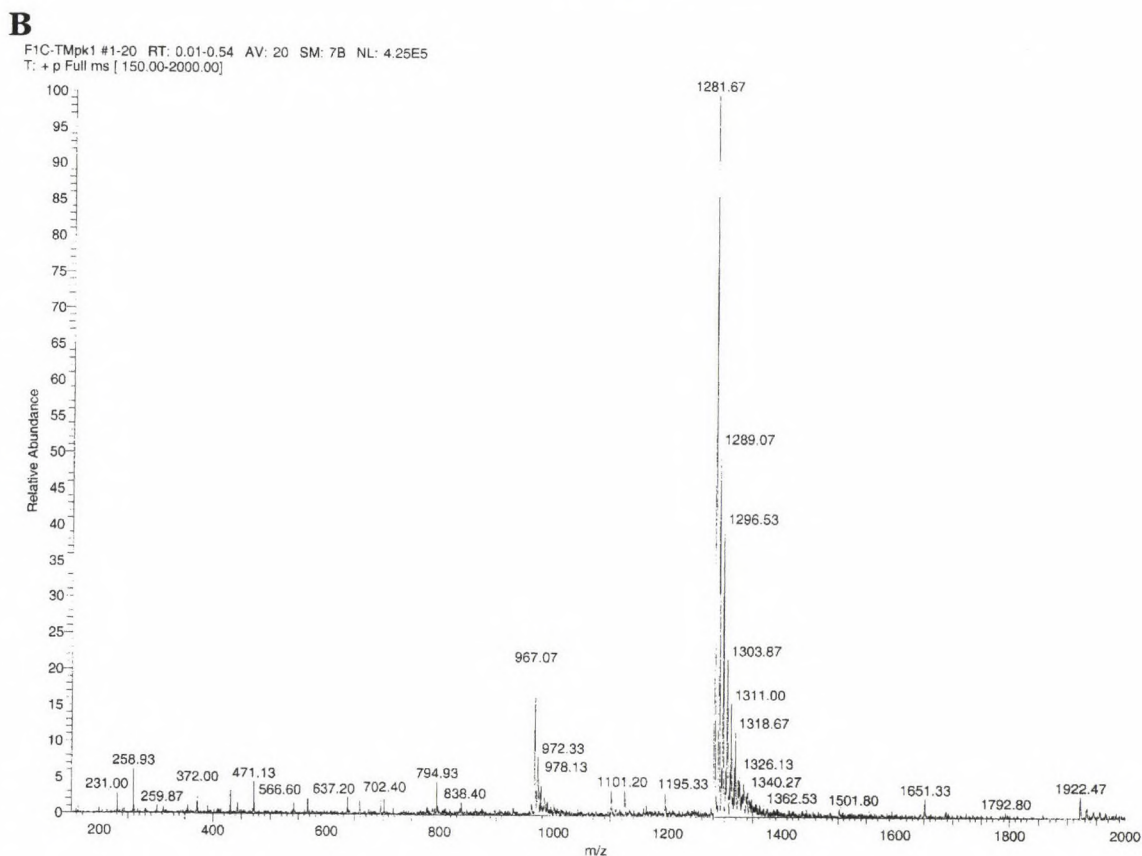
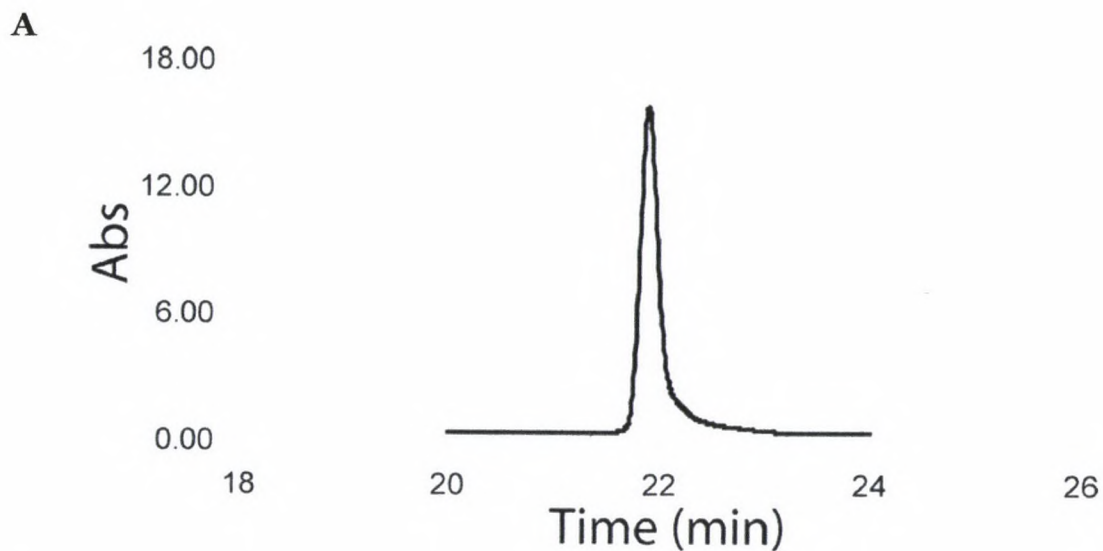


Figure 14. Characterization of HRSV F₁C TM. (A) HPLC of purified material. (B) Electrospray mass spec raw data for purified material ($MW_{\text{calc}} = 3843$; $MW_{\text{obsd}} = 3842$).

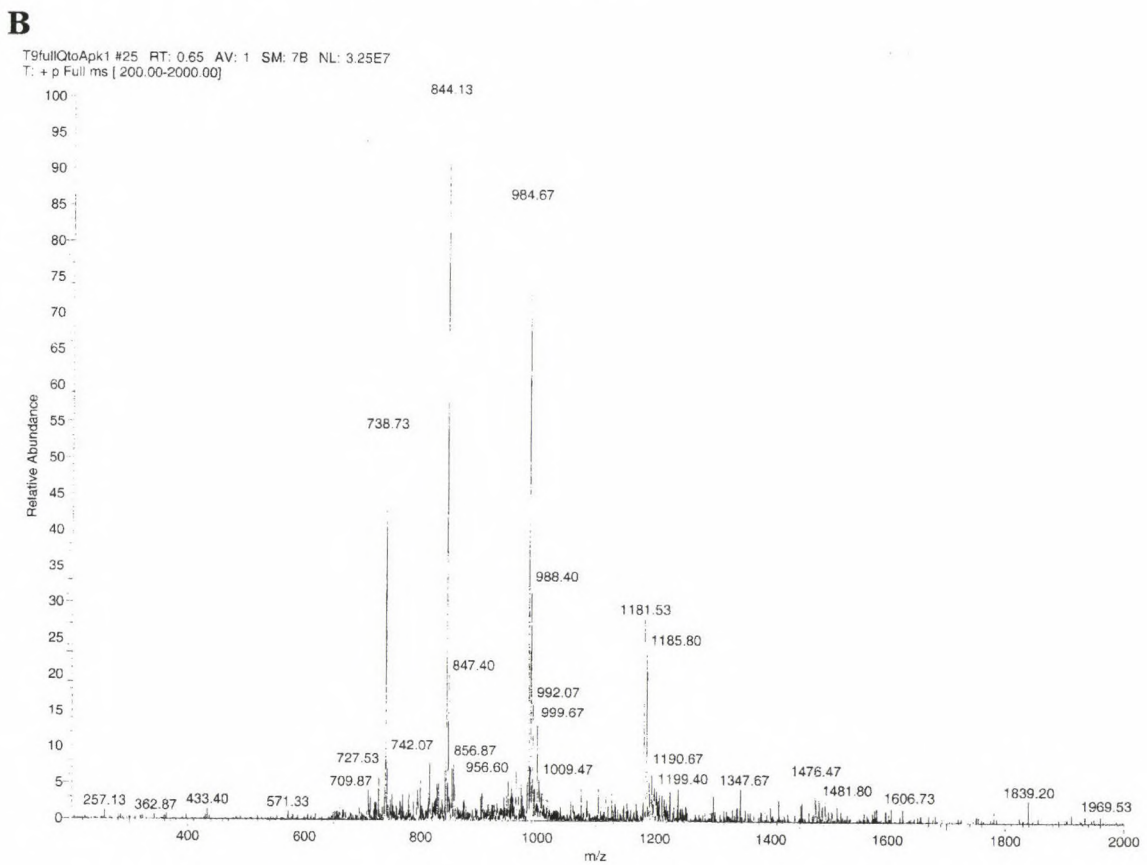
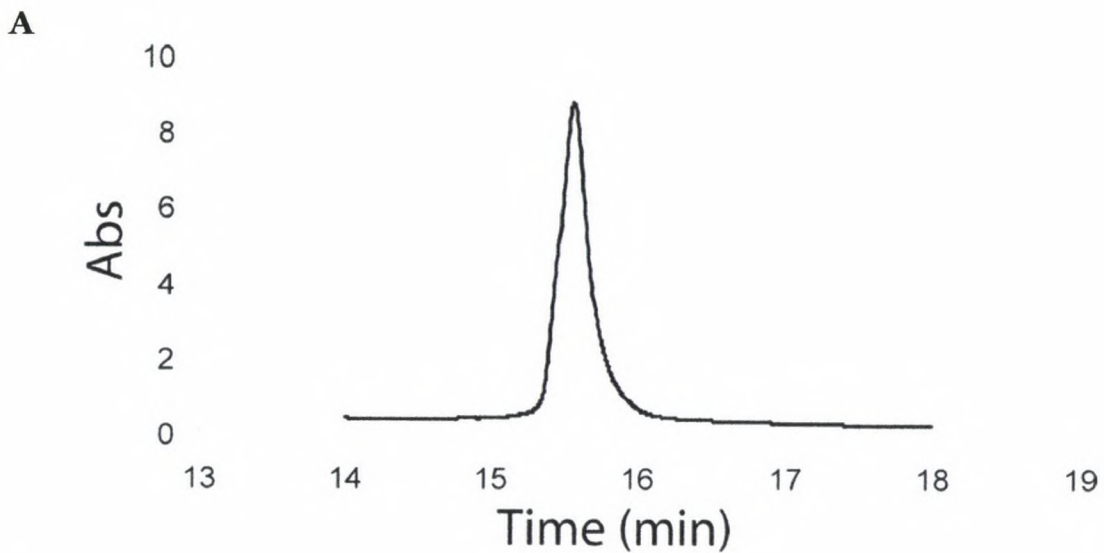


Figure 15. Characterization of T₉HTLVfull Q/A. (A) HPLC of purified material. (B) Electrospray mass spec raw data for purified material (MW_{calc} = 5902; MW_{obsd} = 5902).

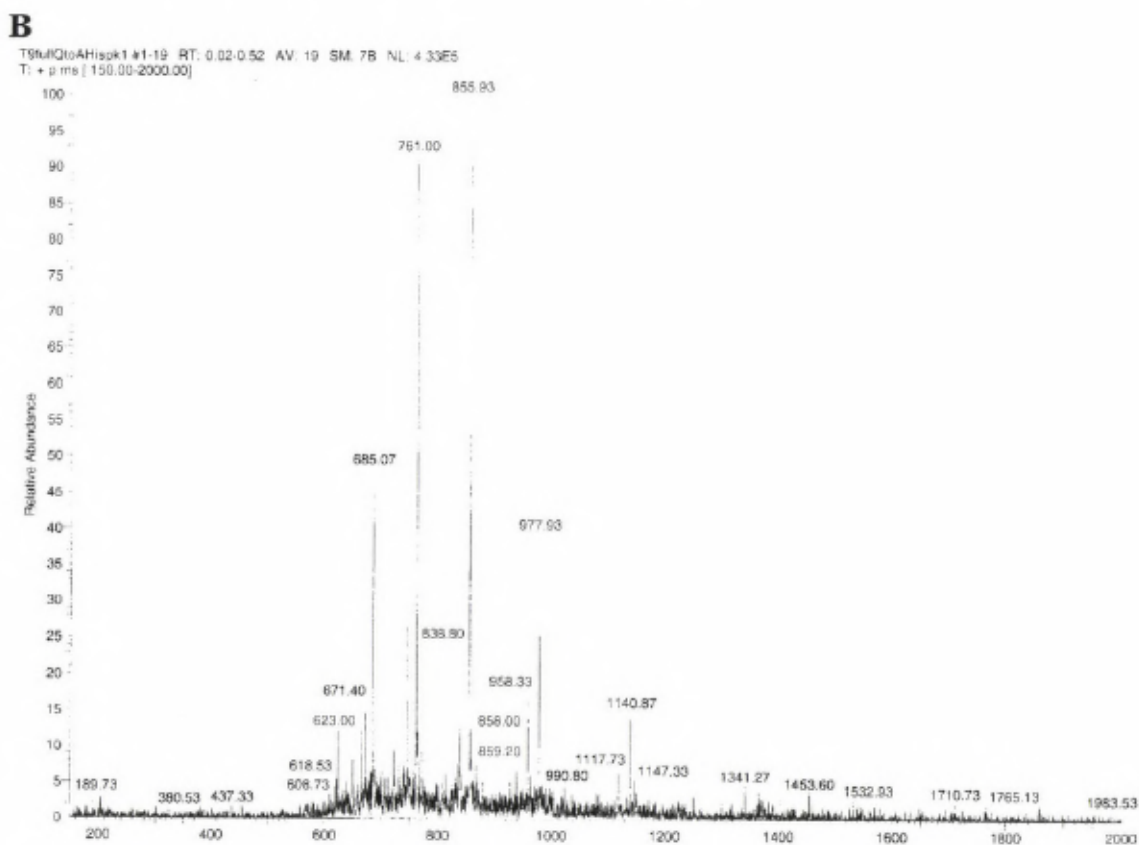
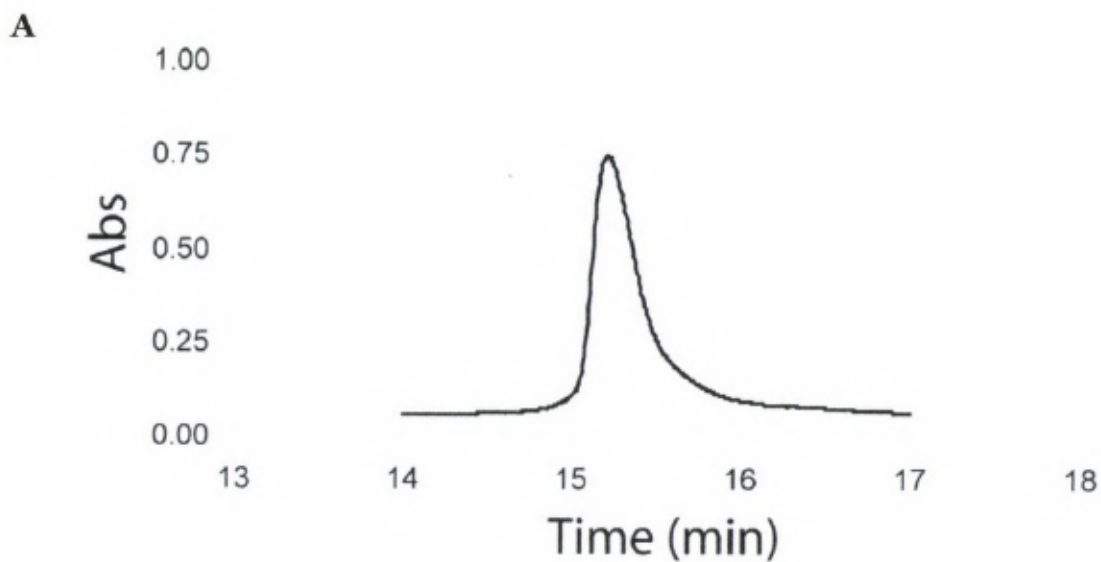


Figure 16. Characterization of T₉HTLVfull Q/A His. (A) HPLC of purified material. (B) Electrospray mass spec raw data for purified material (MW_{calc} = 6839; MW_{obsd} = 6839).

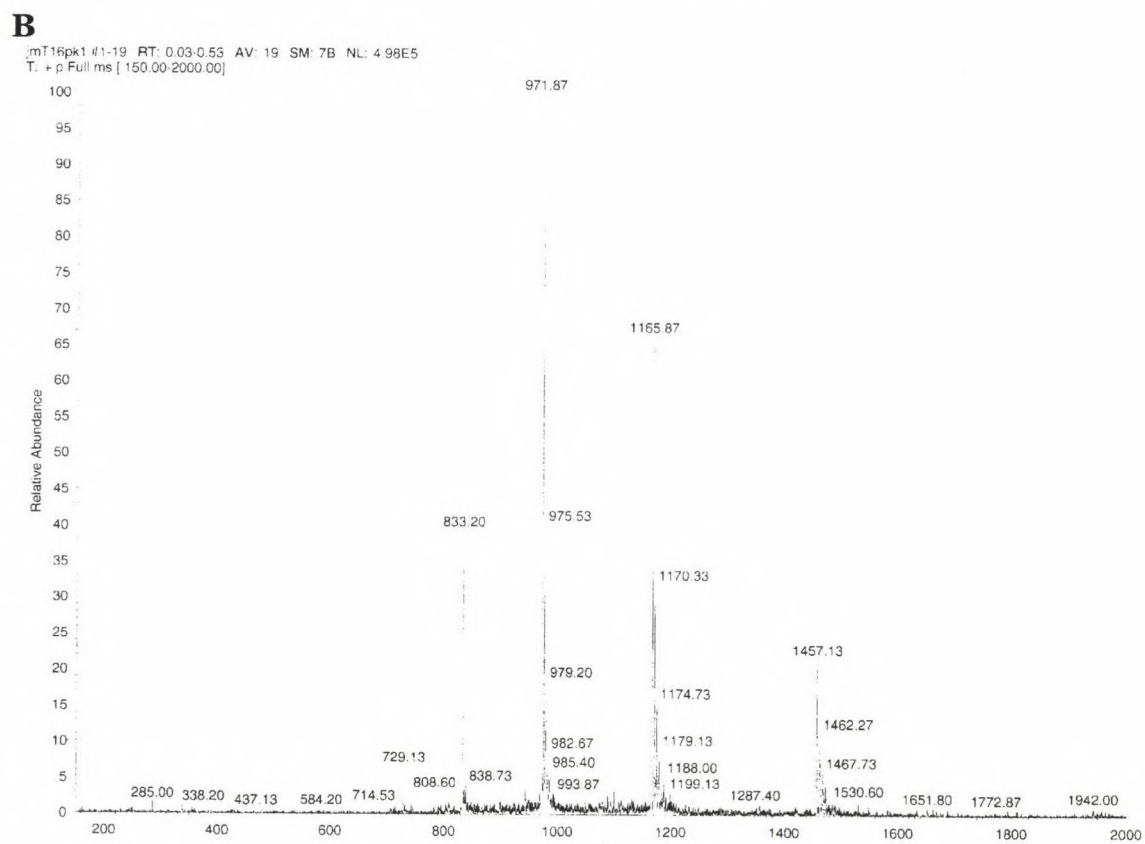
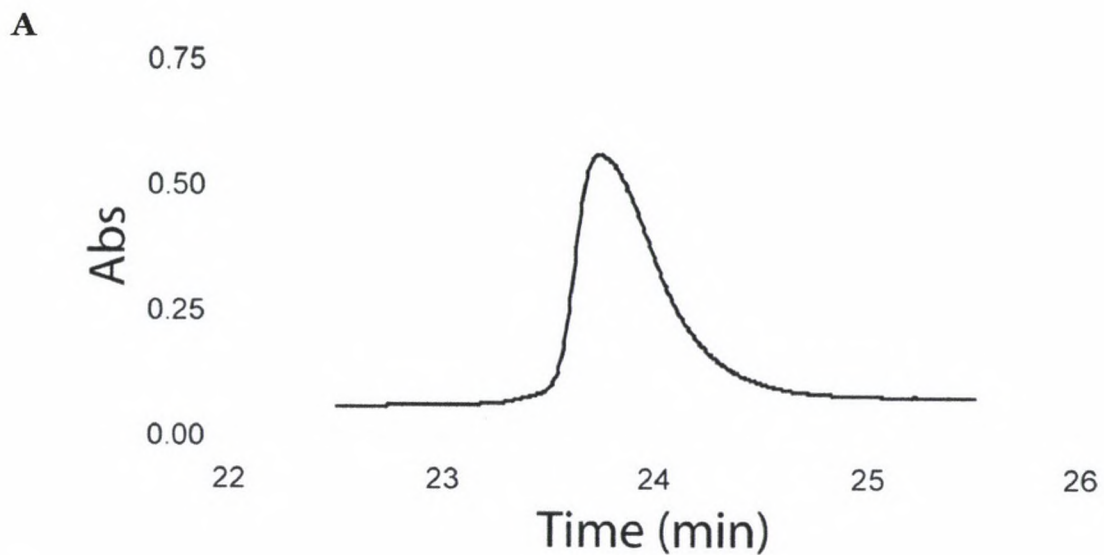


Figure 17. Characterization of T₁₆HTLVfull Q/A. (A) HPLC of purified material. (B) Electrospray mass spec raw data for purified material (MW_{calc} = 5825; MW_{obsd} = 5824).

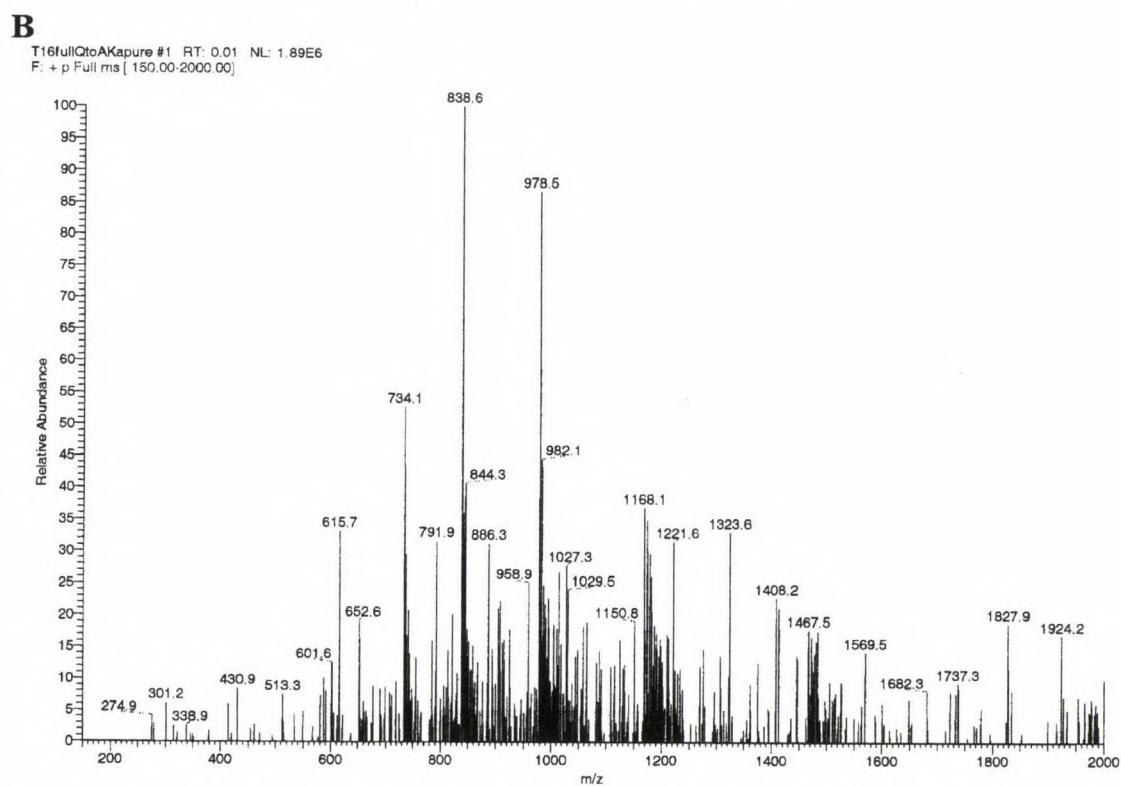
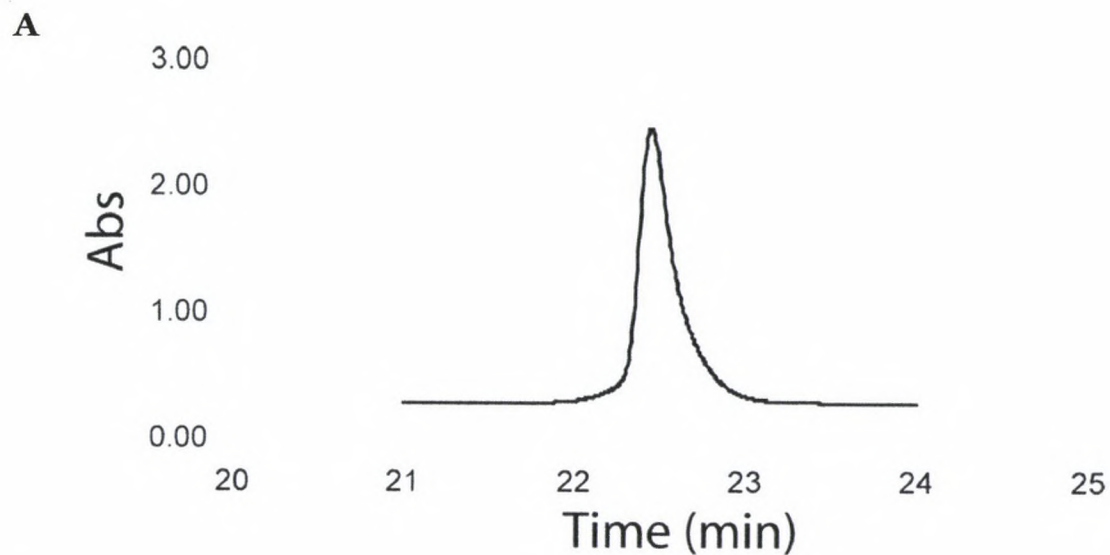


Figure 18. Characterization of T₁₆HTLVfull Q/A K (A) HPLC of purified material. (B) Electrospray mass spec raw data for purified material (MW_{calc} = 5693; MW_{obsd} = 5693).

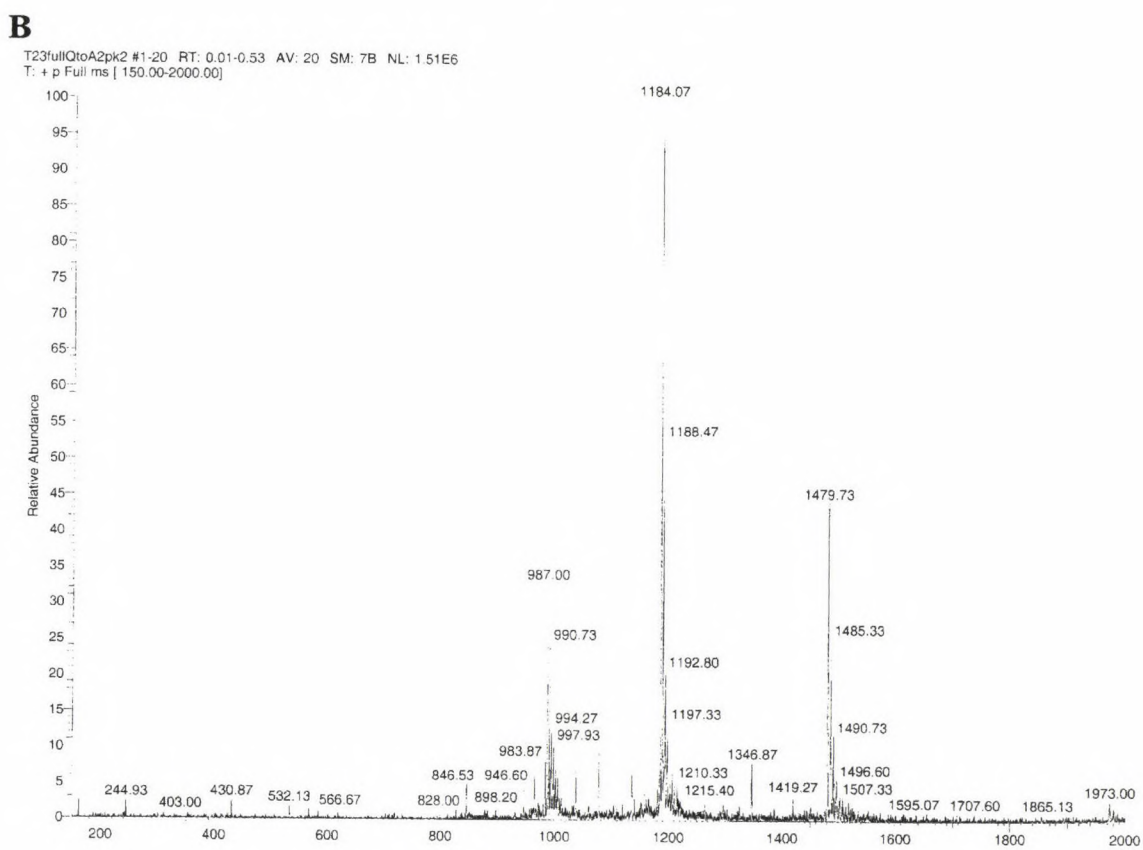
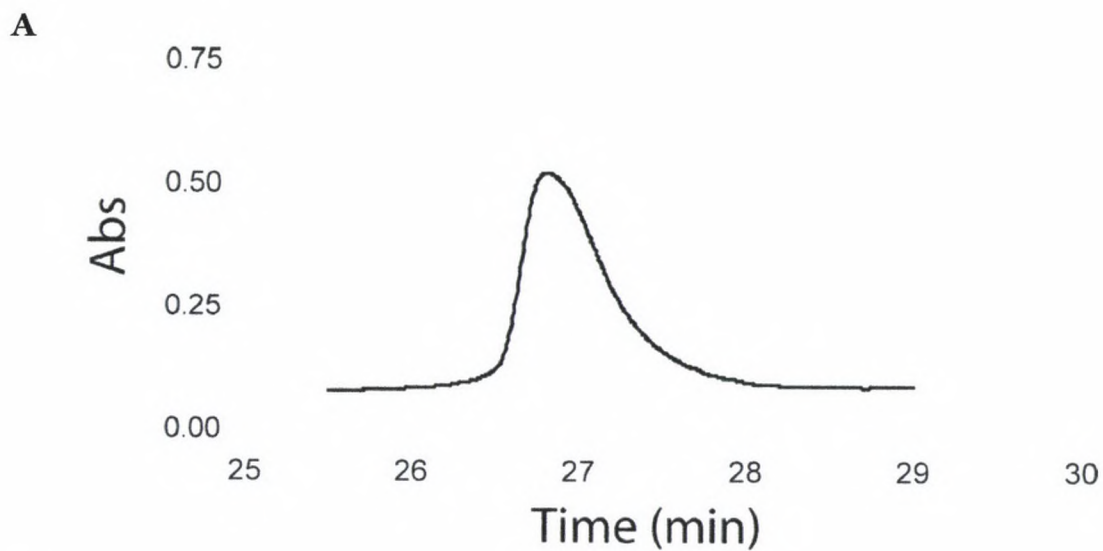


Figure 19. Characterization of T₂₃HTLVfull Q/A. (A) HPLC of purified material. (B) Electrospray mass spec raw data for purified material ($MW_{\text{calc}} = 5916$; $MW_{\text{obsd}} = 5915$).

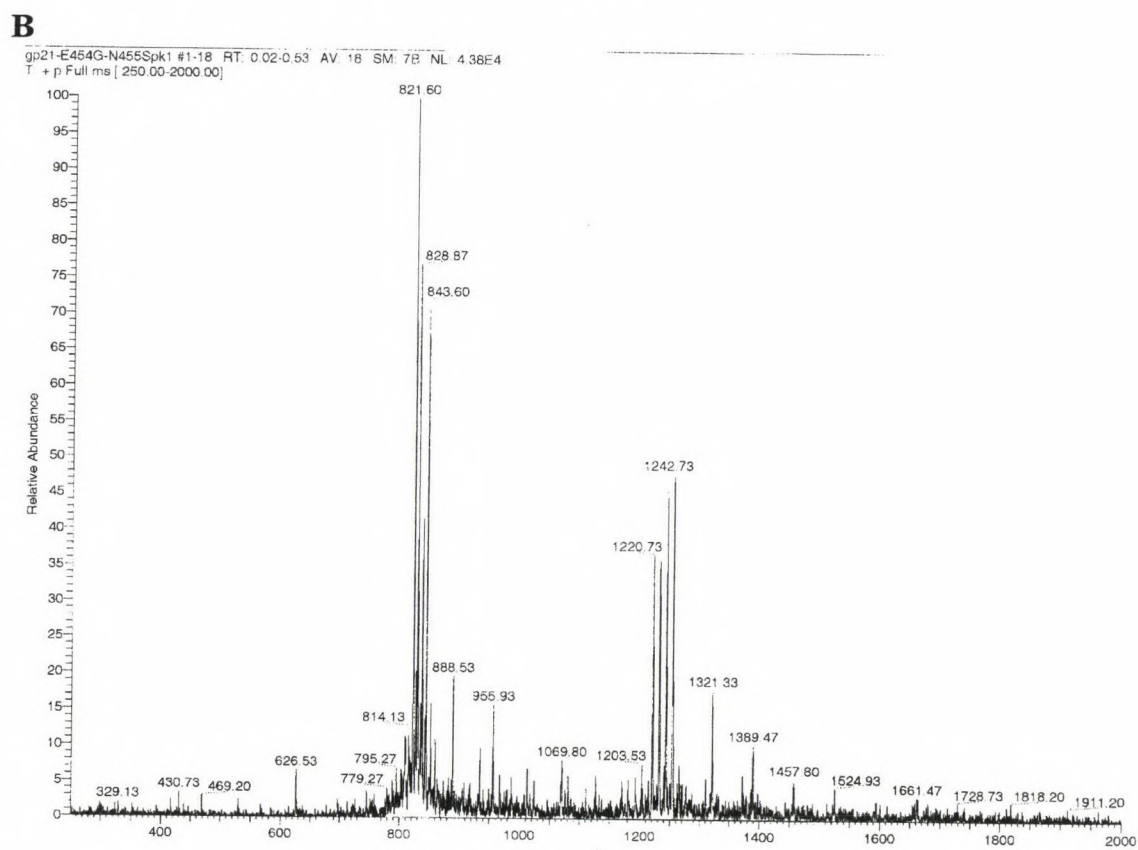
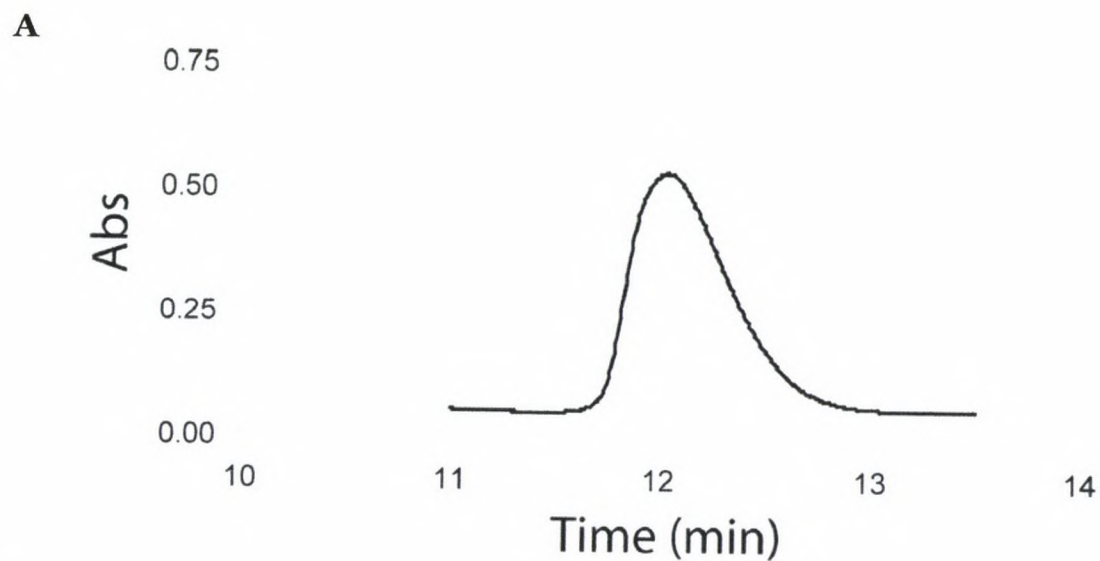


Figure 20. Characterization of HTLV gp21 E&N. (A) HPLC of purified material. (B) Electrospray mass spec raw data for purified material ($MW_{\text{calc}} = 2440$; $MW_{\text{obsd}} = 2439$).

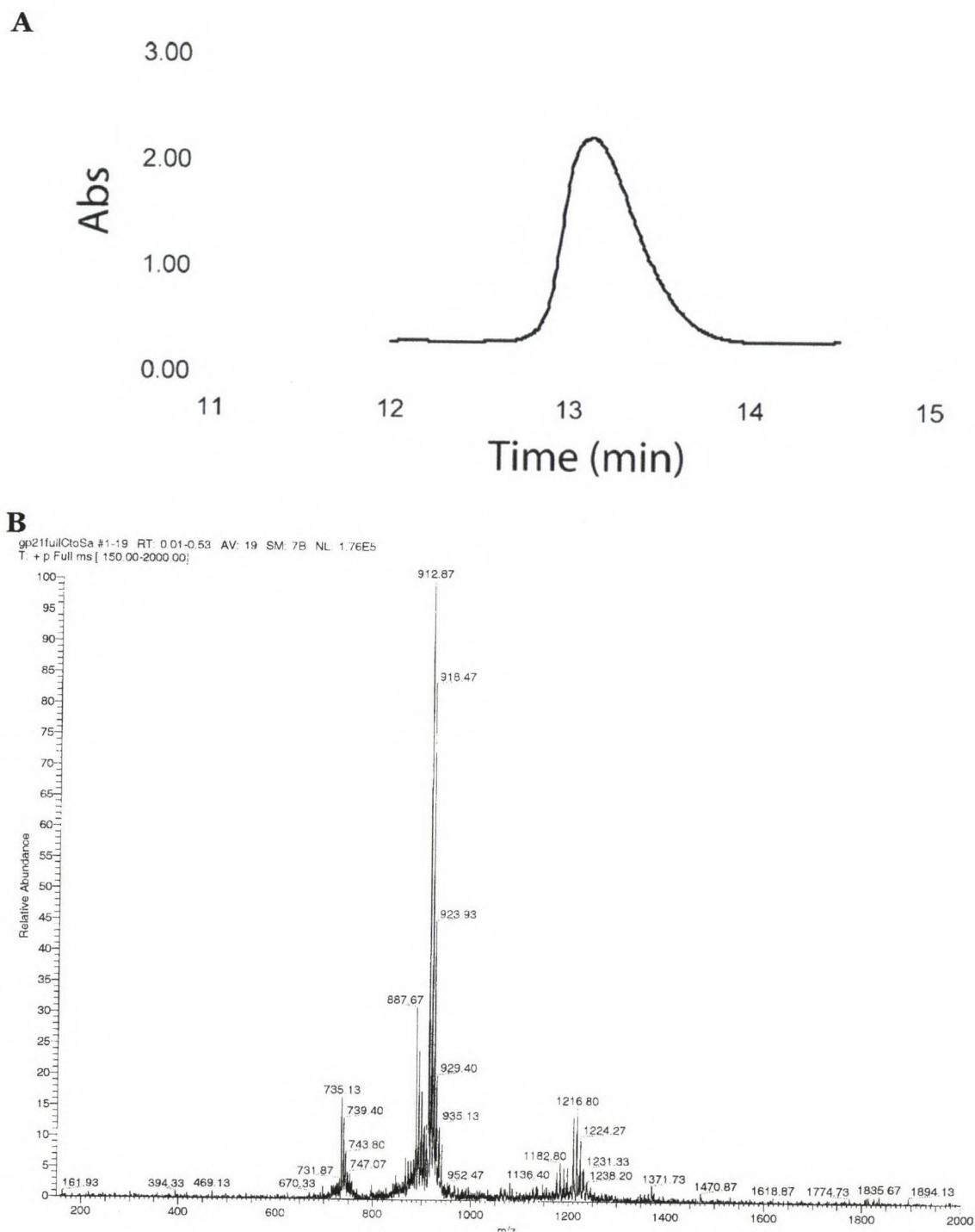
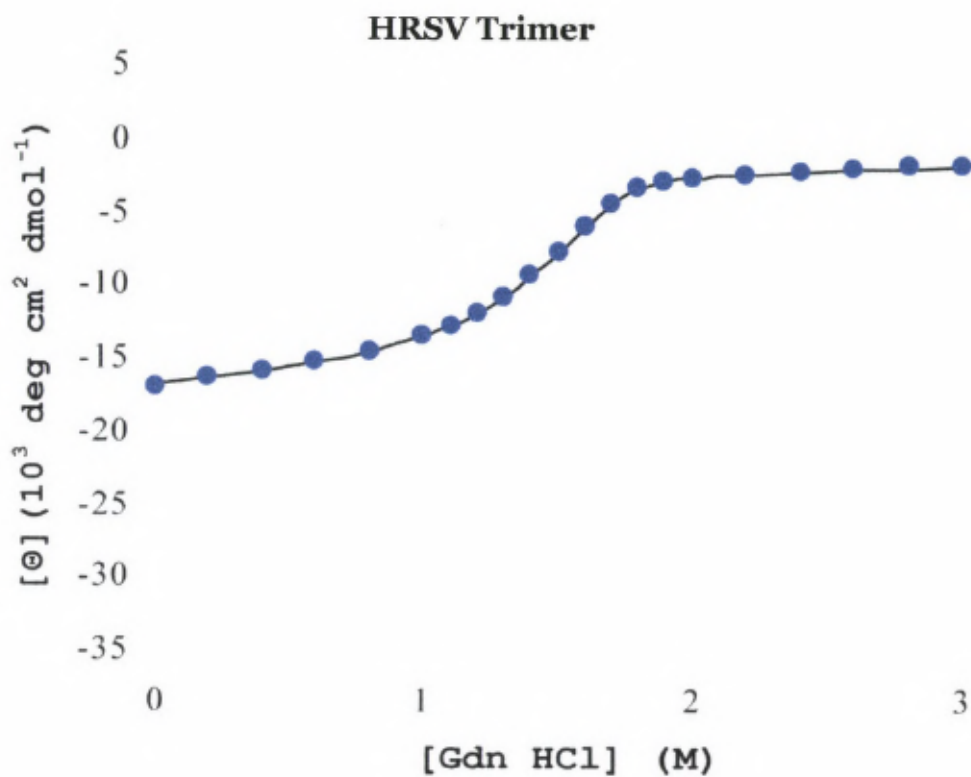


Figure 21. Characterization of HTLV gp21full C/S E&N. (A) HPLC of purified material. (B) Electrospray mass spec raw data for purified material ($MW_{\text{calc}} = 3626$; $MW_{\text{obsd}} = 3624$).

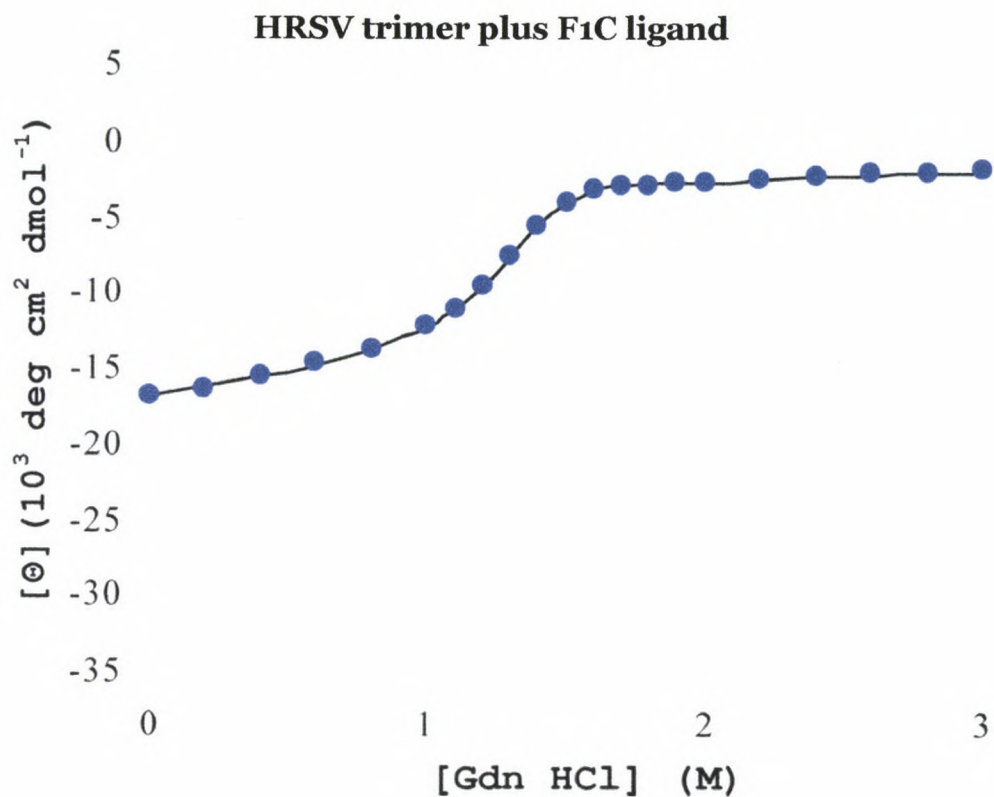
Appendix 2

Guanidine Denaturation Curves



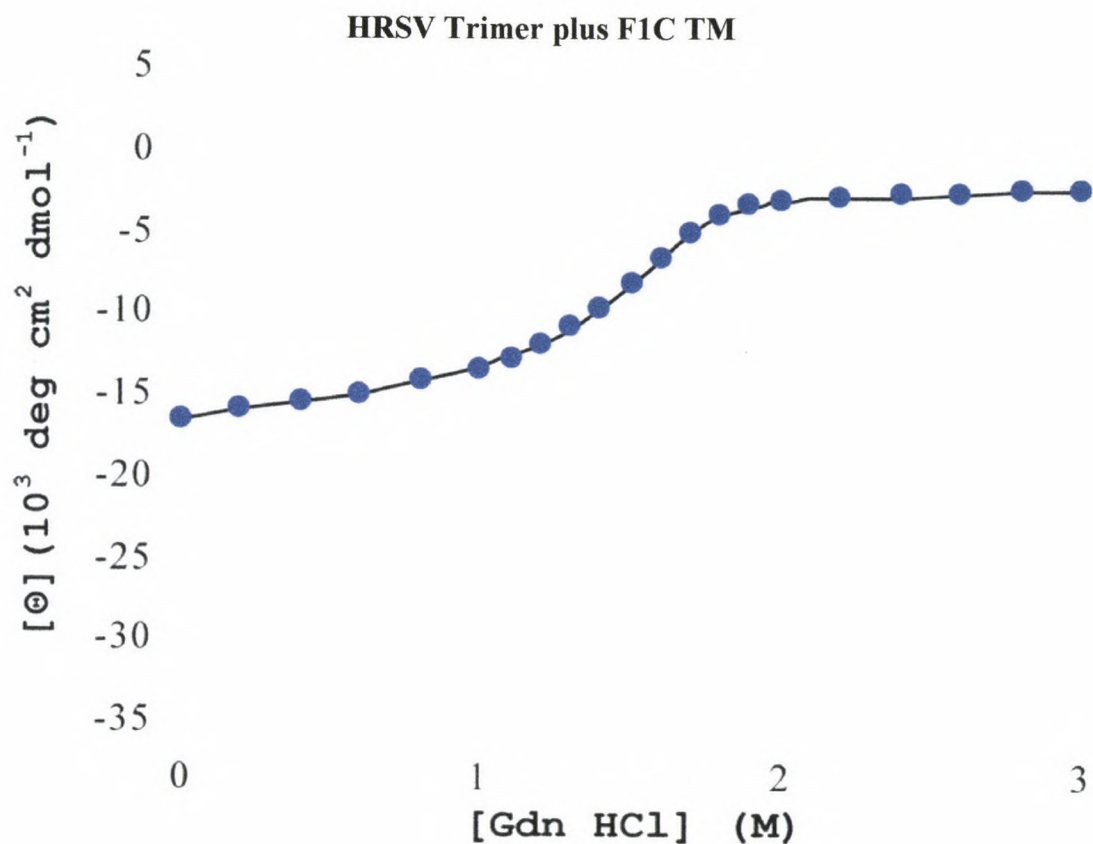
Coefficients	Value	Error
ΔG_{H_2O}	23822	151
m	6790.9	92.2
θf	-17.11	0.02
b	2.3431	0.0642
θu	-4.319	0.088
a	0.7758	0.0351

Figure 1. Guanidine denaturation curve for the HRSV trimer and the associated coefficients of the fit. $\Delta G_{H_2O} = 23.8 \pm 0.2$ kcal/mol.



Coefficients	Value	Error
ΔG_{H_2O}	24954	75
m	8711.4	50.4
θf	-17.02	0.05
b	3.0954	0.1022
θu	-4.155	0.054
a	0.667	0.017

Figure 2. Guanidine denaturation curve for the HRSV trimer plus F₁C and the associated coefficients of the fit. $\Delta G_{H_2O} = 25.0 \pm 0.1$ kcal/mol.



Coefficients	Value	Error
ΔG_{H_2O}	24341	143
m	7018.7	86.6
θf	-16.67	0.02
b	2.2769	0.0510
θu	-4.799	0.077
a	0.7387	0.0305

Figure 3. Guanidine denaturation curve for the HRSV trimer plus F₁C TM and the associated coefficients of the fit. $\Delta G_{H_2O} = 24.3 \pm 0.1$ kcal/mol.